UNIVERSITY OF CALIFORNIA

Los Angeles

Post-transcriptional gene regulation in mature neurons

A dissertation submitted in partial satisfaction

of the requirements for the degree Doctor of Philosophy

in Neuroscience

by

Victoria Meiyi Ho

2013

ABSTRACT OF THE DISSERTATION

Post-transcriptional gene regulation in mature neurons

Victoria Meiyi Ho

Doctor of Philosophy in Neuroscience

University of California, Los Angeles, 2013

Professor Kelsey C. Martin, Chair

Neurons are highly-polarized cells with processes that span great distances and many independent subcompartments. Despite their challenging morphology, neurons are able to respond to external stimuli in a local or cell-wide manner. They are also able to form stable connections with other neurons, while remaining plastic and adaptable to change. To meet these demands, neurons use complex, post-transcriptional mechanisms to regulate gene expression. Two approaches are taken in this dissertation to study post-transcriptional gene regulation in neurons.

First, a cell biological approach was used to study a specific interaction between the microRNA, miR-124, and GluA2 mRNA in dissociated hippocampal neurons. The subcellular localization pattern of miR-124 and GluA2 mRNA was determined by extracting RNA from synaptosome fractions and by direct visualization with fluorescence *in situ* hybridization. The effect of miR-124 overexpression on endogenous GluA2 protein was determined by immunoblotting and again by direct visualization with quantitative immunocytochemistry. These

experiments reveal that miR-124 is dendritically-localized while GluA2 mRNA is somatically-restricted. Both RNAs are present in the cell body, where they interact to downregulate GluA2 proteins in the soma by ~30 %. Synaptic GluA2 protein was not affected by this manipulation, suggesting that post-translational regulatory mechanisms (e.g. trafficking) are in place to maintain appropriate concentrations of GluA2 at the synapse.

Second, a high-throughput sequencing approach was taken to identify general mechanisms of gene regulation during chemical long-term potentiation (chemLTP) in acute hippocampal slices, as well as to screen for interesting candidates for further investigation. RNA was extracted from chemLTP-treated and control slices, and changes in steady-state RNA levels were determined. This study is ongoing but so far, preliminary results suggest that non-neuronal cells may play an important role in the strengthening of neuronal connections. Future analysis will focus on 3' untranslated regions, which determine the post-transcriptional fate of genes.

The two approaches provide different levels of information on the regulation of gene expression in neurons and yield unexpected findings. Together, they illustrate the complexity of regulatory mechanisms in neurons, and that there is much we have left to understand.

The dissertation of Victoria Meiyi Ho is approved.

_____

Douglas L. Black

_____

Giovanni Coppola

_____

Thomas J. O'Dell

_____

S. Lawrence Zipursky

_____

Kelsey C. Martin, Committee Chair

University of California, Los Angeles

2013

DEDICATION

This work is dedicated to my grandmother, Susan Hsu (蘇琇瑋), in loving memory.

TABLE OF CONTENTS

LIST OF FIGURES AND TABLES

ACKNOWLEDGMENTS

I would first like to thank my mentor, Kelsey Martin, for her unwavering guidance and support throughout my PhD training. Thank you for all the opportunities you made possible, the collaborations you set up, and your vast problem-solving abilities. I consider myself incredibly fortunate and privileged to have trained in your lab. You are my role model. Thank you for preparing me to tackle what lies ahead.

Thank you also to my extremely helpful thesis committee – Doug Black, Giovanni Coppola, Tom O'Dell, and Larry Zipursky. Thank you for your insightful feedback on my research projects, and for your guidance throughout my graduate training. I would like to acknowledge Dr. O'Dell. Working with you has taken the projects in our lab to another level, and I am truly grateful. I would also like to acknowledge Dr. Coppola. Thank you for your enthusiasm and support, and for enabling us cell biologists to take advantage of genomic technology.

My graduate training would not be complete without daily mentoring from the knowledgeable and patient post-docs in our lab – Toh Hean Ch'ng, Ji-Ann Lee, and Klara Olofsdotter-Otis. Our conversations always provide me with a lot of clarity and leave me wishing I had sought your advice earlier. I would like to acknowledge Toh-Hean, master of cloning. Your methodical and thoughtful approach to science gives me something to aspire to. Thank you for pushing me to be a better researcher. I would also like to acknowledge Ji-Ann, co-master of cloning. Your expertise and constructive feedback have been an invaluable part of my training. I would like to thank Klara for setting a tone of collegiality and warmth in lab. You

have many times, probably unknowingly, been the center of a spinning wheel for me. I will miss you guys!

Thank you also to Alden Huang and Charles Blum for your hard work and helpful discussions. I am excited to see what our collaboration holds in store. Liane Dallalzadeh, your dedication and fantastic time management really came through for our miR-124/GluA2 project. Thank you for helping make the most of it.

I would like to acknowledge my previous mentors – Julien Sage, Kenneth Caulton, and Lori Watson. Thank you for getting me started in science and for helping me cultivate good habits and attitudes.

I would like to thank all past and present members of the Martin lab. Graduate school can wear a person out, but your friendship and enthusiasm made coming to lab each day thoroughly enjoyable. I am very grateful for our neighbors in the Plath lab – Ritchie Ho, Jason Tchieu, Kostas Chronis, and Rupa Sridharan. Your friendships made long days in lab go by much easier. I also appreciate the non-neuroscience, but still relevant, perspective you guys provided. Rachel Jeffrey and Saadia Hasan, you guys have been wonderful baymates. Thank you to fellow board game geeks for entertainment (initials used to protect privacy): THC, RH, JT, RS, SH, SL, GI, and RM. Thanks also to fellow ramen enthusiasts: Elliott, Sangmok, Ji-Ann, Klara, Toh Hean, Patrick, Martina, and Mariana. Sixty-hour tonkotsu or bust!

I am lucky to have the world's best sisters, Patricia and Valerie Ho, who provide much needed humor, encouragement, and perspective when experiments didn't go as hoped.

Finally, I would like to thank my parents, Mandy and Gaylord Ho, for their unconditional love and support. I know you have made sacrifices in your lives so that your children may have every opportunity to pursue what we love, and I am grateful.

VITA

Education

9/00 to 12/03	Claremont McKenna College, Claremont, CA Biology and Chemistry double major, Computer Science minor B. A., *cum laude*, May 2004

Honors and awards

2011	Neural Repair Predoctoral Training Grant
2009	Neurobehavioral Genetics Predoctoral Training Grant
2003	Honors in Chemistry
2003	Phi Beta Kappa member
2003	McKenna International Fellowship
2001	NSF Research Experience for Undergraduates Fellowship

Research experience

8/08 to present	Prof. Kelsey Martin, University of California at Los Angeles, CA Cellular and molecular mechanisms of synaptic plasticity.
4/04 to 5/06	Prof. Julien Sage, Stanford University, Stanford, CA Molecular mechanisms of the Rb family in cell cycle regulation and tumor suppression.
9/01 to 12/03	Prof. Thomas Poon, Joint Science Department, Claremont, CA

Synthesis and characterization of a nucleoside analog. (senior thesis project)

6/01 to 8/01 Prof. Kenneth Caulton, University of Indiana, Bloomington, Bloomington, IN
Synthesis and reactivity of unsaturated ruthenium diaminocarbenes.

Publications

1. Ho, V.M., Lee, J. A., and Martin, K. C. The cell biology of synaptic plasticity. *Science*, 334(6056), 623-8. (PMCID: PMC3286636)
2. Burkhart, D. L., Ngai, L. K., Roake, C. M., Viatour, P., Thangavel, C., Ho, V. M., Knudsen, E. S., and Sage, J. (2010) Regulation of RB transcription in vivo by RB family members. *Mol. Cell Biol.*, 7, 1729-45. (PMCID: PMC2838078)
3. Ho, V. M., Schaffer, B. E., Karnezis, A. N., Park, K. S., and Sage, J. (2009) The retinoblastoma gene Rb and its family member p130 suppress lung adenocarcinoma induced by oncogenic K-Ras. *Oncogene*, 28(10), 1393-9. (PMCID: PMC2834234)
4. Burkhart, D. L., Viatour, P., Ho, V. M., and Sage, J. (2008) GFP reporter mice for the retinoblastoma-related cell cycle regulator p107. *Cell Cycle*, 7, 2544-52. (PMCID: PMC2730771)
5. Ho, V. M., Watson, L. A., Huffman, J. C., and Caulton, K. G. (2003) Double C(sp^3) dehydrogenation as a route to coordinated Arduengo carbenes: experiment and computation on comparative π-acidity. *New J. Chem.*, 27, 1446-50.

1 The cell biology of synaptic plasticity

The circuitry of the human brain is composed of a trillion (10^{12}) neurons and a quadrillion (10^{15}) synapses, whose connectivity underlies all human perception, emotion, thought, and behavior. Studies of neural circuits in a range of species have revealed that the overall structure of the nervous system is genetically hard-wired but that circuits undergo extensive sculpting and re-wiring in response to a variety of stimuli. This process of experience-dependent changes in synaptic connectivity is called synaptic plasticity. Studies of synaptic plasticity have begun to detail the molecular mechanisms that underlie experience-dependent synaptic changes. This research examines a variety of cell biological processes, including synaptic vesicle release and recycling, neurotransmitter receptor trafficking, cell adhesion, and stimulus-induced changes in gene expression within neurons. Taken together, these studies add to our understanding of how nature and nurture combine to determine our identities. More specifically, research on synaptic plasticity promises to provide insight into the biological basis of many neuropsychiatric disorders in which experience-dependent brain rewiring goes awry.

1.1 History of synaptic plasticity

Working in the late 1800s and early 1900s, the neuroanatomist Ramón y Cajal provided early insights into the biology of synaptic plasticity. Using the Golgi staining technique to visualize the arbor of individual neurons within densely populated nervous tissue, Cajal realized that the brain was composed of individual neurons that elaborate distinct and extensive processes (Figure 1-1). He further noted that processes from individual neurons contacted one another at sites that often contained what he termed “spiny protruberances.” With remarkable prescience,

Cajal hypothesized that neurons communicated with one another at these sites of contacts, that there was a directionality to this communication, and that memories might be stored through the strengthening of these inter-neuronal contacts [1]. Over half a century later, in 1949, the psychologist Donald Hebb proposed a framework for thinking about how synaptic plasticity might mediate experience-dependent behavioral modification, or learning. Hebb's proposal, popularized as "neurons that fire together wire together" has since been substantiated by decades of research on the mechanisms of synaptic plasticity [2].

Electron microscopic analyses in the 1950s directly revealed the ultrastructure of the synapse, with its distinct vesicle-filled axonal presynaptic compartment, a narrow synaptic cleft, and a dendritic postsynaptic compartment (Figure 1-2). Subsequent molecular biological studies increased the level of resolution to the molecular level, with the identification, purification, cloning, and characterization of individual synaptic components. The elucidation of the structure and the composition of the synapse provided a substrate for determining in detail how synapses can change with experience.

The successful study of the cell biology of synaptic plasticity requires a tractable experimental model system. Ideally, such a model should consist of a defined population of identifiable neurons and be amenable to electrophysiological, genetic and molecular cell biological manipulations. In the 1960s and 70s, many investigators developed simple invertebrate systems to study plasticity. As one example, Eric Kandel and colleagues pioneered the use of the marine invertebrate *Aplysia californica* to study the biology of learning-related

Figure 1-1. Drawing of the hippocampus.

Drawing by Ramón y Cajal illustrating the structure and connections in the hippocampus [3].

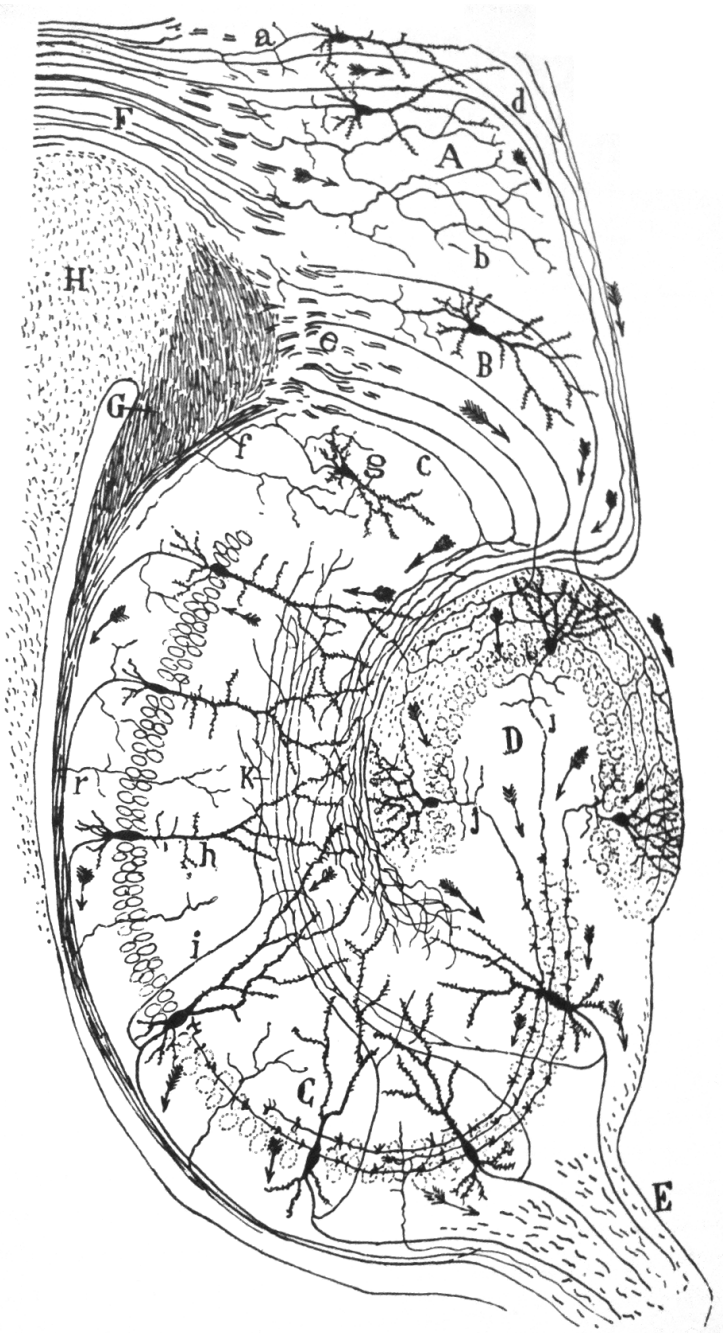

Figure 1-2. The ultrastructure of the synapse.

Neurons communicate with one another at chemical synapses. (**A**) Electron micrograph from area CA1 in adult rat hippocampus. The CA1 dendritic shaft is colorized in yellow, the spine neck and head in green, the presynaptic terminal in orange, and astroglial processes in blue. Scale bar, 0.5 µm. (**B**) Three-dimensional reconstruction of an 8.5-µm-long dendrite (yellow) with the PSDs labeled in red. Note the variation in spine and PSD size and shape. Scale cube, 0.5 µm3. Image reproduced from [4].

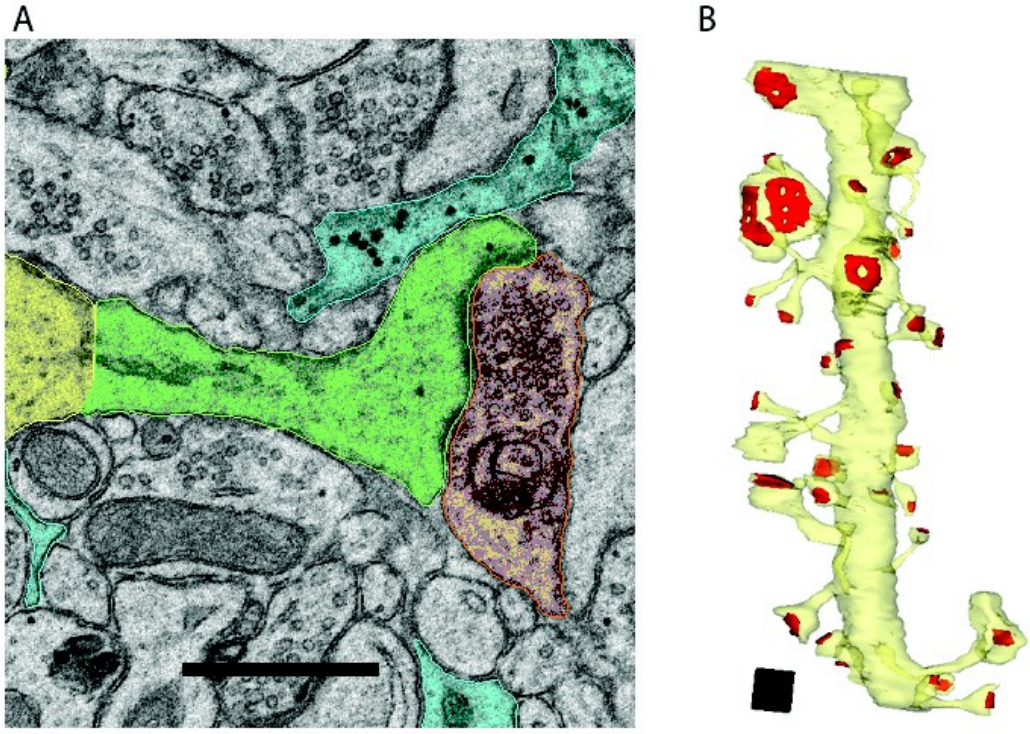

synaptic plasticity. This model system has allowed analysis of plasticity at multiple levels of analysis, from intact behaving animals to individual neurons in culture [5].

Perhaps the best-studied model system for studying plasticity in the adult vertebrate nervous system is the rodent hippocampus [6], a brain region critical for memory formation. The anatomy of the hippocampus renders it particularly suitable for electrophysiological investigation. It consists of a trisynaptic pathway: in the perforant pathway, axons from the entorhinal cortex project to form synapses on dendrites of dentate granule cells; in the mossy fiber pathway, axons of dentate granule cells project to CA3 dendrites; and in the Schaffer collateral pathway, axons of CA3 neurons project to form synapses on CA1 dendrites (Figure 1-3). The dentate, CA3 and CA1 cell bodies form discrete somatic layers, projecting axons and dendrites into defined regions. As such, electrodes can be placed in axonal, dendritic and cell body fields to stimulate and record from defined populations of neurons.

Working in Per Andersen's lab, Terje Lømo and Timothy Bliss published the first report of long-lasting activity-dependent plasticity in the hippocampus in 1973 [7]. Stimulating the perforant pathway in anesthetized rabbits, Bliss and Lømo delivered single test stimuli that elicited a stable synaptic response, measured as excitatory post-synaptic potential (EPSP), in dentate granule cells. Following delivery of a train of high frequency stimuli, however, they observed a sustained increase in EPSP amplitude in response to subsequent single test stimuli, and termed this phenomenon long-lasting potentiation, now known as long-term potentiation (LTP).

Hippocampal plasticity can also be studied in *in vitro* preparations. The hippocampus can be dissected out of the brain and cut into 300-500 micron thick transverse slices that preserve the

Figure 1-3. Hippocampal synaptic plasticity.

The rodent hippocampus can be dissected and cut into transverse slices that preserve all three synaptic pathways. In the perforant pathway (purple), axons from the entorhinal cortex project to form synapses (yellow circles) on dendrites of dentate granule cells; in the mossy fiber pathway (green), dentate granule axons synapse on CA3 pyramidal neuron dendrites; and in the Schaffer collateral pathway (brown), CA3 axons synapse on CA1 dendrites. The dentate, CA3, and CA1 cell bodies form discrete somatic layers (dark blue lines), projecting axons and dendrites into defined regions. Electrodes can be used to stimulate axonal afferents and record from postsynaptic follower cells, as illustrated for the Schaffer collateral (CA3-CA1) pathway. Drawing by Kelsey Martin.

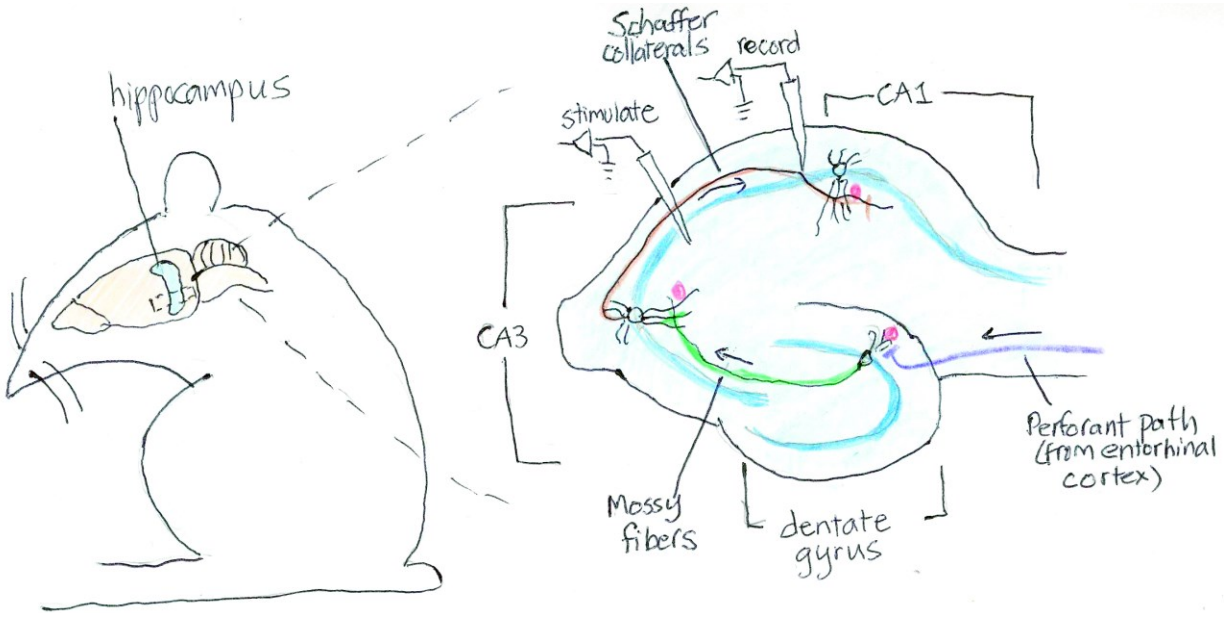

three synaptic pathways. Acute hippocampal slices can be maintained for hours, and electrophysiological techniques can be used to monitor synaptic connectivity. Slices can also be prepared as organotypic slice cultures for weeks, preserving many aspects of their architecture. Finally, hippocampal neurons can be studied in dissociated cultures, which are particularly amenable to manipulation and dynamic imaging of individual neurons and synapses. The development of genetically modified mice and vectors for acute manipulation of gene expression complete a rich tool-kit for studies of the cell and molecular biology of hippocampal synaptic plasticity.

LTP has been studied at all three hippocampal pathways (and in other brain circuits) in *in vivo* and *in vitro* preparations. Distinct stimuli elicit bidirectional changes in synaptic efficacy; while high frequency stimuli produce synaptic strengthening, low frequency stimulation has been shown to produce synaptic weakening, called long-term depression (LTD). LTP and LTD can also be produced by spike timing dependent plasticity, in which the relative timing of pre- and postsynaptic spikes leads to changes in synaptic strength [8]. Further, different patterns of stimulation elicit changes in synaptic strength that persist over various time domains, with long-lasting forms, but not short-term forms, requiring new RNA and protein synthesis [5].

This section will address synaptic plasticity in the adult brain from the perspective of the cell biology of the synapse, focusing on long-lasting forms of plasticity thought to underlie learning and memory. We will consider, in turn, each component of the synapse: the presynaptic compartment, the postsynaptic compartment, and the synaptic cleft. In each case, we will discuss processes that undergo activity-dependent modifications to alter synaptic efficacy. Long-lasting changes in synaptic connectivity require new RNA and/or protein synthesis and so we then turn

our attention to how gene expression is regulated within neurons. We will concentrate on studies of learning-related plasticity in the rodent hippocampus, since these provide the most extensive evidence for the cell biological mechanisms of plasticity in the vertebrate brain, and focus on excitatory chemical synapses.

1.2 Presynaptic mechanisms of plasticity

Neurons communicate at electrical and chemical synapses, both of which show plasticity. Communication at chemical synapses involves the release of neurotransmitter from the presynaptic terminal, diffusion across the cleft, and binding to post-synaptic receptors. Chemical neurotransmission is extremely rapid (occurring in milliseconds) and highly regulated. The presynaptic terminal contains synaptic vesicles filled with neurotransmitter and a dense matrix of cytoskeleton and scaffolding proteins at the site of release, called the active zone (Figure 1-4). Varying the probability of neurotransmitter release, thereby varying the amount of transmitter released, provides one mechanism for altering synaptic strength during neuronal plasticity.

Synaptic vesicle release can be subdivided into distinct steps, including vesicle mobilization, docking, priming, fusion and recycling. While each of these steps may be regulated in an activity-dependent manner, we will highlight three: vesicle mobilization, docking and priming.

1.2.1 Synapsins and synaptic vesicle mobilization

The population of synaptic vesicles within a presynaptic terminal exist in three states, the readily releasable pool docked at the active zone (~1% of synaptic vesicles); the recycling pool, which can be released with moderate stimulation (~15% of synaptic vesicles); and the reserve pool, which is only released in response to strong stimuli (~85% of synaptic vesicles). A family

Figure 1-4. Activity-dependent modulation of pre-, post-, and trans-synaptic components. Presynaptic: Neurotransmitter vesicle cycling. Neurotransmitter release starts with the filling of synaptic vesicles, which then dock and undergo priming at the active zone. Arrival of an action potential induces calcium influx through voltage-sensitive calcium channels (VSCCs), which triggers membrane fusion and exocytosis. The synaptic vesicles are then recycled via local reuse (a; "kiss and stay"), fast recycling (b; "kiss and run"), or clathrin-mediated endocytosis (c). Neurotransmitter release can be regulated during plasticity as exemplified by the regulation of synapsin phosphorylation (1) and the regulation of RIM protein phosphorylation (2). Postsynaptic: AMPA receptor trafficking. Locally and somatically synthesized AMPARs enter a pool of endosomes that undergo constitutive and regulated membrane trafficking. During potentiation, greater receptor insertion (3) increases the concentration of AMPARs at the synapse, where they are anchored by interactions at the PSD. During synaptic depression, AMPARs are endocytosed (3). The preferential location of endocytosis and exocytosis is probably extrasynaptic. Within the plasma membrane, trafficking of AMPARs between the synapse and the point of insertion or removal occurs by lateral diffusion. Extrasynaptic movement of AMPARs increases with neuronal activity (4). Receptor trafficking is modulated by phosphorylation of AMPAR subunits (5), which influences interactions with scaffolding proteins. Trans-synaptic: Synaptic cell adhesion molecules. PSA-NCAM is increased following neuronal activity (6). Lightning bolts indicate activity-dependent processes.

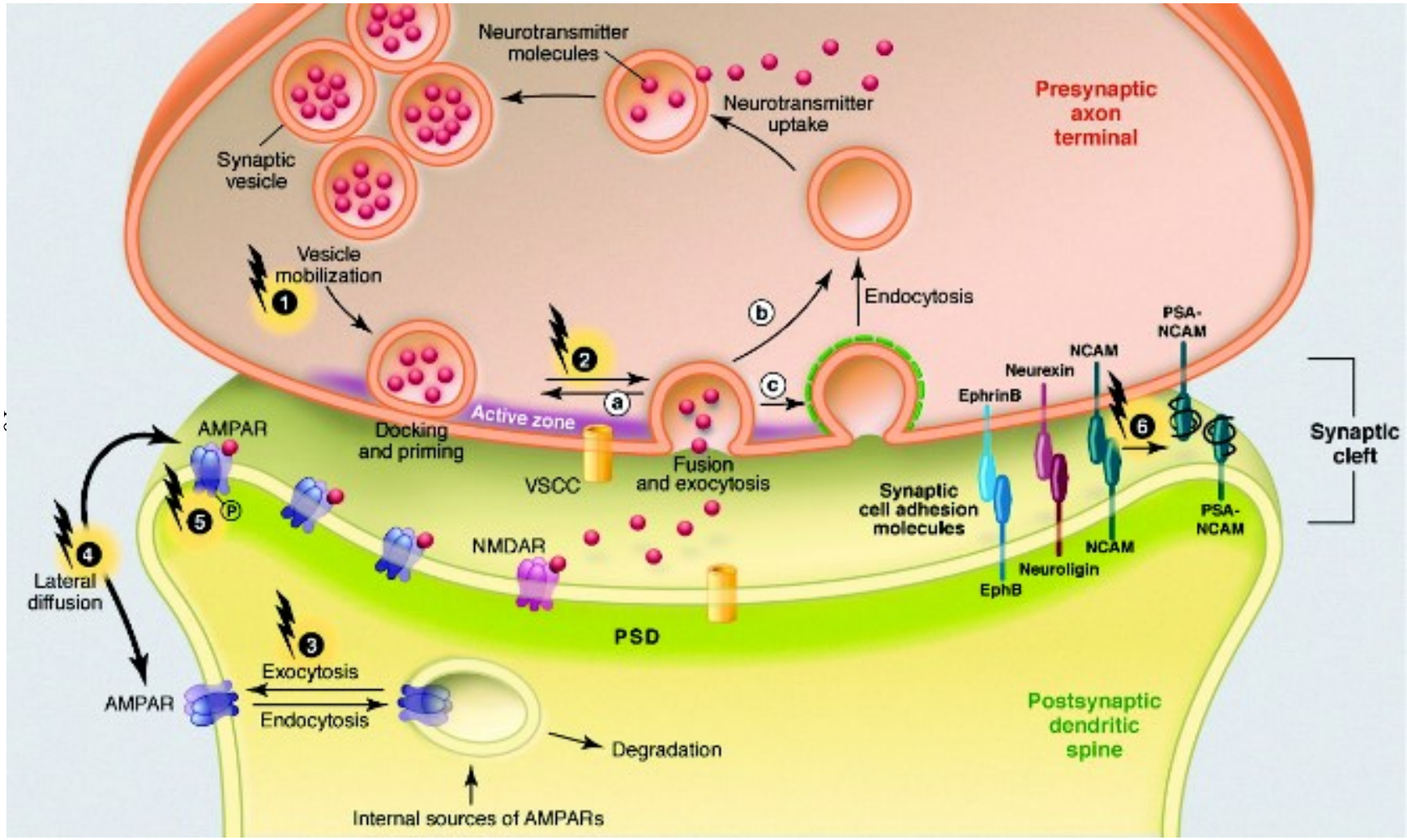
Neurotransmitter molecules
Neurotransmitter uptake
Presynaptic axon terminal
Synaptic vesicle
Vesicle mobilization
1
Endocytosis
b
2
a
c
PSA-NCAM
NCAM
Neurexin
EphrinB
Active zone
AMPAR
Docking and priming
VSCC
Fusion and exocytosis
6
Synaptic cell adhesion molecules
Synaptic cleft
5
P
NMDAR
PSA-NCAM
NCAM
Neuroligin
EphB
4
Lateral diffusion
PSD
3
Exocytosis
AMPAR
Endocytosis
Postsynaptic dendritic spine
Degradation
Internal sources of AMPARs

of phosphoproteins called synapsins tether synaptic vesicles to the actin cytoskeleton and to one another. Neuronal stimulation activates kinases that phosphorylate synapsins to modulate synaptic vesicle tethering [9]. In this way, activity-dependent regulation of synapsin phosphorylation alters the number of synaptic vesicles available for release. While synapsin knockout mice are viable, they have significantly reduced reserve pools of synaptic vesicles, and demonstrate deficits in learning and memory as well as various forms of plasticity [10], indicating that activity-dependent modulation of synaptic vesicle mobilization is critical to neuronal and behavioral plasticity.

1.2.2 SNARES, RIM proteins and synaptic vesicle docking and priming

The final step of neurotransmitter release from the presynaptic bouton involves fusion of the synaptic vesicles with the plasma membrane. Soluble NSF-Attachment Protein Receptor (SNARE) proteins that are present on the vesicle membrane (vSNARE) and target plasma membrane (tSNARE) mediate the fusion. These include the vSNARE synaptobrevin and the tSNARES syntaxin and SNAP-25. SNARE proteins contain a characteristic 60-residue SNARE motif, which, when in contact, can fold into a tight four-helical complex that brings the opposing membranes in close approximation.

For synaptic vesicles to become fusion-competent, they must undergo docking and priming, in which the vSNARE and tSNARE proteins are brought into close contact to allow rapid fusion following calcium influx. The Rab3-interacting molecule (RIM) family of proteins has recently been shown to be critical for this process [11]. A large, multi-domain protein, RIM clusters calcium channels in the active zone [12] and interacts with the Munc-13 protein [13]. The latter is required for efficient SNARE complex formation and membrane fusion. RIM is a

substrate for phosphorylation by Protein Kinase A (PKA). Genetic knockout experiments have shown that RIM is required for mossy fiber LTP and memory [14,15], and studies of cerebellar parallel fiber synapses have shown that PKA phosphorylation of RIM triggers LTP (Lonart et al 2003). Taken together, these findings suggest that RIM proteins regulate not only the coupling between calcium influx and vesicle release, but also vesicle docking and priming. Activity-dependent phosphorylation of RIM proteins by PKA can thus alter synaptic efficacy via multiple mechanisms.

1.3 Postsynaptic mechanisms of plasticity

Following release from the presynaptic bouton, neurotransmitter diffuses across the synaptic cleft to bind to receptors on the post-synaptic side of the synapse. Most postsynaptic principle neurons in the brain are studded with membrane protuberances called dendritic spines, which are the post-synaptic compartments. These spines, Cajal's "spiny protruberances," permit light microscopic detection of postsynaptic compartments. The shape of spines is somewhat heterogeneous, but consists of a bulbous head and a thinner neck that connects the spine to the dendritic shaft; the size of the spine head and the volume of the spine correlates with synaptic strength [16,17]. Spines serve as compartmentalized signaling units, and the number and shape of spines has been shown to change during synaptic plasticity [18]. At the ultrastructural level, the postsynaptic compartment is characterized by an electron-dense post-synaptic density (PSD), which consists of neurotransmitter receptors and an extensive network of scaffolding proteins. The PSD can be isolated biochemically, allowing detailed proteomic analysis of its composition.

1.3.1 Activation of post-synaptic kinases in the spine: CamKIIα and PKMζ

LTP and LTD induction are both dependent on postsynaptic elevations in intracellular calcium [19,20], which activates multiple downstream signaling enzymes including the phosphatase calcineurin and the kinases calcium/calmodulin-dependent protein kinase II (CaMKII) and protein kinase C (PKC). Activation of these enzymes in the postsynaptic compartment plays a major regulatory role during synaptic plasticity. Here we will focus on studies of CaMKIIα and the PKC isoform PKMζ during hippocampal LTP and learning.

LTP induction in the CA1 region of the hippocampus requires CaMKII activity [21,22], and transgenic mice lacking the α isoform have defective LTP and spatial learning [23,24]. CaMKIIα undergoes autophosphorylation in response to elevations in Ca^{2+} bound calmodulin, and this autophosphorylation renders the kinase autonomously active for approximately 30 minutes [25]. This switch-like property of CaMKII enables it to persistently phosphorylate targets. Neuronal activity also translocates CaMKIIα to the PSD, where it can phosphorylate many PSD proteins. CaMKIIα knockout mice were among the first transgenic mice shown to have impairments in hippocampal LTP and learning [24]. Later studies showed specifically that the autophosphorylation of CaMKIIα is essential for LTP induction and, perhaps, its maintenance [26]. More recent findings suggest, however, that autonomous CamKII activity generated by autophosphorylation may be less important for LTP maintenance and long-term memory than previously thought [27].

The brain-restricted atypical PKC isoform, protein kinase M zeta (PKMζ), is constitutively active and thus can persistently phosphorylate targets. PKMζ mRNA is targeted to dendrites where activity-dependent signaling cascades regulate its local translation [28]. Protein concentrations increase or decrease with LTP or LTD inducing stimuli, respectively [29].

Furthermore, studies that exogenously apply PKMζ or pharmacologically block its activity have shown that PKMζ is sufficient and necessary for LTP maintenance [30] and for the maintenance of long-term memories [31]. One way that PKMζ modulates persistent changes in synaptic strength is by regulating AMPAR trafficking [32]. These data have led to the proposal that PKMζ activation perpetuates synaptic plasticity and memory.

1.3.2 Activity-dependent modulation of postsynaptic glutamate receptors

The main excitatory neurotransmitter in the brain is glutamate, which activates several post-synaptic receptors. Two types of ionotropic glutamate receptors – α-amino-3-hydroxy-5-methyl-4-isoxazolepropionic acid (AMPA) and *N*-methyl *D*-aspartate (NMDA) – have central roles in hippocampal synaptic plasticity. Both are ligand-gated ion channels and have unique properties that subserve different phases of synaptic plasticity. NMDA-type glutamate receptors (NMDARs) are calcium permeable and when activated, allow an influx of calcium needed for the induction of long-term potentiation (LTP). However, NMDARs are "coincidence detectors" and require both presynaptic transmitter release and postsynaptic depolarization for activation. As such, activation of the NMDA receptor is considered a molecular exemplar of Hebb's postulate that "neurons that fire together wire together."

AMPA-type glutamate receptors (AMPARs) are important for the expression and maintenance of LTP. Unlike NMDARs, AMPARs can be activated by ligand binding at resting potentials to allow current flow. Studies have found that increased conductance through AMPARs is responsible for the increase in synaptic connectivity during NMDAR-dependent LTP at CA1 synapses [33,34].

Given the importance of AMPARs in determining synaptic connectivity, much effort has focused on delineating the mechanisms that regulate their function. Activity-regulated phosphorylation can change AMPAR function by changing the channel properties and conductances of the receptors. However, changes in channel properties are unlikely to account for the drastic changes in AMPAR function seen with LTP [35]. Instead, changes in AMPAR function during synaptic plasticity are mostly due to phosphorylation-induced changes in its abundance at the synapse. Studies have shown that stimulation of dissociated cultures lead to a redistribution of GluA1 subunits and changes in GluA1 surface expression [36,37]. Furthermore, LTP-induction in slice cultures has been shown to increase the incorporation of AMPARs at the synapse in an NMDA-dependent manner [38]. Conversely, protocols associated with synaptic weakening result in a reduction of AMPARs in spines [39] and an increase in internal AMPARs [40].

AMPARs traffic constitutively to and from the plasma membrane via recycling endosomes [41]. Delivery of AMPARs to synapses is believed to occur first by exocytosis at extrasynaptic sites followed by lateral diffusion within the plasma membrane to PSDs, where the mobility of the receptors is greatly reduced. During removal of synaptic AMPARs, receptors diffuse away from the PSD and then undergo clathrin-mediated, dynamin-dependent endocytosis. AMPAR trafficking occurs constitutively under basal conditions and is modulated by activity through changes in actin dynamics and AMPAR interactions with scaffolding proteins. One of these scaffolding proteins, Stargazin, mediates the interaction between AMPARs and the PSD protein PSD-95, and this interaction is important for synaptic localization of AMPARs [42]. Activity alters the phosphorylation of Stargazin, with phosphorylated Stargazin enhancing

AMPAR function. Blocking Stargazin phosphorylation blocks LTP, while blocking dephosphorylation blocks LTD [43].

AMPARs are tetramers, existing as mostly GluA1/2 or GluA2/3 combinations in the adult hippocampus [44]. The cytoplasmic tails of each subunit contain multiple phosphorylation sites that regulate the trafficking of AMPARs. As one example, PKA phosphorylation of S845 in the long cytoplasmic tail of GluA1 increases GluA1 surface expression due to both enhanced insertion and attenuated internalization [45]. Conversely, NMDA treatment of dissociated cultures and brain slices results in dephosphorylation of S845 and is correlated with an increase in the rate of AMPAR endocytosis [46]. The functional consequences of GluA1 phosphorylation are highlighted by studies in knock-in mice with phosphorylation deficient mutations at both S831A and S845A. These mice display a loss of NMDA-induced AMPAR internalization, deficits in LTP and LTD, and have impaired spatial memory [47]. On the other hand, LTP induction in S831D and S845D phosphomimetic knock-in mice can be achieved with weaker stimulation than in wild-type, suggesting that phosphorylation at these two sites lowers the threshold for LTP [48].

While studies of post-translational modifications at individual sites have established a role for regulating GluA1 trafficking and channel properties, they do not fully account for the changes in GluA1 function observed with synaptic plasticity [49]. Activity-modified residues continue to be discovered, including for example the highly conserved T840 phosphorylation site, which correlates remarkably well with synaptic strength [50] and a phosphorylation site at S818 that appears to have a crucial role in AMPAR trafficking in LTP [49]. It is likely that complex patterns of phosphorylation and of other post-translational modifications (e.g. palmitoylation or

ubiquitination) combine to regulate AMPAR localization. Taken together, these studies underscore the importance of activity-dependent modulation of AMPAR trafficking as a means of regulating synaptic strength.

1.4 Trans-synaptic signaling: the synaptic cleft

The synaptic cleft is a remarkably regular junction of approximately 20 nm between the pre- and post-synaptic compartments, consisting of a space through which presynaptically released neurotransmitters diffuses to bind postsynaptic receptors, as well as a network of cell adhesion molecules (CAMs) that keeps the synapse together. These adhesive interactions are so strong that it is impossible to biochemically separate intact pre- from post-synaptic compartments.

1.4.1 Role of CAMs in synaptic plasticity

The CAMs that localize to the synaptic cleft include, among others, members of the cadherin, integrin, immunoglobulin (Ig)-containing CAMs, as well as neurexins and neuroligins. Much research has focused on trying to understand whether and how CAMs mediate synapse specificity during neural circuit formation [51]. Here we will focus on studies of regulation of synaptic CAMs during experience-dependent synaptic plasticity, limiting our discussion to just two of many examples.

One example of activity-dependent changes in adhesion at synapses involves the addition of large sialic acid homopolymers to the Neural Cell Adhesion Molecule NCAM to form polysialylated NCAM (PSA-NCAM), which decreases hemophilic adhesion. The ratio of PSA-NCAM to NCAM is increased following hippocampal learning tasks [52,53] and inactivation of the enzyme that adds the poly-sialic moieties blocks hippocampal learning and plasticity [53,54].

The time course of these changes suggests that the increase in PSA-NCAM is required to promote synaptic remodeling during persistent forms of plasticity.

Another family of CAMs that play a role in hippocampal plasticity includes the synaptically localized receptor tyrosine kinase ephrins and ephrin receptors (Eph receptors), which mediate bidirectional signaling at the synapse. Initially studied in the context of neural development, ephrins and Eph receptors have also been found to be essential for hippocampal LTP and LTD in the adult brain [55]. Specific ephrins and Eph receptors interact with and regulate the localization and function of NMDA receptors, and can thereby modulate synaptic strength in response to activity. Experiments using inhibitory ephrin and Eph Receptor peptides have revealed that both molecules are required, in a kinase-independent manner, for mossy fiber hippocampal LTP [56].

1.4.2 Trans-synaptic signaling by retrograde messengers

Another means of trans-synaptic signaling involves diffusible, membrane soluble messengers. Here we will briefly review recent work outlining a role for endocannabinoids as trans-synaptic retrograde signals critical to many forms of synaptic plasticity [57]. The CB1 and CB2 cannabinoid receptors were initially identified as receptors for cannibinoid, the active ingredient of THC/marijuana. This in turn led to the identification of endogenous CB1 and CB2 ligands, called endocannabinoids. These include the arachidonate-based lipids anandamide (*N*-arachidonoylethanolamide, AEA) and 2-arachidonoylglycerol (2-AG). Discovered only 10 years ago, endocannabinoids have emerged as important modulators of plasticity at synapses throughout the brain. Depolarization and activation of a variety of receptors (including metabotropic glutamate receptors) have been shown to activate release of endocannabinoids

from the postsynaptic compartment and binding to presynaptic CB receptors, resulting in a suppression of neurotransmitter release. This form of plasticity is called endocannabinoid-LTD, or eCB-LTD. Studies using CB1 knockout mice or CB1 receptor antagonists have shown that endocannabinoid signaling is required for the extinction but not the acquisition of spatial memories [58-61]. Future studies are likely to reveal additional functions for endocannabinoids as retrograde messengers that modulate brain plasticity.

1.5 The tripartite synapse: glia and synaptic plasticity

Once thought of as the "support cells" of the nervous systems, glial cells are now considered essential partners in synapse formation, synaptic transmission and plasticity [62]. Astrocytes ensheath the synapse (Fig x), forming a "tripartite synapse," composed of neuronal pre- and post-synaptic compartments as well as surrounding astrocytes. Synaptically-localized glia release neuroactive molecules that influence neuronal communication. For example, release of D-serine (a co-activator of the NMDA receptor) from glia has been shown to be required for LTP of hippocampal Schaffer collateral synapses [63] (although see also [64]). Ephrin and Eph receptor signaling between neurons and glia has been shown to regulate the uptake of glutamate through glial glutamate transporters, and thereby affect neurotransmission and synaptic plasticity [65]. The release of lactate from astrocytes and uptake by neurons has also been reported to be required for long-term hippocampal memory and plasticity [66]. As these examples illustrate, future research in this relatively new field is likely to uncover a multitude of ways in which glia contribute to synaptic plasticity.

1.6 Regulating gene expression within neurons during plasticity

While post-translational modifications are adequate for short-term plasticity, long-lasting forms of plasticity require new transcription and translation [5].

1.6.1 Signaling from synapse to nucleus to regulate transcription

The requirement of new RNA for long-lasting synaptic plasticity indicates that synaptic signals must be relayed to the nucleus to regulate transcription. Synapse to nucleus signaling poses a unique set of challenges in neurons, where the distance between the synapse and nucleus can be significant. Neurons are specialized for rapid communication between compartments via electrochemical signaling, and depolarization at the synaptic terminal leads to depolarization at the soma within milliseconds, followed by calcium influx and calcium-dependent nuclear signaling. Calcium influx can occur through voltage-gated ion channels, through NMDA or AMPA glutamate receptors. Cytosolic calcium can also be elevated following activation of Gq coupled receptors such as the metabotropic glutamate receptor. Interestingly, each route of calcium influx induces different programs of gene induction. For example, transcription of brain-derived neurotrophic factor (BDNF) is highly induced following calcium entry through L-type voltage-sensitive calcium channels (VSCCs) in excitatory neurons, but not following calcium entry through NMDA receptors or other VSCCs [67].

Soluble signals can also be transported from the synapse to the nucleus by slower, microtubule and motor protein-dependent pathways [68]. This class of signals includes kinases such as the extracellular regulated kinase ERK as well as transcriptional regulators such as CREB2 [69,70]. These slower pathways of signaling to the nucleus may sustain changes in gene expression for time periods extending beyond the initial stimulus.

To obtain a global view of how transcription is altered during activity-dependent plasticity, many groups have measured changes in transcription following depolarization of cultured mouse neurons. Such studies have identified over 300 activity-regulated genes [71]. Genome-wide analyses of transcription factor binding sites of the activated genes have revealed that the transcription factors CREB, MEF2, and Npas4 control the activity-dependent transcription of a large number of downstream activity-regulated genes [72,73]. A larger number of transcription factors also contribute to neuronal-activity driven transcription, including SRF, ELK, NFAT, NFκB, DREAM, NeuroD, SP4, and CREST. These transcription factors regulate the expression of overlapping but distinct subsets of activity-regulated genes, suggesting that the precise temporal, spatial, and stimulus-specific cellular response is achieved by the combinatorial control by different transcription factors.

1.6.2 Local protein synthesis

Despite requiring new transcription, LTP and LTD can occur in a synapse-specific manner, raising the question of how gene expression in neurons can be restricted to subsets of synapses and not generalized to the entire cell. One way of locally changing the proteome in neurons is through regulated translation of localized mRNAs (Figure 1-5) [74].

Protein synthesis was historically thought to occur exclusively in neuronal cell bodies. The existence of local translation in dendrites of mature neurons was first suggested by electron micrographic identification of polyribosome in hippocampal dendrites [75]. Studies in hippocampal slices in which dendrites had been severed from cell bodies were found to retain the ability to express long-lasting LTP and LTD, indicating that local translation can mediate long-term modification of synaptic strength [76,77]. Studies from many labs have since identified

Figure 1-5. Local regulation of the synaptic proteome.

Synaptic plasticity modifies gene expression at many levels. Strong stimulation of synapses triggers signals that are sent to the nucleus to modify RNA synthesis. Synaptic activity also modifies protein synthesis, and has been found to act at several key steps during translation: (1) Relief of repression, e.g., RISC-mediated repression; (2) modification of translational initiation to allow 4E-4G interaction and recruitment of 40*S*; (3) formation of the preinitiation complex; and (4) dephosphorylation of eEF2 to allow for catalysis of ribosome translocation during translational elongation. To counterbalance local protein synthesis, local protein degradation also occurs at synapses (5). Together, these regulated steps in protein addition and removal allow for rapid, spatially restricted control of the synaptic proteome. Lightning bolts indicate activity-dependent processes. RBP, RNA binding proteins such as exon junction complexes, RISC machinery, Staufen, CPEB, etc. (Note: Although local translation in dendrites is a well-accepted phenomenon, it has not been demonstrated to occur in spines.)

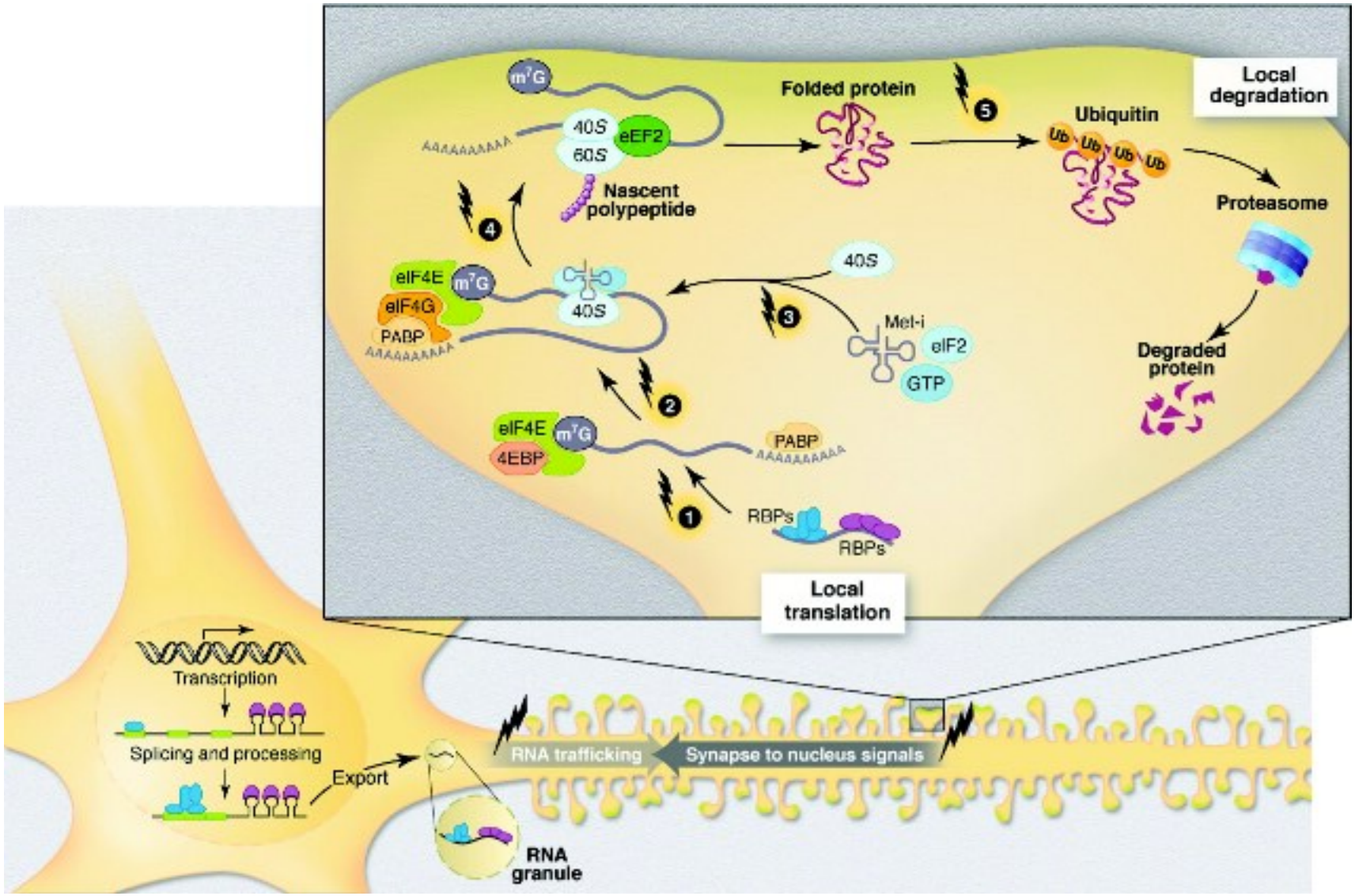
m7G
AAAAAAAAAA
40S
60S
eEF2
Nascent polypeptide
Folded protein
5
Ubiquitin
Ub
Local degradation
Proteasome
Degraded protein
4
eIF4E
m7G
eIF4G
PABP
AAAAAAAAAA
40S
3
Met-i
eIF2
GTP
2
eIF4E
m7G
4EBP
PABP
AAAAAAAAAA
1
RBPs
RBPs
Local translation
Transcription
Splicing and processing
Export
RNA granule
RNA trafficking
Synapse to nucleus signals

localized mRNAs that undergo stimulus-induced translation, and have used a number of approaches to directly visualize translation at dendrites and synapses [78,79].

Studies of mRNA localization have led to the identification of *cis*-acting RNA elements that bind to RNA-binding proteins to undergo export from the soma into the dendrite [80]. Although several dendritic localization elements have been identified, there is to date no consensus in their sequence or structure. Among the best-studied RNA binding proteins involved in dendritic mRNA localization are Staufen, HuD/Elav, and hnRNPA2 [81]. These proteins bind *cis*-acting elements and assemble transcripts into larger RNA transport granules, which travel in a kinesin-dependent manner along microtubules to their final destination. Whether localized RNAs undergo directed targeting, anchoring or stabilization at specific sites remains an open question.

In terms of translational regulation, studies have revealed activity-dependent regulation of translation initiation and elongation. One well-studied mechanism of regulating translation initiation involves the phosphorylation of eIF2α, part of the preinitiation complex. eIF2α, phosphorylation decreases translation initiation. L-LTP inducing protocols, but not E-LTP protocols, have been shown to reduce eIF2α phosphorylation [82]. Mice heterozygous for a phosphorylation resistant mutation in eIF2α show a lowered threshold for plasticity and memory [83]. Conversely, pharmacologically increasing levels of phosphorylated eIF2α prevents L-LTP induction while having no effect on E-LTP. Whether and how this pathway is regulated locally at synapses (as opposed to in the soma) is unclear.

A mechanism of translational regulation known to occur at synapses involves the cytoplasmic polyadenylation element (CPE) binding protein (CPEB). CPEB increases the polyA

tail of mRNAs by binding to CPEs in the 3'UTR. Poly(A) binding protein (PABP) is recruited to the elongated poly(A) tail, which in turn recruits eIF4G, which then interacts with eIF4E to promote translation initiation [84]. CPEB localizes to synapses [85], and has been shown to regulate translation of dendritically localized CamKIIα mRNA [85,86].

Another activity-dependent means of regulating translation initiation involves phosphorylation of eIF4E binding proteins (4E-BPs). Hypo-phosphorylated 4E-BPs bind eIF4E and prevent translation initiation; phosphorylated 4E-BP dissociates from eIF4E and relieves translational inhibition [87,88]. In neurons, activity increases 4E-BP phosphorylation in a manner that correlates with enhanced translation [89,90] (Raught 2000 sonenberg textbook). Studies in 4E-BP2 knockout mice found that E-LTP stimulation protocols could induce L-LTP in brain slices. Recently, two additional 4E-BPs have been identified in neurons: neuroguidin and the cytoplasmic FMRP interacting protein (CYFIP). While 4E-BP1 and 2 are believed to affect general translation, these new 4E-BPs may preferentially affect subgroups of transcripts within dendrites [91,92].

Activity can also regulate translational elongation during synaptic plasticity. As one example, the elongation factor eEF2 has been shown to undergo activity-dependent changes in phosphorylation. Phosphorylation of eEF2 decreases the rate of translation. Schuman and colleagues have shown that while action potentials decrease eEF2 phosphorylation (thereby increasing translation), spontaneous release increases eEF2 phosphorylation and decreases translation. These effects occur locally at synapses, indicating that one function of spontaneous release of neurotransmitter may be to suppress local translation and thereby stabilize synapses.

Translation may also be regulated through the microRNA (miRNA) pathway, which can potentially regulate hundreds of transcripts and hence provide a way of coordinating the expression of many genes. Expression profiling has shown that many miRNAs are enriched in, or even restricted to, the brain [93]. While miRNAs can regulate cell-wide levels of translation, their post-transcriptional mode of actions makes them especially well-suited to regulating distally localized transcripts. Consistent with a role in local translation, miRNAs have been found in dendrites and at synapses. Further, components of the RNA-induced silencing complex (RISC) machinery itself have been found to be altered by activity [94].

1.6.3 Local protein degradation

The local proteome can be regulated not only by local translation but also by regulated local protein degradation through the ubiquitin proteasome system. One of the first demonstrations of a role for protein degradation in regulating synapse function was the finding in *Aplysia* sensory neurons that the regulatory subunit of the cAMP-dependent protein kinase (PKA) underwent ubiquitin-mediated degradation during long-term synaptic plasticity, leading to persistent PKA activity [95]. In mammals, recent studies identified widespread deficits in synaptic plasticity and learning in mice lacking Ube3a, a brain-expressed ubiquitin ligase that is mutated in Angelman syndrome [96]. Other studies have shown that both protein synthesis and degradation are required for the maintenance of late-phase LTP, suggesting tight coupling of protein synthesis and degradation in learning-related plasticity [97,98].

Like local translation, protein degradation can be regulated within dendrites. In support of locally regulated degradation, ubiquitin and proteasomal subunits have been found in dendrites and at synapses [99]. Glutamatergic stimulation of cultured hippocampal neurons leads to

bidirectional changes in the ubiquitin conjugation of proteins and to proteasome-dependent changes in protein concentrations in PSD fractions [100]. Activity-dependent degradation involves redistribution of proteasomes from dendritic shafts to spines [101]. The occurrence of both translation and degradation at the synapse suggests that proper synaptic function requires tight control of the local proteome.

1.7 Perspectives

As the above examples indicate, cell biological approaches have provided a detailed understanding of certain aspects of activity-dependent plasticity. By focusing on molecular processes occurring within individual neurons and subcellular compartments, we now understand specific processes that are modulated by experience to change synaptic efficacy. These involve alterations in neurotransmitter release, trans-synaptic signaling, post-synaptic receptor dynamics and gene expression within neurons. The results of such studies provide molecular tools to further probe the mechanisms of brain plasticity, and potential therapeutic targets for diseases in which brain plasticity is dysfunctional. However, they fall significantly short of elucidating how complex circuits are altered by experience so as to store information and alter behavior. A challenge in the field is to study plasticity in neural circuits in living animals, and to develop methods to examine how all the components of circuit (excitatory and inhibitory neurons, synapse, glia and vasculature) are regulated to alter circuit function dynamically over various time domains. The development of methodologies for high-resolution time-lapse imaging of synapses, neurons, and circuits in live animals promises to move the field forward towards a more nuanced and complete understanding of the experience-dependent plastic changes in the brain that mediate learning and memory.

1.8 Acknowledgements for this section

This section is adapted from a review article published in Science [102], and co-authored by Ji-Ann Lee and Kelsey C. Martin. The authors thank J. T. Braslow, T.J. O'Dell, and F.E. Schweizer for comments on the manuscript.

2 GluA2 mRNA distribution and regulation by miR-124 in hippocampal neurons

2.1 Introduction

Precise control of gene expression at synapses is important for proper communication between neurons. Among the proteins that are tightly controlled are members of the 2-amino-3-(3-hydroxy-5-methyl-isoxazol-4-yl) propanoic acid (AMPA)-type glutamate receptor subunit family, GluA1-4 [103]. AMPA receptors (AMPARs) are mediators of fast, excitatory transmission between neurons, and their concentration at the synapse plays a central role in determining synaptic strength [104]. Increased synaptic AMPAR levels are correlated with increased synaptic strength and vice versa. Given their importance, AMPARs have been heavily studied and have been shown to undergo nuanced regulation at many levels of gene expression [103,105-109].

How AMPARs arrive at their synaptic locations is an active area of investigation with several, non-mutually exclusive theories [103]. One theory is that that the receptors are synthesized on the rough endoplasmic reticulum and assembled in the cell body. They are then trafficked to synaptic sites along the cytoskeleton [110-113]. Alternatively, the assembled AMPARs may be inserted into the plasma membrane at the cell body, and then transported to synapses via lateral diffusion [114]. Another theory is that AMPARs are locally translated in dendrites and processed in Golgi outposts before being inserted at synapses [115]. In support of local translation, GluA1 and GluA2 messenger RNA (mRNA) transcripts have been found to be present in dendrites of cultured rat neurons [116,117]. Furthermore, stimulation of cultured hippocampal neurons has been shown to alter the dendritic localization of both GluA1 and

GluA2 mRNAs [117], and overexpression studies have revealed local translation of GluA1 and GluA2 in dendrites that have been severed from the cell body [118,119].

The occurrence of stimulus-responsive local translation indicates that regulatory mechanisms exist to ensure that translation occurs when and where the encoded proteins are needed. One potential regulatory mechanism is through the microRNA pathway. MicroRNAs (miRNAs) are non-coding, endogenous RNAs of about ~22 nucleotides in length that downregulate gene expression via the RNA-induced silencing complex (RISC). Within RISC, the 5' end of the miRNA has a "seed" site that recognizes targets by partial complementarity to sequences in the 3' untranslated region (3'UTR) of target mRNAs [120,121]. Upon recognition of a target mRNA, miRNAs repress translation either by reducing translational efficiency or by destabilizing the transcript [122-124]. The post-transcriptional and potentially reversible mode of action of miRNAs makes them well-suited to regulate local translation.

In this study, we investigated the post-transcriptional regulation of the GluA2 subunit. Among the AMPAR subunits, GluA2 is unique because its inclusion in an AMPAR makes the receptor calcium impermeable [125]. Hence, GluA2 levels at the synapse influence calcium influx through AMPARs after glutamate binding to the receptor [126]. We used a computational algorithm to predict potential miRNA target sites in the GluA2 3'UTR, and identified miR-124 as a favorable candidate. The prediction was first validated in 293T cells using luciferase assays, and then further tested in dissociated hippocampal cultures using lentivirus-mediated miR-124 overexpression in dissociated hippocampal cultures. Fluorescence *in situ* hybridization (FISH) and reverse transcription quantitative polymerase chain reaction (RT-qPCR) were used to determine the subcellular localization patterns of miR-124 and GluA2-mRNA. Our results

support miR-124 regulation of GluA2 in neurons, but indicate that this interaction regulates GluA2 translation primarily in the somatic cytoplasm rather than in dendrites.

2.2 Materials and methods

Luciferase assays

The 3' UTR of GluA2 was cloned downstream of the renilla luciferase coding region in plasmid pRL-TK (Promega). The sequences cloned correspond to nucleotides 3,203 - 3,298 of the flip and flop isoforms (NM_001083806.1 and NM_013540.2), which have identical 3' UTRs. Reporter constructs with the predicted miR-124 target site deleted or point-mutated were generated by site-directed mutagenesis. A mixture of renilla luciferase reporter plasmid (0.35 ug), firefly luciferase control plasmid (0.05 ug) (pGL3, Promega), carrier plasmid (0.4 ug) (pBSK), and miRNA mimic (25 nM final concentration; Thermo Scientific Dharmacon; mimic-124: UAAGGCACGCGGUGAAUGCCA, mimic-124*: GCAUUCACCGCGUGCCUUAUU, mimic-124PM: UAACGGACGCGGUGAAUGCCA, mimic-124 PM*: GCAUUCACCGCGUCCGUUAUU) was transfected using Lipofectamine 2000 (Invitrogen) into one well of HEK293T cells that were plated at a density of 50,000 cells/well in a 24-well plate the day before. At 24 hours post-transfection, luciferase expression was assayed with the Dual-Luciferase® Reporter Assay System (Promega) according to manufacturer's instructions and measured on a Molecular Devices Analyst AD microplate reader (Analyst AD 96-384). Renilla luciferase signals were first normalized to firefly luciferase signals, and then normalized to the control samples (each construct, without miRNA added). The assays were performed four times in triplicate.

Synaptosome fractionation

Synaptosome fractions were prepared from 2-3 month old C57BL/6J mice. Ten mice were used for each fractionation. The mice were anesthetized with isofluorane and sacrificed by cervical dislocation. All centrifugation steps were performed at 4 ^{o}C and solutions were kept on ice. Forebrains were dissected and homogenized in solution A (0.32 M sucrose, 1 mM $NaHCO_3$, 1 mM $MgCl_2$, 0.5 mM $CaCl_2$, 10 mM $Na_4P_2O_7$). An aliquot of the total homogenates were removed at this point for RNA and protein extraction. The remaining homogenates were spun at 1,400 g and the supernatant was saved. The pellet was resuspended in solution A and spun at 700 g. The supernatants from both spins were pooled and an aliquot representing the cytosolic fraction was removed. The supernatants were then spun at 13,800 g to pellet synaptosomes and other organelles. The pellet was resuspended in solution B (0.32 M sucrose, 1 mM $NaHCO_3$), and layered onto a discontinuous gradient with 1.2 M, 1.0 M, and 0.8 M sucrose layers prepared in 1 mM $NaHCO_3$. The gradient was spun at 82,500 g for 2 hours. Synaptosomes separate into the band between the 1.0 M and 1.2 M layers. This band was collected and spun at 100,000 g for 20 min to pellet the synaptosomes.

Protein extraction and immunoblotting

RIPA buffer (50 mM Tris, 150 mM NaCl, 0.1 % SDS, 0.5 % Na deoxycholate, 0.1 % SDS, 1 % NP-40*)* with cOmplete protease inhibitor (Roche) and benzonase (Sigma #E1014) was used for protein extraction from synaptosomes and neuronal cultures. For synaptosome preparations, total protein levels were determined with by BCA protein assay (Pierce) and 5 mg of protein was loaded per lane. For neuronal cultures, proteins were extracted and the same volumes were loaded for each condition. All protein samples were run on 10 % polyacrylamide

gels and transferred to a PVDF membrane for immunoblotting. Blots were scanned using the Odyssey imaging system (Li-Cor) and quantified with ImageJ software.

Antibodies

We used the following antibodies. Vendors, catalog numbers, and dilutions are shown within parenthesis. PSD-95 (Abcam 18258; 1:1000), GluA2 (Invitrogen 32-0300; 1:200), MAP2 (PhosphoSolutions 1100-MAP2; 1:20,000), copGFP (Evrogen AB513; 1:3,000), Synapsin I (Abcam AB8; 1:1000), GFAP (Millipore MAB360; 1:1000), Tuj1 (Millipore AB15708; 1:1000), Alexa Fluor® 488 goat anti-rabbit (Invitrogen 11008; 1:20,000), Alexa Fluor® 488 goat anti-mouse (Invitrogen 11001; 1:20,000), Alexa Fluor® 555 goat anti-mouse (Invitrogen A21422; 1:20,000), Alexa Fluor® 633 goat anti-chicken (Invitrogen A21103; 1:20,000), IRDye® 680LT goat anti-mouse (Li-Cor 926-68020; 1:20,000), IRDye® 800CW goat anti-rabbit (Li-Cor 926-32211; 1:20,000)

RNA extraction and quantification

The miRNeasy Mini kit (Qiagen) was used according to manufacturer's protocol for extraction of total RNA and DNaseI treatment. The amount of RNA extracted was measured with a NanoDrop ND-1000 spectrophotometer (NanoDrop Technologies). For miRNA RT-qPCR assays, RNA was diluted to below 10 ng/μL and measured with the Qubit RNA assay kit on a Qubit fluorometer (Invitrogen).

Reverse transcription and quantitative PCR (RT-qPCR)

For mRNA RT-qPCR, the amount of starting material in each reaction was normalized to total RNA. Transcripts were primed with random hexamers and reverse transcribed with SuperScript III (Invitrogen). The resulting cDNA was then used for comparative qPCR with

SYBR Green (Applied Biosystems) and gene specific primers (GluA2 – fwd: CCATCGAAAGTGCTGAGGAT, rev: AGGGCTCTGCACTCCTCATA; Camk2α – fwd: TCTGAGAGCACCAACACCAC, rev: CCATTGCTTATGGCTTCGAT; c-Fos – fwd: CACACAGGACTTTTGCGC, rev: GACACGGTCTTCACCATTCC; Fads3 – fwd: ATGACCTACCAGGCGACAAG, rev: CAATCAACAGGGGTTTCAGG; pre-miR-124 – fwd: GTGTTCACAGCGGACCTTG, rev: ATTCACCGCGTGCCTTAAT). Looped primers specific for mature miRNAs were used for RT, and TaqMan® probes were used for qPCR (Applied Biosystems). Standard curves were determined for all genes quantified, all of which had amplification efficiencies within 100 ± 10%.

Dissociated hippocampal cultures

Hippocampi were dissected from postnatal day 0 C57BL/6J mice (Jackson Laboratory) and dissociated by trypsin treatment and trituration. The dissociated neurons were plated on culture plates or on HCl-etched coverslips (Deckgläser #1001/12). Culture plates and coverslips were coated with 0.1 mg/mL poly-DL-lysine (Sigma #P-9011) overnight at 37 ^{o}C. Plating medium consisted of B-27 supplement (1 mL/50 mL media), 0.5 mM glutamine (Gibco #21103-015), 25 μM glutamate (Sigma #G-5889), and β-mercaptoethanol (25 μM; Sigma #G-57522) diluted in Neurobasal-A media (Gibco #21103). Neurons for FISH and immunocytochemistry (ICC) were plated at low density (approximately 210 cells/mm^2 or 40,000 cells/well in a 24-well plate). Neurons for RNA or protein extraction were plated at high density (approximately 630 cells/mm^2 or 240,000 cells/well in a 12 well plate).

Fluorescence in situ hybridization

Neurons (14-21 DIV) were processed for FISH using the QuantiView mRNA and miRNA kits according to manufacturer's protocol (Affymetrix). Each QuantiGene® mRNA probe set consists of a mixture of 20 pairs of short oligonucleotides that are complementary to different regions of the transcript. Each pair hybridizes to the target mRNA at adjacent sites and amplifies the signal through sequential hybridization of branched DNA molecules. The resulting signal comes from fluorophore-conjugated oligonucleotides. This technology can provide up to 8,000-fold signal amplification and is reported to have single molecule sensitivity. The QuantiGene® miRNA probes undergo a similar amplification system with branched DNA molecules, however differs in that only one pair of olignucleotides is used. Also, the final amplification step for the miRNA FISH is an enzymatic reaction with the Fast Red chromogenic substrate. After the last FISH amplification and wash steps, neurons were blocked in 10% goat serum and processed as described for immunocytochemistry.

Image acquisition

Images were acquired on a Zeiss LSM700 microscope by an experimenter blind to the treatment. Confocal images of FISH and ICC experiments were acquired with a 40 x/1.3 oil objective. For FISH images, Z-stacks of an area including the cell body and dendritic processes were taken. Images of surface GluA2 ICC experiments were acquired in single sections with a pin hole of 1 airy unit. For total GluA2 ICC images, single sections were acquired with different pinhole settings. The pin hole was first set to 5.62 airy units to capture dendritic signal from 5 μm sections. Then, for the same field, the pin hole was maximized to 14.07 airy units and the plane of focus was adjusted to capture somatic signal from 12.4 μm sections. The copGFP transduction marker was partially quenched by fixation, but could still be seen in the cell body

and this signal was used to confirm transduction. The gains for signals to be quantified were set at subsaturation levels. Live images to assess transduction efficiency were acquired with a 10 x/0.3 air objective.

Image analysis

Images were analyzed by an experimenter blind to the treatment and quantified with ImageJ software. To measure FISH puncta distribution, stack images of FISH staining were converted to maximum projection intensities. Somatodendritic compartments were linearized using the "Straighten" function in ImageJ with a width setting of 25 pixels (corresponding to ~4 μm). Somatodendritic compartments were selected on the basis of MAP2 staining. Measurements of dendritic distance began at the center of the cell body and extended out along the dendrite until the boundary of the image. Only dendrites that did not overlap with cell bodies were selected. Then, the ImageJ "Find Maxima" function with a noise tolerance of 10 was used to identify individual puncta and report the distance of the puncta from the center of the cell body. Since dendrites of different lengths were imaged, only dendrites longer than 150 μm and only puncta within 150 μm were included in the analyses. To measure total somatic and proximal GluA2 protein expression by ICC, regions of interest were defined manually based on MAP2 staining. For dendrites >20 μm from the soma, regions of interest were defined based on dilated MAP2 masks. The mean pixel intensity and integrated densities were determined using the "Measure" function and corrected for background signal. To measure synaptic GluA2 protein expression by ICC, synapsin I puncta were used as synaptic markers in images of surface GluA2 staining. Dendrites greater than 20 μm from the soma were linearized with the "Straighten" function and a width setting of 40 pixels (corresponding to ~6 μm). The "Analyze Particles"

function was used to select Synapsin I puncta that were between 4-500 pixel units and with a circularity between 0.5-1.0. The number of puncta identified was used as an approximation of the number of synapses. Then, the "Find Peaks" function in the GDSC plugin was used to identify GluA2 puncta and report their total intensity. Finally, the "Match Calculator" function in the GDSC plugin was used to identify GluA2 puncta that were within 8 pixels (corresponding to ~1 μm) of Synapsin I puncta. Matched GluA2 puncta were considered synaptic.

Statistical methods

To compare the distributions of FISH puncta across cell groups, we performed two types of analysis. First, we developed a mixed effects analysis of variance (ANOVA) model of mean puncta distance, with variation between cell groups represented as a fixed effect, and variation between dendrites represented as a nested random effect. The analysis therefore controls for between-dendrite variation in estimating cell group effects on mean distance from cell body. Second, we classified puncta as either somatic, proximal, or non-proximal according to distance from cell body, and developed one way ANOVA models of the mean proportion of puncta in each of the three bins. Variation between cell groups was represented as a fixed effect in these models. This second analysis enables us to compare puncta density between cell groups for particular dendrite segments. SAS version 9.3 was used to fit the models, and SPSS version 21 was used. One-tailed t-tests were used to compare GluA2 ICC intensity between control and miR-124 overexpression conditions.

Lentiviral transduction

The pMIRNA1-124 overexpression plasmid was purchased from Systems Biosciences. This plasmid was modified to introduce two point mutations in the seed site for the

overexpression control plasmid. For the sponge plasmids, the pre-miR-124 sequence was deleted and sponge sites were cloned into the 3'UTR of copGFP, as described by Ebert et al. The plasmids were packaged in HEK293T cells with Δ8.9 and VSVG, and concentrated by ultracentrifugation. Neurons were transduced at 13 DIV. During transduction, half of the media was removed and stored at 4 ^{o}C. Virus was mixed with the remaining media and applied to the neurons. Transduction media was replaced with the saved media the next day (16-24 hour incubation). At 21 DIV (8 DIV post transduction), transduced neurons were harvested for RNA or protein extraction, or fixed for immunocytochemistry.

Immunocytochemistry

Neurons grown on coverslips were fixed in 4% paraformaldehyde for 10 minutes, permeabilized in 0.1% Triton-X for 5 minutes, blocked in 10% goat serum for 30 minutes, and incubated in primary antibody 16-24 hours at 4 ^{o}C. Secondary antibodies and Hoechst (1:1000, Invitrogen H3570) were incubated for 1 hour in the dark. Coverslips were mounted using Aqua PolyMount (Polysciences #18606) and allowed to dry overnight before imaging. All steps were performed at room temperature unless otherwise noted. For surface staining of GluA2 (also see Appendix, Protocol 1), neurons were first incubated live at 37 ^{o}C for 30 minutes in GluA2 antibody diluted with artificial cerebrospinal fluid (ACSF; 119 mM NaCl, 26.2 mM $NaHCO_3$, 2.5 mM KCl, 1 mM NaH_2PO_4, 1.3 mM $MgCl_2$, 10 mM glucose, 2.5 mM $CaCl_2$). The ACSF used was first bubbled with carboxygen (5 % CO_2/95 % O_2) to pH 7.35, adjusted to 293 mmOsm with glucose, and filtered with a 0.22 μm filter. Then, neurons were fixed, permeabilized, and stained for intracellular proteins (i.e. MAP2, Synapsin I) as described above.

2.3 Results

2.3.1 Prediction and initial validation of the GluA2/miR-124 interaction

We identified a predicted target site for miR-124 in the 3'UTR of GluA2 mRNA using the TargetScan algorithm (Version 4.0), which considers both the thermodynamic stability of RNA:RNA interactions and the degree of target site conservation across species [127] (Figure 2-1A). To validate the prediction, we used a dual luciferase reporter assay system in 293T cells (Figure 2-1B). In one set of assays, the GluA2 3'UTR containing the miR-124 target site was fused to the 3' end of a luciferase reporter construct. Co-transfection of this reporter with a synthetic miR-124 duplex resulted in a 50% knockdown of luciferase signal (Figure 2-1B). This interaction depended on the miR-124 seed sequence, as transfection with a mutant miR-124 duplex with two point mutations did not produce significant knockdown in luciferase expression (Figure 2-1C). In another set of assays, the miR-124 target site was deleted from the reporter. Co-transfection of this construct with miR-124 did not reduce luciferase expression compared to transfection of the target-deleted construct alone (Figure 2-1C). To confirm the importance of sequence complementarity between the miR-124 seed and GluA2 target site, a luciferase construct with point mutations complementary to those in the mutant miR-124 was made. With seed-target complementarity restored, the transfected miRNA once again repressed luciferase expression (Figure 2-1D). These studies indicate that miR-124 inhibits translation of target GluA2 mRNA reporters in a sequence-specific manner.

2.3.2 Determining the subcellular distribution of GluA2 mRNA and miR-124

GluA2 mRNA and miR-124 must be present in the same subcellular compartment to be able to interact. To determine whether they are both present at synapses, we prepared synaptosome fractions from mouse forebrain. The enrichment of synaptic terminals was

Figure 2-1. The GluA2 3' untranslated region (UTR) has a functional miR-124 target site.

(A) Schema showing the position of the fully complementary miR-124 target site at the 5' end of the GluA2 3' UTR. The seed region of miR-124 is shown in bold. Vertical bars depict Watson-Crick base pairs.

(B-D) Wild type and mutant reporter constructs were transfected into HEK293T cells with miR-124 mimics or mutant miR-124 mimics with two point mutations in the seed region (underlined). Luciferase activities are reported relative to reporter only controls.

(B) Transfection of the wild type reporter ("WT") with miR-124 resulted in robust knockdown of luciferase activity while transfection with mutant miR-124 did not. Significance determined by one-way analysis of variance (ANOVA) with Bonferroni correction.

(C) Transfection of miR-124 with a reporter lacking the miR-124 target site ("TD") did not reduce luciferase activity. ˆ site of deletion. Significance determined by two-tailed t-test.

(D) Transfection of a mutant reporter with two point mutations in the miR-124 target site ("PM") did not show knockdown by miR-124. Knockdown was restored when the mutant reporter was transfected with the complementary mutant miR-124. Significance determined by one-way ANOVA with Bonferroni correction. ***$p<0.001$; error bars show standard error of the mean (S.E.M.); N = 4 per group.

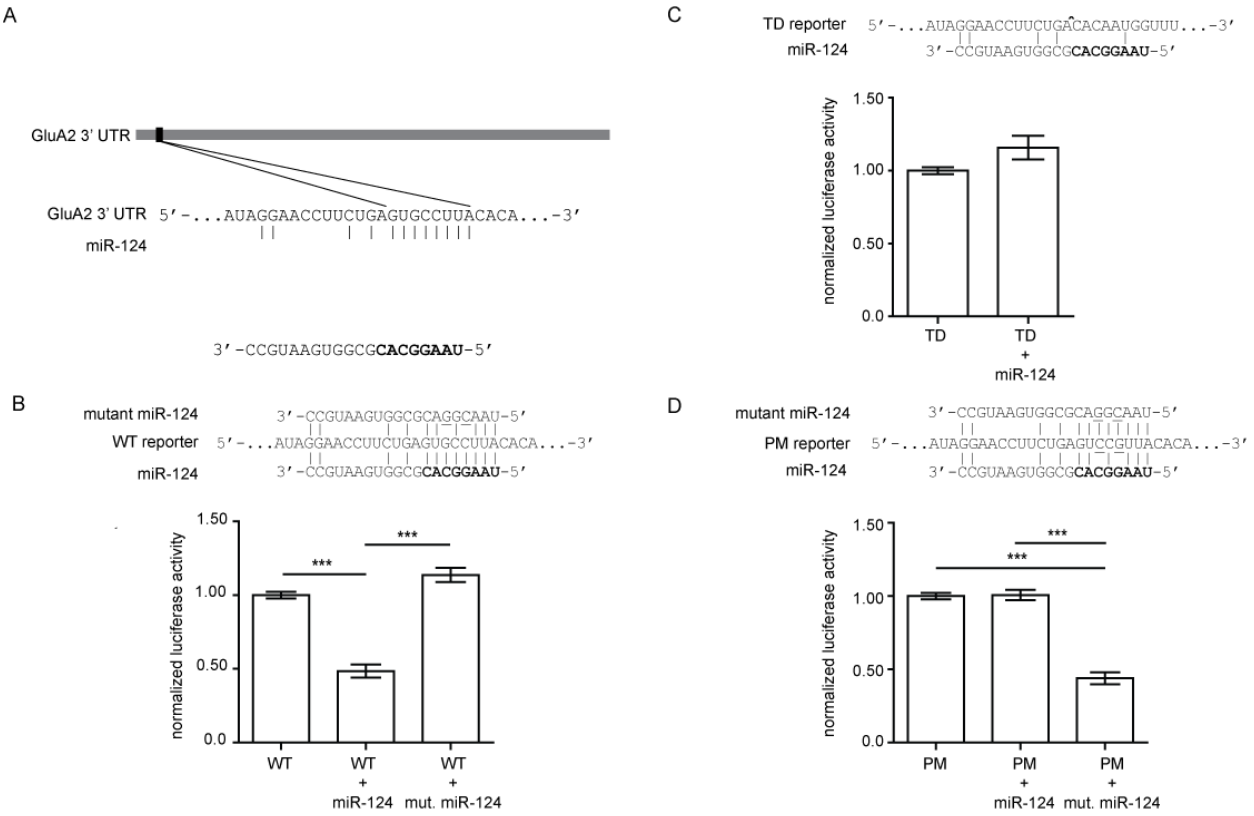
A
GluA2 3' UTR
GluA2 3' UTR 5′-...AUAGGAACCUUCUGAGUGCCUUACACA...-3′
miR-124
3′-CCGUAAGUGGCGCACGGAAU-5′
B
mutant miR-124 3′-CCGUAAGUGGCGCAGGCAAU-5′
WT reporter 5′-...AUAGGAACCUUCUGAGUGCCUUACACA...-3′
miR-124 3′-CCGUAAGUGGCGCACGGAAU-5′
normalized luciferase activity
1.50
1.00
0.50
0.0
***
***
WT
WT + miR-124
WT + mut. miR-124
C
TD reporter 5′-...AUAGGAACCUUCUGACACAAUGGUUU...-3′
miR-124 3′-CCGUAAGUGGCGCACGGAAU-5′
normalized luciferase activity
1.50
1.00
0.50
0.0
TD
TD + miR-124
D
mutant miR-124 3′-CCGUAAGUGGCGCAGGCAAU-5′
PM reporter 5′-...AUAGGAACCUUCUGAGUCCGUUACACA...-3′
miR-124 3′-CCGUAAGUGGCGCACGGAAU-5′
normalized luciferase activity
1.50
1.00
0.50
0.0
***
***
PM
PM + miR-124
PM + mut. miR-124

confirmed by western blotting for the post-synaptic scaffold protein, PSD-95 (Figure 2-2A). RNA was extracted and relative concentrations of GluA2 mRNA and mature miR-124 were measured by comparative RT-qPCR (Figure 2-2B). The synaptosome:total ratios for GluA2 mRNA and miR-124 were 0.14 and 1.52 respectively. To help put these ratios into context, we measured Camk2α mRNA (ratio = 0.90), which has been widely reported to be present in distal compartments [128-132]. We also measured miR-134 (ratio = 2.14) as a positive miRNA control for distal localization [133]. For a negative control, we chose Fads3 mRNA (ratio = 0.20), which has been reported to be somatically-restricted [116]. These results suggest that GluA2 mRNA is as de-enriched from synapses as Fads3 mRNA, and that miR-124 is more synaptically-enriched than Camk2α mRNA.

Since synaptosome preparations are subject to contamination by closely-associated glial components, we performed FISH on dissociated hippocampal cultures to complement these findings. FISH allows us to visualize the subcellular distribution patterns of GluA2 mRNA and miR-124 in individual cells. Again, Camk2α and Fads3 mRNA were used for comparison. Using the QuantiGene® (Affymetrix) detection system, all four RNAs appear as discrete puncta that are present at high concentrations in the cell body (Figure 2-3A).

The extent of dendritic localization varied greatly between genes and, to a lesser extent, between individual neurons and dendrites. Because of the variability between different neurons and dendrites, we imaged many neurons to determine the overall distribution pattern for each gene. In Figure 2-3B, we estimated the distance of a typical puncta from the center of the cell body. The mean distances for miR-124 and Camk2α mRNA were 33.27 μm (95% CI [31.64, 34.89]) and 33.46 μm (95% CI [32.36, 34.55]) respectively, placing them in the dendritic

Figure 2-2. miR-124 is enriched at synapses.

(A) Synaptosome fractions were prepared from adult forebrain. Western blotting shows enrichment for PSD-95 in the synaptosome fraction. 5 μg of total protein was loaded in each lane. (B) Comparative RT-qPCR on RNA extracted from total and synaptosome fractions of mouse forebrain. Error bars show 95% confidence intervals. N = 3 fractionations.

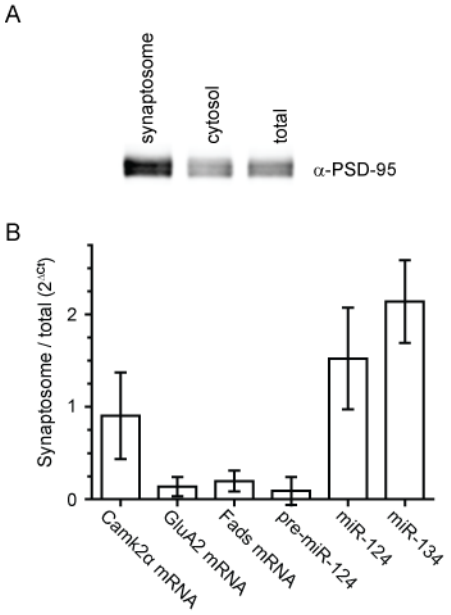

Figure 2-3. GluA2 mRNA and miR-124 have different distribution patterns.

(A) Representative fluorescence *in situ* hybridization (FISH) images of straightened dendrites. Top: red, FISH puncta; cyan, MAP2; blue, Hoechst. Bottom: FISH puncta in gray scale. Arrowheads show puncta positions in the non-proximal dendrite. Scale bar = 20 μm.

(B) Group data for average puncta distance from the center of the cell body. Error bars show 95% confidence intervals. Pairwise comparisons of each gene are reported in Figure 2-4C.

(C) Puncta were classified into three subcompartments and the percentage of puncta in each subcompartment is shown. Error bars show 95% confidence intervals. One-way ANOVA comparisons between genes are reported in Figure 2-4D.

(D) Table showing the absolute number of puncta per μm in each subcompartment, along with number of dendrites measured for each gene. Dendrites were imaged from 4 to 7 independent experiments.

A

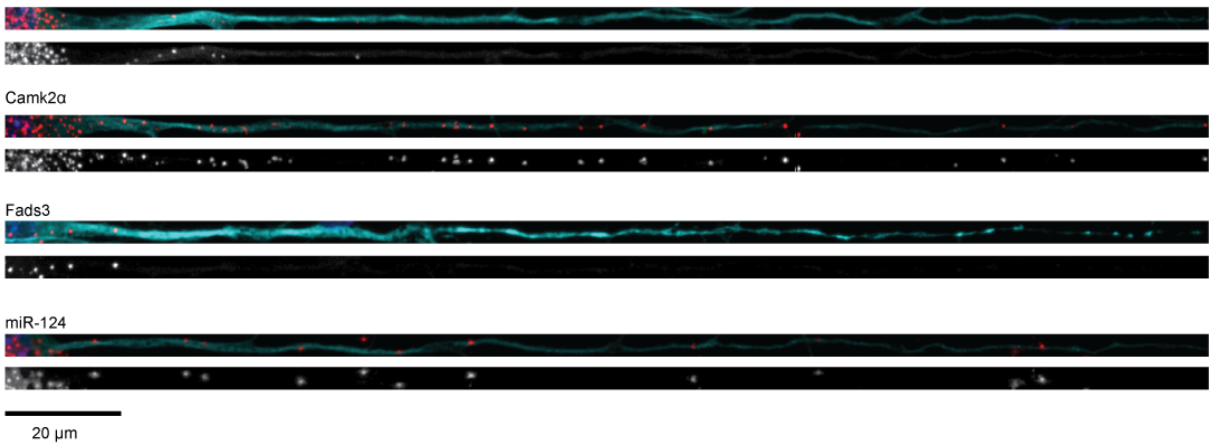

B

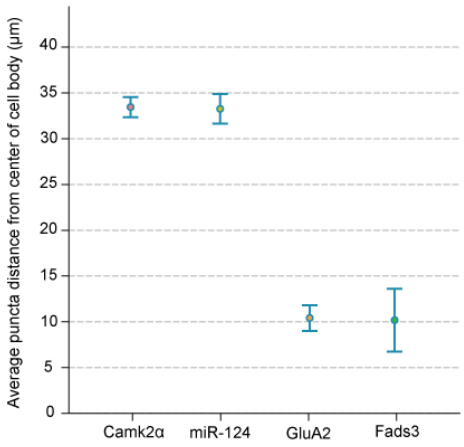

C

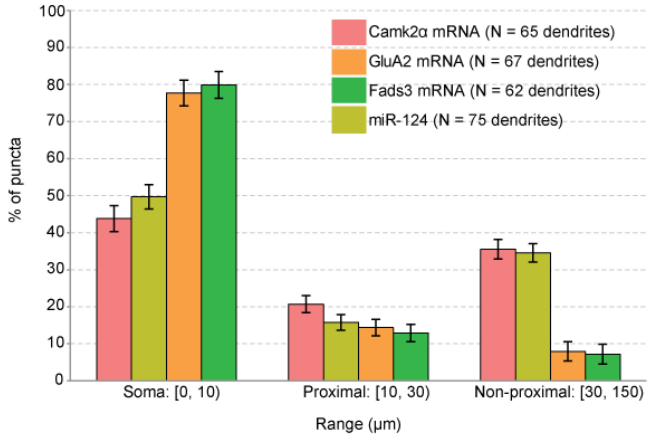

D

	Camk2α mRNA puncta/μm			GluA2 mRNA puncta/μm			Fads3 mRNA puncta/μm			miR-124 puncta/μm		
	Mean	**95%CI**	**N**	**Mean**	**95%CI**	**N**	**Mean**	**95%CI**	**N**	**Mean**	**95%CI**	**N**
Soma	2.797	0.209		2.810	0.179	67	0.689	0.081		1.269	0.130	
Proximal	0.774	0.120	65	0.295	0.063	67	0.066	0.019	62	0.226	0.041	75
Non-proximal	0.216	0.031		0.027	0.007	67	0.007	0.002		0.076	0.010	

subcompartment. The mean distances for GluA2 and Fads3 mRNA were 10.42 μm (95% CI [9.02, 11.82]) and 10.18 μm (95% CI [6.75, 13.62]) respectively, which lie in the cell body or proximal dendrite. Pairwise comparisons of the average distance between genes showed that there was sufficient evidence to distinguish between the location of miR-124 and GluA2 puncta, while there was insufficient evidence to distinguish between miR-124 and Camk2α puncta or GluA2 and Fads3 puncta locations (Figure 2-4C).

For further analysis, we divided the puncta into three subcompartments (cell body; proximal dendrite, up to 20 μm from cell body; and non-proximal dendrite, 20-140 μm from cell body), which were chosen based on the distribution patterns of the different RNAs (Figure 2-4A and B). We quantified the proportion of puncta in each subcompartment to account for differences in expression levels between the transcripts. The proportion of FISH puncta in the soma and non-proximal dendrites are shown in Figure 2-3C. This analysis reveals a significant difference in the somatic/dendritic distribution of miR-124 and GluA2 puncta, with no significant difference between the somatic/dendritic distribution of miR-124 and Camk2α (known to be dendritically localized) or between GluA2 and Fads3 (known to be somatically localized) (Figure 2-4D). The conclusion is that GluA2 is a predominantly somatically restricted mRNA, while miR-124 is present in somata and in dendrites.

We performed several controls to confirm that the FISH signals we observed were specific. The specificity of GluA2 and Fads3 probes were verified by hybridization with sense probes, which did not produce any signal (Figure 2-5A and D). The specificity of the miR-124 probe was verified by hybridization in the presence of a competitive inhibitor that has full complementarity to miR-124, which produced a marked reduction in signal (Figure 2-6C). In

Figure 2-4. Group data of puncta distribution.

(A) Fraction of puncta present in arbitrary bins. The 0-10 μm bin corresponds to the soma. Bins beyond 10 μm are in the dendrite. Error bars show standard deviation.

(B) Inverse cumulative distribution of puncta in arbitrary bins.

(C) Pairwise comparisons of average puncta distance shown in Figure 2-3B.

(D) Table to accompany Figure 2-3C. Left, fraction of puncta in each of the three subcompartments – soma, proximal, and non-proximal dendrites. Right, pairwise comparisons between genes in each subcompartment. Comparisons that are significantly different are in bold.

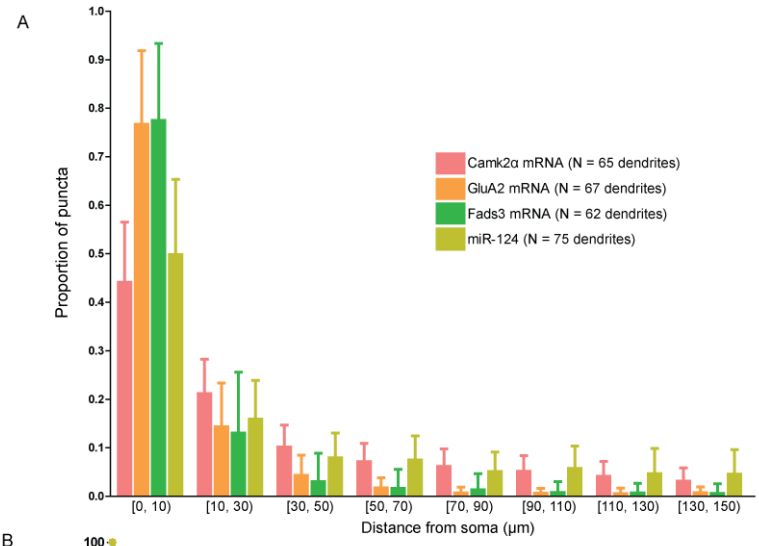

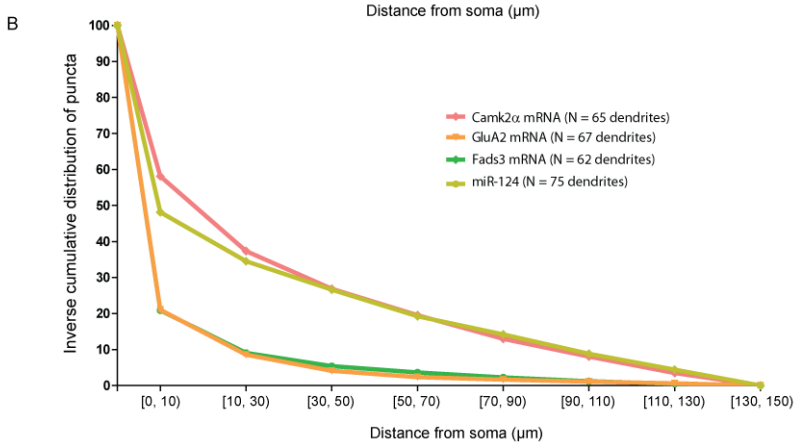

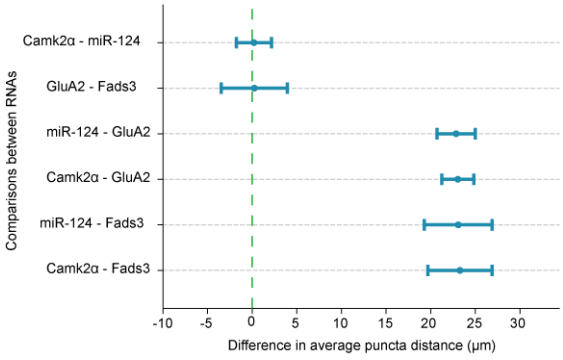

D

Mean Puncta Proportion Observed in Soma Range -- [0, 10) Microns

Gene	Proportion
Camk2α	0.438
Fads3	0.799
GluA2	0.777
miR124	0.497

Gene 1	Gene 2	Difference	95% CI Limits		Pr > |t|
Camk2α	**Fads3**	**-0.361**	**-0.411**	**-0.311**	**< 0.001**
Camk2α	**GluA2**	**-0.339**	**-0.388**	**-0.290**	**< 0.001**
Camk2α	**miR124**	**-0.059**	**-0.107**	**-0.011**	**0.016**
Fads3	GluA2	0.022	-0.028	0.072	0.384
Fads3	**miR124**	**0.302**	**0.254**	**0.351**	**< 0.001**
GluA2	**miR124**	**0.280**	**0.232**	**0.328**	**< 0.001**

Mean Puncta Proportion Observed in Proximal Range -- [10, 30) Microns

Gene	Proportion
Camk2α	0.207
Fads3	0.129
GluA2	0.144
miR124	0.158

Gene 1	Gene 2	Difference	95% CI Limits		Pr > |t|
Camk2α	**Fads3**	**0.078**	**0.045**	**0.111**	**< 0.001**
Camk2α	**GluA2**	**0.063**	**0.031**	**0.095**	**< 0.001**
Camk2α	**miR124**	**0.049**	**0.018**	**0.081**	**0.002**
Fads3	GluA2	-0.015	-0.047	0.018	0.373
Fads3	miR124	-0.029	-0.060	0.003	0.078
GluA2	miR124	-0.014	-0.045	0.017	0.384

Mean Puncta Proportion Observed in Non-proximal Range -- [30, 150) Microns

Gene	Proportion
Camk2α	0.355
Fads3	0.072
GluA2	0.079
miR124	0.346

Gene 1	Gene 2	Difference	95% CI Limits		Pr > |t|
Camk2α	**Fads3**	**0.283**	**0.245**	**0.321**	**< 0.001**
Camk2α	**GluA2**	**0.276**	**0.239**	**0.313**	**< 0.001**
Camk2α	miR124	0.010	-0.026	0.046	0.600
Fads3	GluA2	-0.007	-0.045	0.030	0.702
Fads3	**miR124**	**-0.274**	**-0.310**	**-0.237**	**< 0.001**
GluA2	**miR124**	**-0.266**	**-0.302**	**-0.231**	**< 0.001**

Mean Puncta Distance from Cell Body (in Microns)

Gene	Distance
Camk2α	33.457
Fads3	10.184
GluA2	10.419
miR124	33.265

Gene 1	Gene 2	Difference	95% CI Limits		Pr > |t|
Camk2α	**Fads3**	**23.273**	**19.672**	**26.875**	**< 0.001**
Camk2α	**GluA2**	**23.038**	**21.258**	**24.818**	**< 0.001**
Camk2α	miR124	0.192	-1.768	2.152	0.848
Fads3	GluA2	-0.235	-3.944	3.473	0.901
Fads3	**miR124**	**-23.081**	**-26.879**	**-19.284**	**< 0.001**
GluA2	**miR124**	**-22.846**	**-24.995**	**-20.697**	**< 0.001**

Figure 2-5. Controls for mRNA FISH.

(A) GluA2 sense probe does not bind non-specifically. Red, GluA2 mRNA sense probe; cyan, MAP2; blue, Hoechst. Scale bar = 20 μm.

(B) GluA2 antisense signal is absent from astrocytes. Red, GluA2 mRNA antisense probe; green, GFAP; cyan, MAP2; blue, Hoechst. Scale bar = 20 μm.

(C) Camk2α antisense signal is not in inhibitory neurons. Red, Camk2α mRNA; green, GAD67; cyan, MAP2; blue, Hoechst. Scale bar = 20 μm.

(D) Fads3 sense probe does not bind non-specifically. Scale bar = 20 μm.

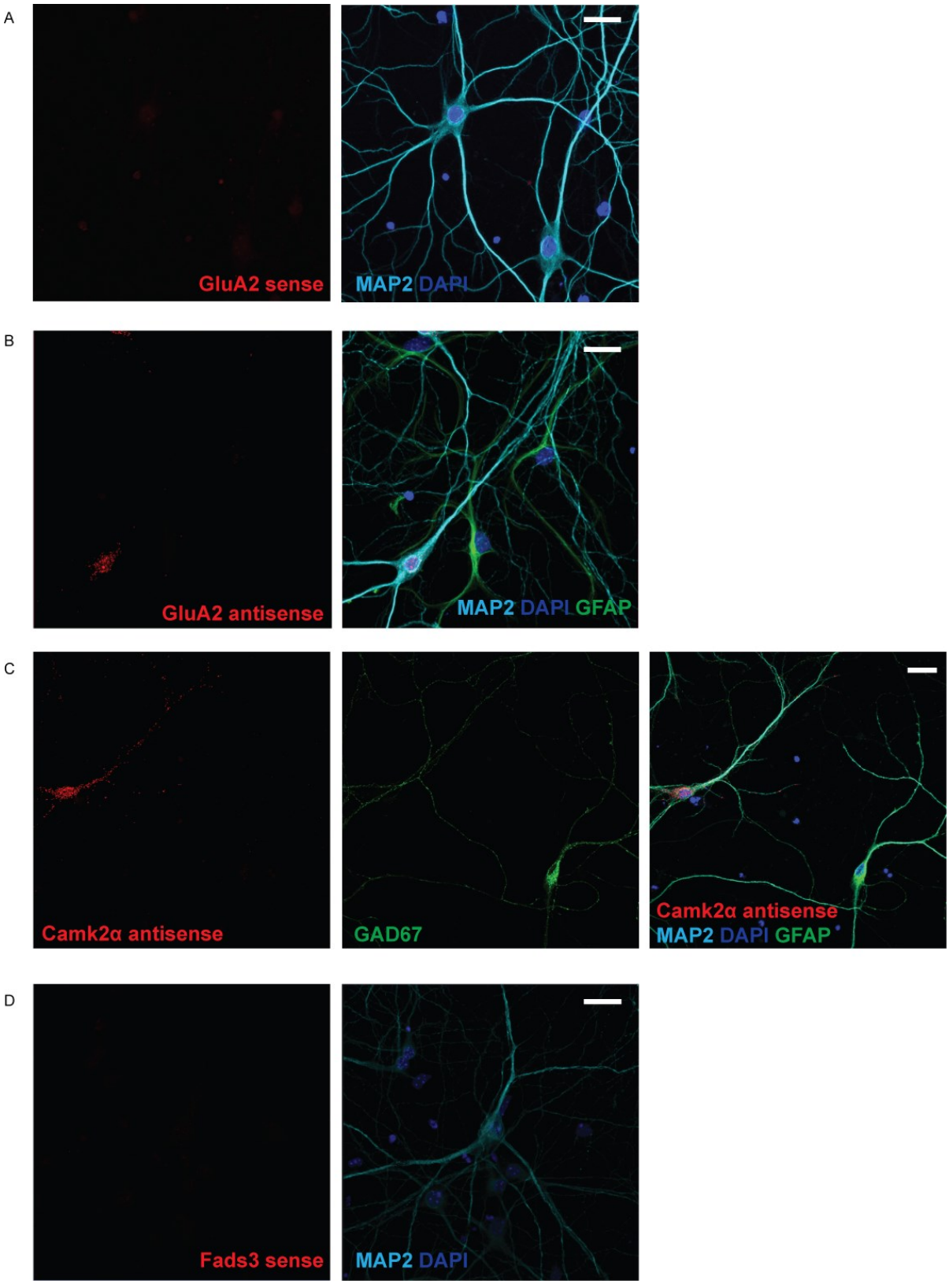
A
GluA2 sense
MAP2 DAPI
B
GluA2 antisense
MAP2 DAPI GFAP
C
Camk2α antisense
GAD67
Camk2α antisense
MAP2 DAPI GFAP
D
Fads3 sense
MAP2 DAPI

Figure 2-6. Controls for miR-124 FISH.

(A) The DapB negative control, which is not complementary to any miRNA sequences, does not bind non-specifically.

(B) miR-124 signal is absent from astrocytes. Red, miR-124, green, GFAP; cyan, MAP2; blue, Hoechst.

(C) miR-124 signal is drastically reduced in the presence of a competitive inhibitor at 10X concentration. The inhibitor is fully complementary to mature miR-124. Red, miR-124; green, GFAP; cyan, MAP2; blue, Hoechst. Scale bar = 20 μm.

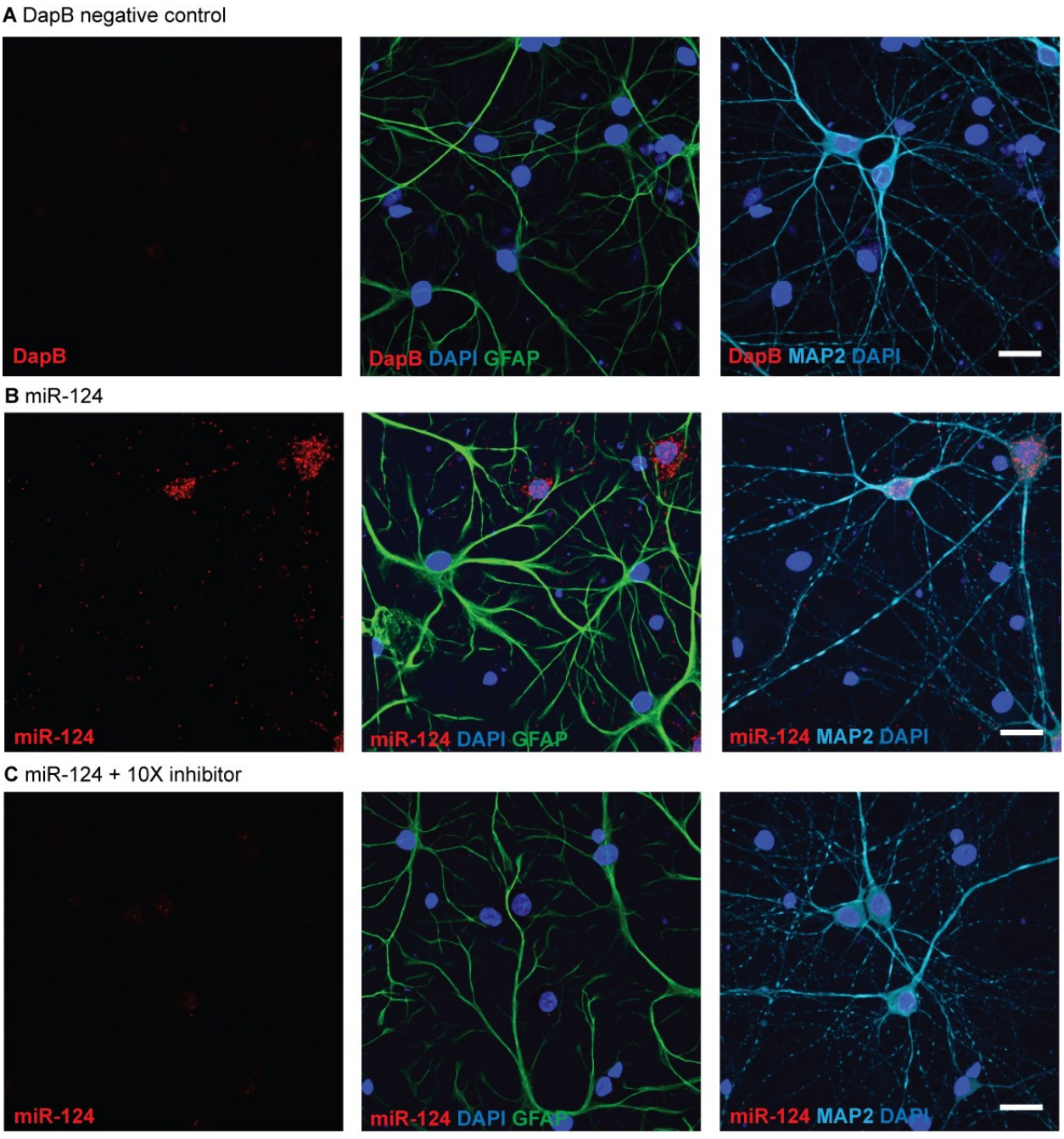
A DapB negative control
DapB
DapB DAPI GFAP
DapB MAP2 DAPI
B miR-124
miR-124
miR-124 DAPI GFAP
miR-124 MAP2 DAPI
C miR-124 + 10X inhibitor
miR-124
miR-124 DAPI GFAP
miR-124 MAP2 DAPI

addition, the DapB control probe for miRNA FISH did not produce any signal (Figure 2-6A). As yet another indication of probe specificity, both miR-124 and GluA2 antisense probes hybridize to MAP2 positive neurons and do not produce signal in GFAP positive astrocytes (Figure 2-5B and 6B). Finally, signal from the Camk2α antisense probe was absent from GAD67 positive inhibitory cells (which do not express Camk2α, Figure 2-5C). Taken together, these controls indicate that the FISH probes are highly specific.

Since miRNA FISH probes can recognize both mature and precursor miR-124 (pre-miR-124), we measured pre-miR-124 in synaptosome fractions. The RT-qPCR results show that pre-miR-124 is depleted from synaptosomes (ratio = 0.09), indicating that the miR-124 FISH signal in non-proximal dendrites is likely from mature miR-124 (Figure 2-2).

Since our findings contrasted with previous reports showing that GluA2 mRNA localized to dendrites, we asked whether activity altered the distribution pattern of miR-124 or GluA2 mRNA by silencing neuronal cultures with the sodium channel antagonist tetrodotoxin (TTX; 1 μM), or by stimulation with the $GABA_A$ receptor antagonist bicuculline (BIC; 40 μM), which drives glutamatergic transmission. Neither silencing nor stimulation altered the dendritic localization of GluA2 puncta at any time point examined (15 minutes, 1 hour, or 3 hours, Figure 2-7). As a positive control, we probed for cFos mRNA, an immediate early gene that is strongly induced by activity [134], which was absent in the TTX- treated cultures, but was highly expressed in the cell body of bicuculline-treated cultures.

2.3.3 The effects of overexpressing miR-124 levels on endogenous GluA2 levels

To test the effects of manipulating miR-124 levels on GluA2 expression in neurons, we transduced dissociated hippocampal cultures with lentivirus to overexpress either pre-miR-124

Figure 2-7. GluA2 FISH on cultures with different levels of activity.

(A) Cultures treated with tetrodotoxin (TTX; 1 μM) or with bicucullin (BIC; 40 μM) for 3 hours before processing for FISH. Red, GluA2 or c-Fos mRNA; cyan, MAP2; blue, Hoechst. Scale bar = 20 μm.

(B-D) Distribution of FISH puncta after activity treatments. Dissociated neurons were treated with TTX (1 μM) or BIC (40 μM) for (A) 15 min, (B) 1 hr, and (C) 3 hr. Results are plotted as an inverse cumulative distribution (i) and as proportions of puncta binned by cell compartment (ii). From each condition, 4 to 6 dendrites were quantified. Error bars show standard deviation. The distribution of miR-124 is included as a point of reference.

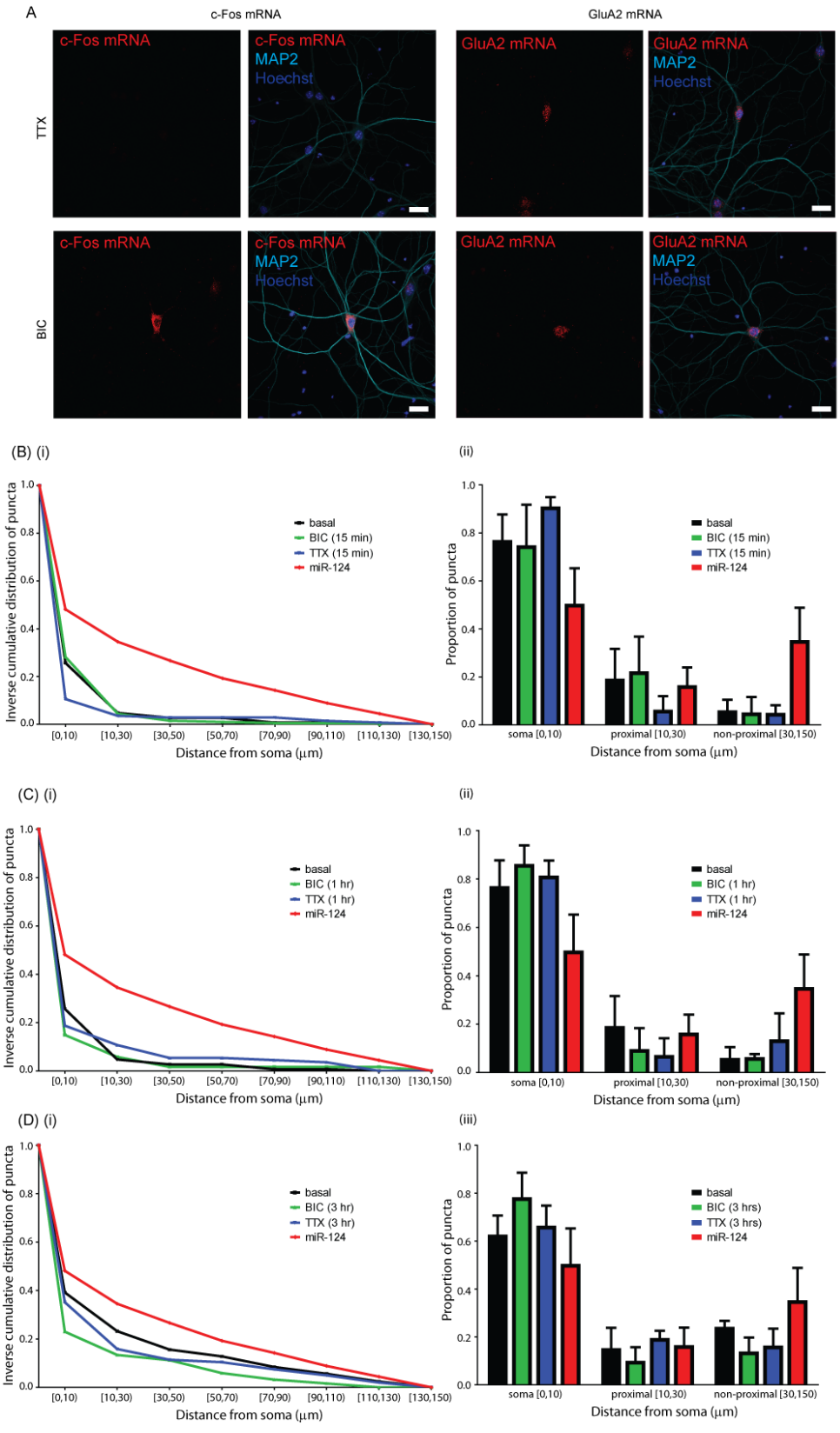
A
c-Fos mRNA
GluA2 mRNA
TTX
BIC
c-Fos mRNA
MAP2
Hoechst
GluA2 mRNA
(B) (i)
(ii)
(C) (i)
(ii)
(D) (i)
(iii)
Inverse cumulative distribution of puncta
Proportion of puncta
Distance from soma (μm)
basal
BIC (15 min)
TTX (15 min)
BIC (1 hr)
TTX (1 hr)
BIC (3 hr)
TTX (3 hr)
BIC (3 hrs)
TTX (3 hrs)
miR-124
[0,10)
[10,30)
[30,50)
[50,70)
[70,90)
[90,110)
[110,130)
[130,150)
soma [0,10)
proximal [10,30)
non-proximal [30,150)

(pMIRNA1-124), which is processed by the Dicer pathway into mature miR-124 [135], or a control with point mutations in the seed region similar to the mutant used in the luciferase assays (pMIRNA1-124P.M.) (Figure 2-8A). Co-expression of copGFP from the same vector indicated that transduction efficiency was high, with over 90% of neurons being transduced (Figure 2-8B). Transduction of the overexpression construct increased mature miR-124 expression by 3.2-fold while GluA2 mRNA levels were not significantly changed at 1.1-fold relative to control (Figure 2-8C). However, total GluA2 protein levels were reduced by 27% (Figure 2-8D), as determined by western blotting on whole cells lysates. This result indicates that miR-124 represses translation of endogenous GluA2 in a manner that is dependent on the seed region.

To complement this approach with experiments in which we reduced endogenous miR-124, we designed sponge constructs with bulged miR-124 binding sites in the 3' UTR of copGFP (sponge-124) as well as a previously published control sponge that does not recognize miRNAs (sponge-CXCR) (Figure 2-9) [136]. By having multiple miRNA binding sites, sponges are believed to divert miRNAs from binding their endogenous targets. However, when we transduced cultures with sponge-124, we noticed that the copGFP marker was almost exclusively expressed in non-neuronal cells and no change in GluA2 protein was observed (Figure 2-9C). Visual inspection of the cultures and Tuj1 immunoblotting did not indicate reduced neuronal viability (Figure 2-9). Instead, we suspect that the endogenous concentration of miR-124 was so high that it repressed copGFP expression and overwhelmed the transduced sponge-124. This possibility is supported by tests in HEK293T cells that show that increasing concentrations of miR-124 do repress copGFP expression from sponge-124 (data not shown). Of note, miR-124 is

Figure 2-8. miR-124 overexpression in dissociated cultures.

(A) Overexpression and control lentiviral constructs.

(B) Live images of transduced cultures taken before harvesting for protein or RNA. Co-expression of copGFP identifies transduced cells. Scale bar = 50 μm. DIC, differential interference contrast.

(C) Comparative RT-qPCR measurement of miR-124 and GluA2 mRNA fold changes in neurons transduced with pMIRNA1-124 relative to control. Error bars show S.E.M. N = 3 independent experiments.

(D) Western blot analysis of protein lysates from transduced cultures. Band intensities were quantified and normalized to Tuj1. The difference relative to control is shown below with standard error. N = 4 independent experiments.

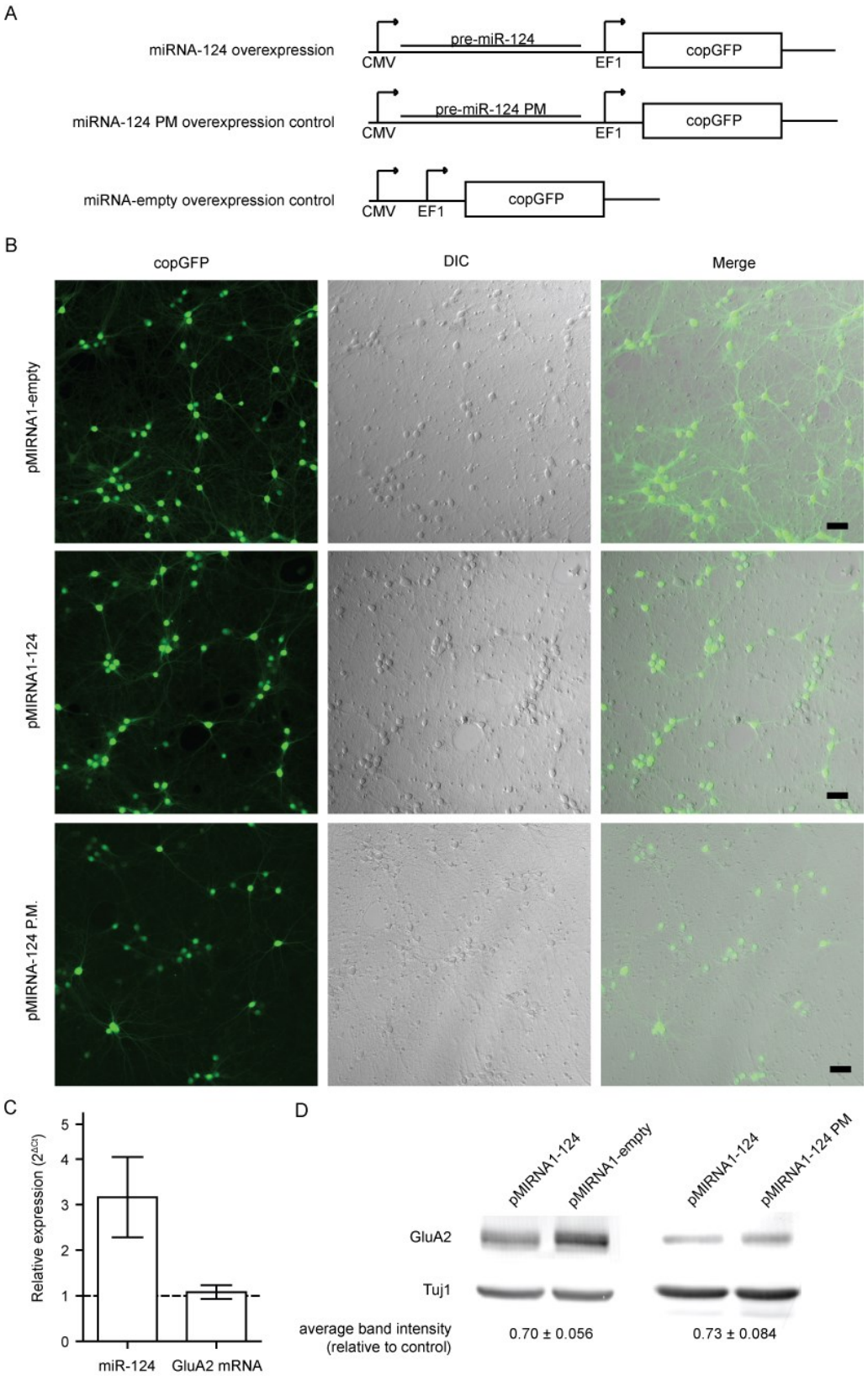
A
miRNA-124 overexpression
pre-miR-124
CMV
EF1
copGFP
miRNA-124 PM overexpression control
pre-miR-124 PM
CMV
EF1
copGFP
miRNA-empty overexpression control
CMV
EF1
copGFP
B
copGFP
DIC
Merge
pMIRNA1-empty
pMIRNA1-124
pMIRNA-124 P.M.
C
Relative expression (2^ΔCt)
0
1
2
3
4
5
miR-124
GluA2 mRNA
D
pMIRNA1-124
pMIRNA1-empty
pMIRNA1-124
pMIRNA1-124 PM
GluA2
Tuj1
average band intensity
(relative to control)
0.70 ± 0.056
0.73 ± 0.084

Figure 2-9. Sponge transduction in cultured neurons.

(A) Sponge-124 and control sponge-CXCR lentiviral constructs.

(B) Western blot analysis of protein lysates from transduced cultures. Band intensities were quantified and normalized to Tuj1. The difference relative to control is shown below with standard error. N = 4 independent experiments.

(C) Live images of transduced cultures taken before harvesting for protein. Co-expression of copGFP identifies transduced cells. Scale bar = 50 μm. Scale bar = 50 μm.

A

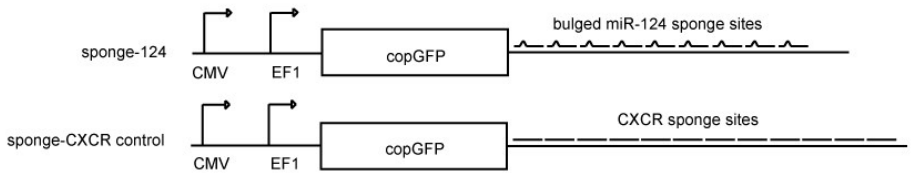
sponge-124
CMV
EF1
copGFP
bulged miR-124 sponge sites
sponge-CXCR control
CMV
EF1
copGFP
CXCR sponge sites

B

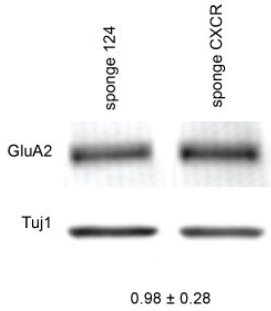
sponge 124
sponge CXCR
GluA2
Tuj1

0.98 ± 0.28

C

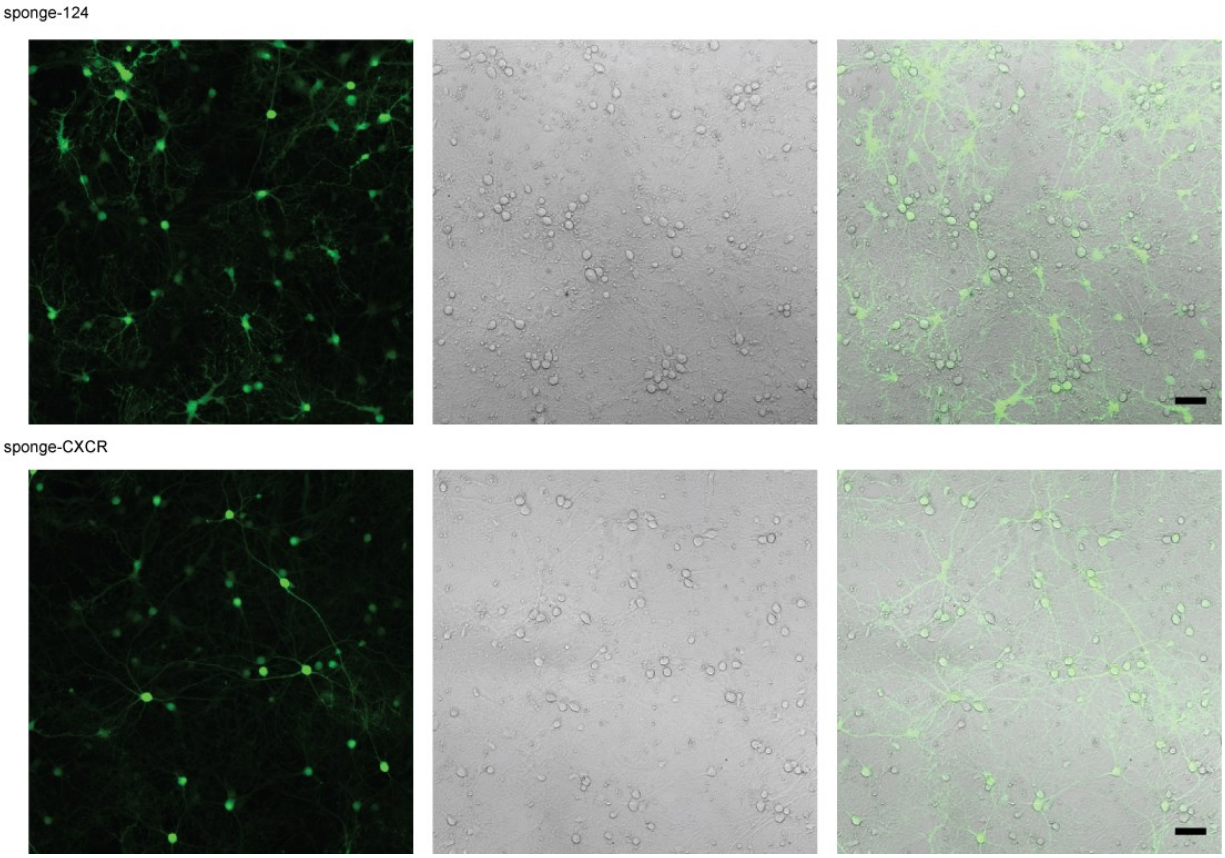
sponge-124
sponge-CXCR

the most abundant miRNA in the mouse brain [137]. As a result, we were not able to knockdown miR-124 in hippocampal neurons with our sponge-124 construct.

In addition to immunoblotting whole cell lysates, subcompartment-specific GluA2 expression was also measured using quantitative ICC. As with the FISH analysis, the cell body, proximal, and non-proximal dendritic regions were analyzed. GluA2 immunostaining was performed on permeabilized neurons to measure total GluA2 expression. Quantification of mean GluA2 signal intensity show that miR-124 overexpression significantly reduced GluA2 expression in all three regions of the neuron: the cell body, proximal, and non-proximal regions showed 33%, 30%, and 17% reductions in mean pixel intensity respectively (Figure 2-10A-C). The integrated intensity per cell body was also reduced by 33% (Figure 2-10Aiii). This observation is consistent with the immunoblotting results.

To measure synaptic GluA2 expression, GluA2 immunostaining was performed on nonpermeabilized neurons using an antibody that recognizes an extracellular N-terminal epitope. In the absence of permeabilization, only surface-expressed GluA2 proteins are labeled. Since functional synapses should have both pre- and post-synaptic compartments [138], we used antibodies against the pre-synaptic protein, synapsin I, to mark presynaptic compartments, and focused on GluA2 signals that were apposed to synapsin-immunoreactive puncta. Quantification of synaptic GluA2 puncta intensities did not reveal a significant difference between miR-124 overexpression and control (Figure 2-10D). Together, these data indicate that overexpression of miR-124 decreases the total expression of GluA2 but does not alter the concentration of GluA2 at synapses.

Figure 2-10. Overexpression of miR-124 downregulates cytoplasmic but not synaptic GluA2 protein levels.

(A-C) Measurement of total GluA2 protein expression by immunocytochemistry (ICC).

(A) GluA2 expression in the cell body. (i) Representative images of cell bodies of transduced neurons. Red/gray, GluA2 protein; green, copGFP. (ii) Mean GluA2 intensity per pixel. (iii) GluA2 intensity per cell body. (B) GluA2 expression in proximal dendrites (i) Representative images. Red/gray, GluA2 protein; cyan, MAP2 (ii) Mean GluA2 intensity per pixel.

(C) GluA2 expression in non-proximal dendrites (i) Representative images. Red/gray, GluA2 protein; cyan, MAP2 (ii) Mean GluA2 intensity per pixel. N = 5 independent experiments, 3 to 5 fields per experiment.

(D) Measurement of synaptic GluA2 protein expression by ICC. (i) Representative images of surface expressed GluA2. Red, GluA2; cyan, Synapsin. (ii) Fraction of Synapsin puncta that are within 8 pixels (1.248 μm) of GluA2 puncta. (iii) Integrated intensity of GluA2 puncta that are within 8 pixels of Synapsin puncta. N = 3 independent experiments, each with dendrites from 5 different neurons quantified. P values were determined by one-tailed *t*-tests. *P<0.05, **P<0.01, ***P<0.001. Error bars show S.E.M.

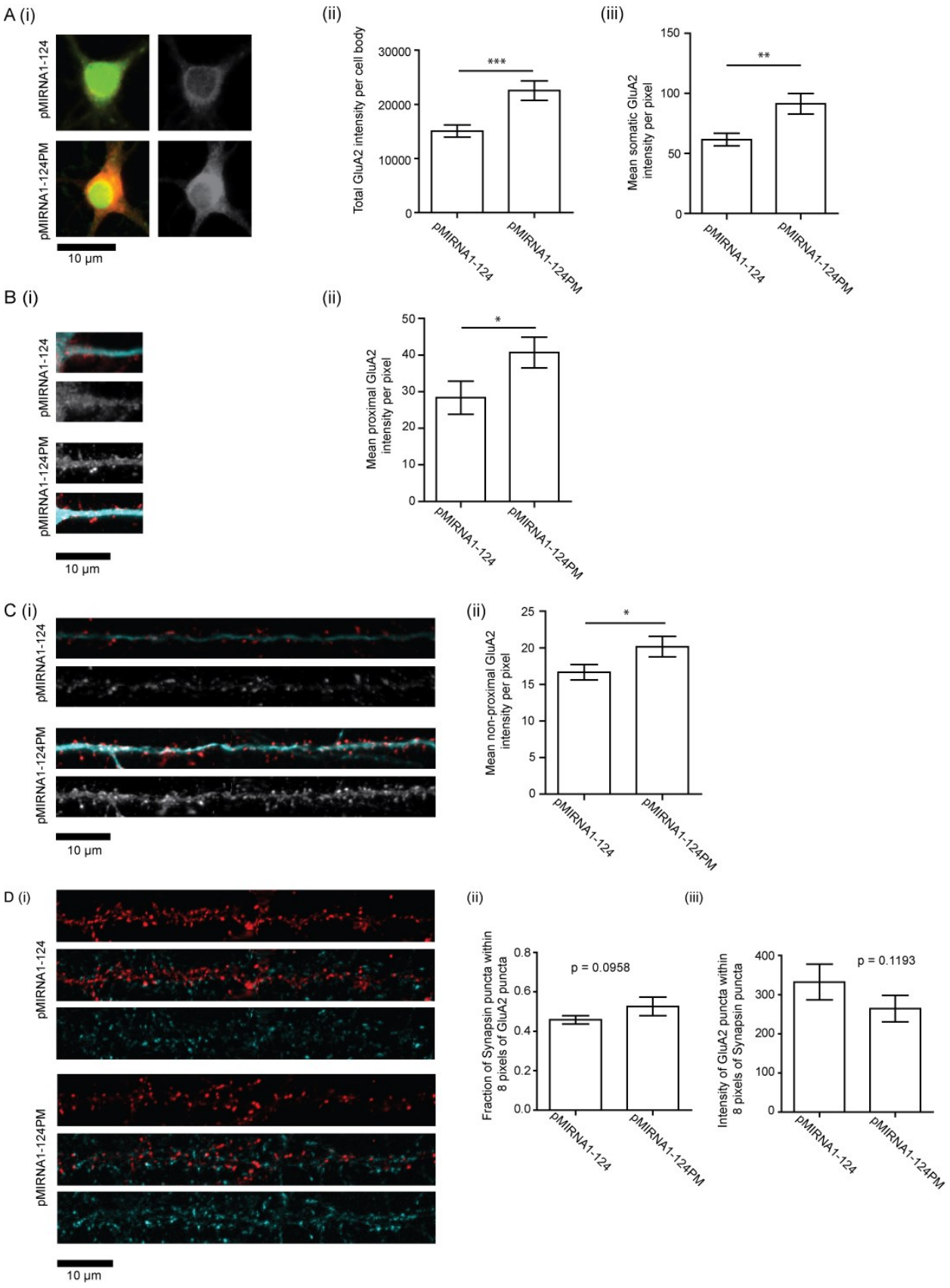
A (i)
pMIRNA1-124
pMIRNA1-124PM
10 µm
(ii)
Total GluA2 intensity per cell body
30000
20000
10000
0
***
pMIRNA1-124
pMIRNA1-124PM
(iii)
Mean somatic GluA2 intensity per pixel
150
100
50
0
**
pMIRNA1-124
pMIRNA1-124PM
B (i)
pMIRNA1-124
pMIRNA1-124PM
10 µm
(ii)
Mean proximal GluA2 intensity per pixel
50
40
30
20
10
0
*
pMIRNA1-124
pMIRNA1-124PM
C (i)
pMIRNA1-124
pMIRNA1-124PM
10 µm
(ii)
Mean non-proximal GluA2 intensity per pixel
25
20
15
10
5
0
*
pMIRNA1-124
pMIRNA1-124PM
D (i)
pMIRNA1-124
pMIRNA1-124PM
10 µm
(ii)
Fraction of Synapsin puncta within 8 pixels of GluA2 puncta
0.8
0.6
0.4
0.2
0.0
p = 0.0958
pMIRNA1-124
pMIRNA1-124PM
(iii)
Intensity of GluA2 puncta within 8 pixels of Synapsin puncta
400
300
200
100
0
p = 0.1193
pMIRNA1-124
pMIRNA1-124PM

2.4 Discussion

This study was aimed at determining whether and how miR-124 regulates translation of GluA2 in neurons. Computational identification of a conserved miR-124 site in the 3'UTR of GluA2 gave rise to the hypothesis that miR-124-mediated regulation of GluA2 could produce rapid changes in GluA2 expression. Since the GluA2 subunit is calcium-impermeable, such local changes would have important functional consequences on synaptic strength and connectivity. We were particularly intrigued by the possibility that local regulation could occur in dendrites given previous reports that GluA2 mRNA localized to dendrites [117], and that GluA2 underwent local, activity-dependent translation in dendrites [118].

As a first test of whether miR-124 might regulate GluA2 expression in dendrites, we asked whether both RNAs localized to dendrites and/or synapses. Our synaptosome RT-qPCR (Figure 2-2) and FISH (Figure 2-3) results showed that this was not the case: GluA2 transcripts were largely restricted to the cell body, while miR-124 was present in significant concentrations in dendrites. These observations suggest that miR-124 most likely regulates GluA2 transcripts in the cell body rather than in dendrites.

Our findings conflict with previous reports that GluA2 mRNA is dendritically localized and that miR-124 is somatically restricted in neurons [117,139]. Although we are confident about the specificity of the FISH probes we used (especially since both GluA2 signals were present in neurons but not in astrocytes), we did explore a number of explanations for the discrepancy between our results and previously published reports. To address whether the discrepancy might arise from technical differences in FISH methodologies, we used additional approaches for FISH, including digoxigenin-modified riboprobes for GluA2 FISH and locked

nucleic acid (LNA) for miR-124 FISH. GluA2 FISH using riboprobes did not reveal dendritic localization of GluA2 mRNA in cultured hippocampal neurons (data not shown), and the results using LNA probes to detect miR-124 were inconclusive, as the signal for the antisense LNA was not significantly different from the signal from the sense LNA (data not shown). In considering the lack of dendritic localization of GluA2 mRNA, it is possible that RNA binding proteins on some transcripts may block probe recognition and lead to underestimation of dendritic localization. However, we do not think this is likely as the QuantiGene mRNA probes used recognize 20 different regions on each transcript. Additionally, pre-treating the neurons with proteinase K to improve probe accessibility did not increase the number of transcripts detected (data not shown). A possible explanation for the lack of detection of miR-124 in dendrites in Kye et al. is that the locked nucleic acid probe used did not hybridize well with miR-124. This possibility is supported by the low level of miR-124 signal detected in the cell body, which was only slightly higher than their negative control. One would expect a much stronger signal, considering that miR-124 is the most abundant miRNA in the mouse brain [137]. Another possible source of the discrepancy between our results and those of Grooms et al. and Kye et al. is that their FISH experiments were performed on rat hippocampal neurons while we used mouse hippocampal neurons. Finally, we addressed the possibility that levels of activity regulate GluA2 and/or miR-124 localization in dendrites of cultured neurons by incubating cultures with TTX or bicuculline, but were not able to detect significant GluA2 signal in dendrites under any condition (Figure 2-7).

We next sought to evaluate dendritic localization of RNA in a manner that was independent of concentration, since differences in absolute RNA concentration might affect

measurements of RNA distribution. All RNAs are abundant in the cell body, where they are transcribed. However, by carefully quantifying the somatic signal, and directly comparing it to the signal in dendrites in the same cell, rather than saturating the somatic signal in order to detect signal in the dendrites, we were able to quantify and compare the proportion of FISH signal in three compartments: the soma, the proximal dendrite (0 to 20 μm from the soma) and the non-proximal dendrite (greater than 20 μm from the soma). These analyses revealed that Camk2α mRNA and miR-124 were significantly more dendritically-localized than either GluA2 or Fads3 mRNAs (Figure 3). Since we compared the proportion of each RNA, these differences are probably due to an RNA-specific mechanism and not just an effect of transcript or miRNA abundance. We hope that these methods and methods of analyses will provide a useful reference for future studies on transcript and miRNA localization in neurons.

Our luciferase assays and overexpression studies in neurons show that miR-124 downregulates GluA2 expression in a manner that is dependent on the seed sequence (Figures 2-1, 8 and 10). Overexpression of miR-124 in neurons reduces endogenous GluA2 protein levels without affecting mRNA levels, suggesting that miR-124 acts by repressing translation and not by degrading GluA2 target transcripts (Figure 2-8). While total protein levels are reduced, we did not detect a change in the concentration of GluA2 at synapses (Figure 2-10). It appears that at this modest level of downregulation (~30% by immunoblot), post-translational mechanisms exist to maintain normal levels of synaptic GluA2 expression. These mechanisms may include enhanced trafficking of GluA2-containing AMPARs, which is a well-studied mechanism of AMPAR regulation involving post-translational modifications and several interacting proteins [140-143]. Taken together, the colocalization of miR-124 and GluA2 localization in the cell

body but not in the dendrite, and the effects of overexpression of miR-124 on total but not synaptic GluA2 protein in neurons, are most consistent with a model in which the majority of GluA2 protein is synthesized in the soma and subsequently transported into dendrites and synapses [110-113].

Several previous studies have suggested that GluA2 is a likely candidate for post-transcriptional regulation. GluA2 translation following pilocarpine-induced status epilepticus has been shown to be regulated in a 3' UTR-dependent manner [144]. Furthermore, GluA2 mRNA immunoprecipitates with FMRP, a RISC component, and GluA2 translation following DHPG treatment is dysregulated in FMRP knock-out mice [145]. miR-124 has also been shown to found with FMRP in the mouse brain [146]. The work presented here further suggests a role for post-transcriptional regulation of GluA2 mRNA by miR-124, and indicates that majority of this interaction likely takes place in the cell body. Although miR-124 does not affect synaptic GluA2 expression by itself, there are several other predicted miRNA target sites its 3' UTR, including a validated interaction with miR-181. Saba et al. have found that transfection of a miR-181 duplex into hippocampal cultures reduces surface GluA2 puncta size [147]. Collectively, these findings indicate that the concentration of GluA2 in neurons and at synapses is fine-tuned by multiple mechanisms, some of which occur in the cell body and others of which occur locally at synapses. Our findings suggest that the local mechanisms do not involve local translation, but rather consist predominantly of post-translational processes.

2.5 Acknowledgements for this section

This section was adapted from a manuscript prepared for publication [148], and co-authored by Liane O. Dallalzadeh, Nestoras Karathanasis, Mehmet F. Keles, Sitaram Vangala, Tristan Grogan, Panyiota Poirazi, and Kelsey C. Martin.

3 Using high-throughput sequencing to identify gene expression changes during chemical long-term potentiation in acute slices

3.1 Introduction: activity dependent changes in gene expression

Neurons are highly polarized cells, extending many elaborate processes with numerous synaptic subcompartments. These subcompartments are capable of responding independently from one another to external stimuli. Furthermore, the responses can be long-lasting, in a manner that requires new transcription and translation [5]. These features impose unique challenges on the spatial regulation of gene expression, which the neuron employs a fascinating repertoire of mechanisms to fulfill.

Regulation of activity-dependent changes in gene expression occurs at both the transcriptional and translational level. A number of studies have found that neuronal stimulation induces profound changes in the transcriptome, including changes in transcript levels, splicing, and polyadenylation [127,149-152]. Neuronal activity can also affect protein synthesis by modifying translational regulators [153].

We use high-throughput RNA sequencing to survey changes in the transcriptome during a physiologically relevant model of learning – chemical long-term potentiation (chemLTP) in acute hippocampal slices. We will also sequence the polyribosome bound fraction of mRNAs to infer changes in the proteome. This approach will allow us to identify: (1) genes that are important for long-lasting changes in synaptic plasticity, and (2) general mechanisms that regulate gene expression during these changes.

3.1.1 Transcription

Maintenance of long-lasting changes in synaptic plasticity requires new gene expression and has been shown to be transcription and translation dependent. In a study of plasticity in acute rat hippocampal slices, Nguyen et al. found that application of transcriptional inhibitors during the induction of long-term potentiation blocks the persistence of this potentiation at 100 min [154]. This effect was observed with both actinomycin D and DRB, which inhibit transcription by intercalating DNA or by preventing transcriptional elongation respectively.

These observations suggest that neurons require new RNA synthesis in order to support the long-lasting enhancement of synaptic strength seen during LTP. The new RNAs probably serve a purpose beyond replenishing transcripts lost during basal turnover. Nguyen et al. [1994] found that blocking transcription after LTP induction does not affect potentiation in the time frame studied, indicating that temporarily halting the replenishment of transcripts does not measurably alter synaptic strength. Instead, the new RNA synthesis likely contributes to the pool of RNAs necessary to meet the new requirements for protein synthesis, suggesting that the new transcription occurring during LTP induction plays an integral role in its maintenance. The newly synthesized RNAs may also be noncoding and contribute important regulatory functions to establishing a long-lasting change in synaptic strength.

To change transcription, synaptic activity generates signals that travel long distances to the nucleus [68]. One way the signal travels is through the trafficking of soluble proteins. Studies have identified transcription factors and activators that are basally tethered at synaptic sites, and undergo translocation to the nucleus in a synapse- and stimulus-specific manner [69,155-157]. Once in the nucleus, they initiate transcriptional programs that are necessary for long-lasting responses. Neuronal stimulation can also affect chromatin structure [158,159]. However, only a

few of the necessary transcriptional products have been identified. Also, it is not understood how different external stimuli activate different transcriptional programs.

Genome-wide studies using microarrays have found that the transcriptome is altered by various forms of neuronal activity, including depolarization of cultured neurons [160], LTP induction in acute slices [161], and seizure induction in animals [162,163].

3.1.1.1 Promoter usage

Neuronal activity can modify gene expression by altering transcription factor function. Activity-dependent transcription factors have been identified by studying the proximal promoter regions of activity-induced genes. One well-characterized gene is c-Fos, which is induced by glutamatergic stimulation and by calcium influx during depolarization [164,165]. Mutational analysis of the c-Fos promoter region identified a cAMP response element (CRE)-like element that binds CRE binding protein (CREB) [166]. The c-Fos promoter region also contains a serum response element that mediates calcium-dependent transcription by interacting with the serum response factor [167]. In a different approach using transcriptome profiling, the transcription factor MEF2 was also found to play a role in the regulation of gene induction during depolarization [160]. The MEF2 family of transcription factors is also activated by calcium. However, while CREB is activated by both calcium and cAMP, MEF2D activation is antagonized by cAMP [168].

There are several reports of genes switching promoter usage with activity. The gene encoding BDNF expresses several different 5'UTR isoforms that result from alternative promoter usage. These isoforms have been found to be differentially upregulated after kainite-induced seizures in rat brain [169]. The mechanism underlying the switch has not been identified,

although may involve epigenetic modifications as incubation of C6 and N2A cell lines with DNA methyltransferase and histone deacetylase inhibitors differentially alters isoform expression [170]. The post synaptic density signaling protein, SynGAP, is another gene that shows activity-dependent alternative promoter usage, giving rise to isoforms with opposing effects on synaptic strength [171].

3.1.2 Co-transcriptional RNA processing

Neuronal activity also alters the processing of nascent RNA. Activity-dependent change in splicing is an active area of study and more recently there has been increasing interest in the closely related process of cleavage and polyadenylation.

3.1.2.1 Alternative splicing

Newly transcribed coding RNA (called "pre-mRNA") usually consists of several exons that are spliced together to form messenger RNA (mRNA). The exons may be "constitutive," meaning that they are always included in the fully processed mRNA, or they may be "alternative" and only included in mRNA sometimes. The inclusion or exclusion of alternative exons is called "alternative splicing", and increases transcript diversity and diversity in the encoded proteins. Recently, a study across tissue types in primates and mice found that the forebrain has the highest proportion of alternatively spliced exons [172], supporting the idea that neurons have a flexible gene expression program. Several activity-regulated alternative splicing events have been identified in genes that encode proteins with important roles in synaptic plasticity [151]. In many of these events, the switch in splicing has been found to be regulated by CaMKIV. One example is the big potassium (BK) channel, which is involved in repolarizing neurons after an action potential. Depolarization represses the inclusion of the STREX exon in BK transcripts

through an upstream CamKIV responsive RNA element, making the BK channels less sensitive excitable [173]. Activity also represses the alternative splicing of GluN1 in a CaMKIV-dependent manner [152].

Many splicing proteins participate in other aspects of RNA metabolism and can shuttle between the nucleus and cytoplasm [151]. In the cytoplasm, splicing factors function in polyadenylation, translation, and turnover [151].

3.1.2.2 Cleavage and polyadenylation

Another RNA processing event that occurs after transcription has begun and before it has terminated is cleavage and polyadenylation (CPA) (although strictly speaking, transcript termination and cleavage are coupled events). The site of CPA is important as it defines the boundaries of the 3' UTR (discussed in Section 1.1.4). There are several elements that influence where CPA occurs: (1) an AAUAAA sequence or variant that is 15-30 nt 5' to the CPA site, (2) a GU-rich downstream sequence element that is 0-20 nt 3' to the CPA site and not part of the final mRNA, (3) a U-rich upstream element that is 0-20 nt 5' to AAUAAA, and (4) the nucleotides at the actual site of CPA [174]. These *cis* elements, called the polyadenylation signal (PAS), recruit the cleavage and polyadenylation specificity factor (CPSF) and the cleavage stimulatory factor (CstF) with varying efficiency that is dependent upon the actual sequences present [174].

Genes often have several potential PASs and as a result, can produce transcripts with alternative 3' UTRs. High throughput sequencing of the 3' end of transcripts from various mouse tissues found that 79 % of genes have an alternative 3' UTR isoform [175], which is much higher than the 32 % previously identified by studying cDNA/EST databases and demonstrates why

known annotations cannot be completely relied on to study 3'UTRs [176]. In addition to the CPSF and CstF complexes, and increasing number of splicing factors have been implicated in the process of CPA (e.g. U1, U2AF65, ELAV, Nova, etc.) [177]. There are two main types of alternative 3'UTR isoforms: splicing independent or splicing dependent (Figure 3-1). The splicing independent type is most common and arises from use of different PASs within the same last exon [176]. These isoforms have the same coding sequence and share only part of their 3'UTRs. The longer isoform has an extended 3'UTR that may contain regulatory elements not present in the shorter isoform. Alternative isoforms of this type encode the same protein but undergo different post-transcriptional regulation. The splicing dependent alternative 3'UTR isoforms have different coding regions and hence produce different proteins. These proteins differ in their C-terminal and can have markedly different functions. Some or none of the 3'UTR sequence is shared between these isoforms.

The choice of which PAS to use is probably determined by an interplay between the splicing and CPA factors present and their levels of activity [178,179]. Interestingly, PAS selection is dynamically regulated in several cell types, including neurons. A well-studied example of a transcript that switches 3' UTRs is Homer1, which favors a shorter isoform upon many different types of neuronal stimulation, in a manner that may be mediated by the MAPK cascade [73,180-183]. The shorter isoform encodes a truncated protein that disrupts the interactions of full-length Homer1, leading to smaller and fewer dendritic spines [180]. In addition to Homer1, a previous study using microarrays and KCl depolarization of dissociated hippocampal cultures has identified 58 other genes that switch 3'UTRs with activity [160].

Figure 3-1. Types of alternative 3'UTRs.

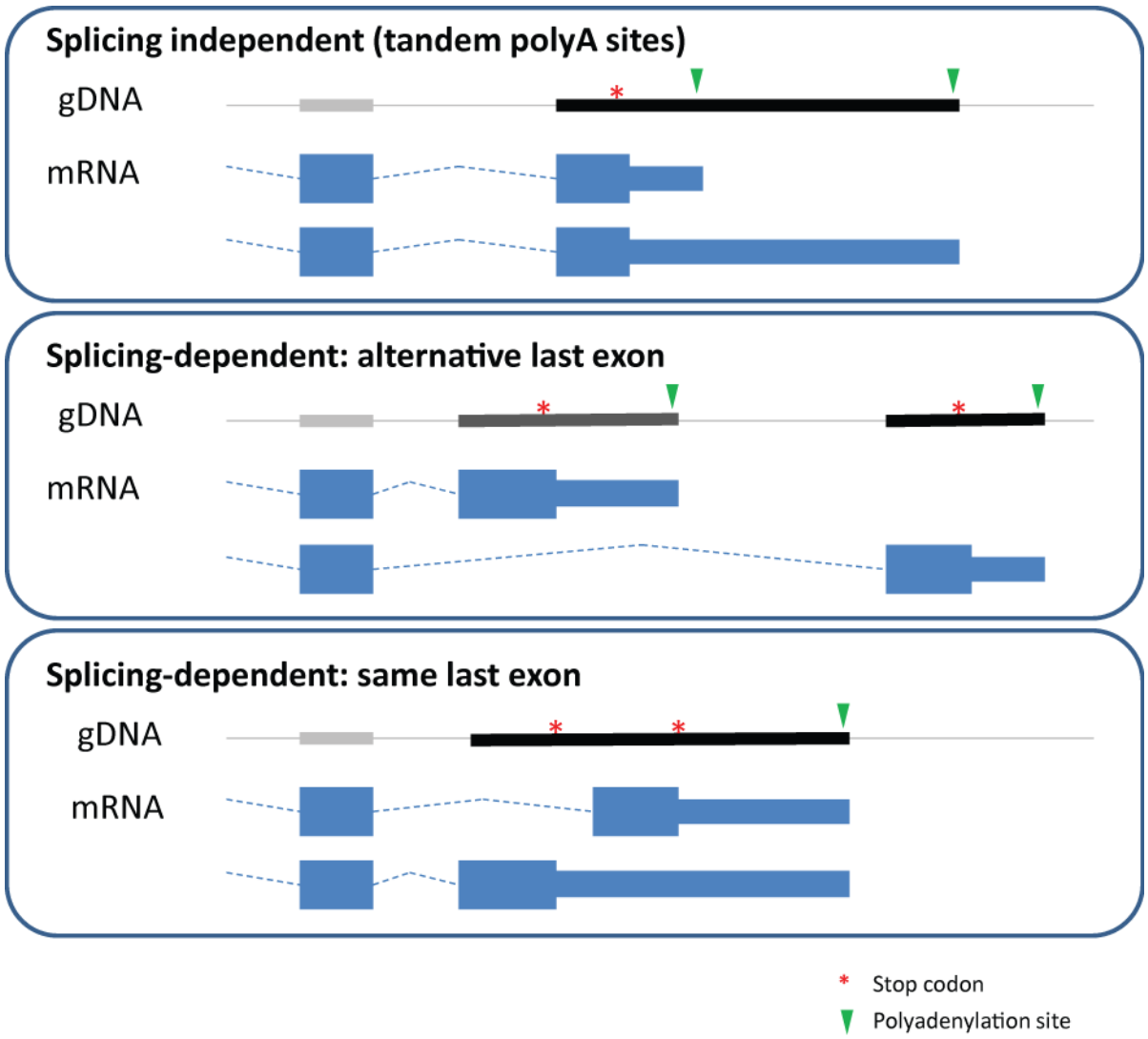

3.1.3 Post-transcriptional regulation

The 3'UTR contains *cis* regulatory elements that determine the post-transcriptional fate of mRNAs. The regulatory elements may alter transcript stability, localization, and translational efficiency, providing a flexible and diverse means for neurons to regulate gene expression. Transcripts from the brain have the longest 3'UTRs among different tissues [184], indicating an important role for post-transcriptional regulation in neurons. Brain 3'UTRs are 500 nt longer on average than Ensembl annotations and contain additional regulatory sequences, such as miRNA target sites [184].

In conjunction with having longer 3'UTRs with more *cis* regulatory sequences, the brain has also been found to express 323 of 380 putative RNA binding proteins (RNABPs), which may act as *trans* factors to determine the post-transcriptional fate of mRNAs [185]. It has been hypothesized that RNABPs coordinately regulate groups of genes involved in synaptic plasticity [186].

3.1.3.1 Regulation by miRNAs

MicroRNA array studies have shown that expression of many miRNAs is highly enriched in, or even restricted to, the brain [93]. Further, a large number of miRNAs have been detected in neuronal dendrites [139], and some have been found to be enriched at synapses[187]. Since they regulate gene expression post-transcriptionally and in a potentially reversible manner, miRNAs are well-suited to direct rapid changes that are restricted to subcellular compartments (e.g. by regulating local translation). Furthermore, miRNAs enable transcript-specific regulation and have even been found to selectively regulate different isoforms of the same gene [188].

Most miRNAs are transcribed by pol II as primary miRNA transcripts (pri-miRNA; ~1000 nt) that are capped and polyadenylated. Pri-miRNAs are processed in the nucleus by Drosha and DGCR8 into precursor miRNAs hairpins (pre-miRNA; ~70 nt) that are exported into the cytoplasm [189]. Pre-miRNAs are cleaved by Dicer into miRNA duplexes (~21 bp). Either strand of the duplex may be incorporated by RISC and function as a mature miRNA, although usually only one strand functions as a miRNA (the guide strand) while the other strand is degraded (the passenger or "*" strand) [189].

Mature miRNAs recognize targets by partial complementarity to sites in the 3' UTR of target transcripts. Target sites have also been found in the 5' UTR and coding regions of transcripts. The most important determinant of whether miRNA/mRNA interaction occurs is base paring between the target and the 2-8 nts at the 5' end of the miRNA (the "seed") [189].

Within RISC, miRNAs repress gene expression by either destabilizing the transcript or by repressing its translation. The exact mechanisms involved in repression are an area of active investigation. Destabilization most likely occurs by deadenylation of target transcripts, but may also occur through decapping. Both deadenylation and decapping make transcripts more prone to degradation by exonucleases. Also, the RISC component, Ago2, has RNAseH activity that is capable of endonucleolytically cleaving targets. *In vitro* assays have found that translational repression by miRNAs is dependent up on the 5' m^7G cap. Ago2 may compete with eIF4F binding to the cap and prevent circularization of the mRNA during translational initiation. Repression may also occur by preventing the recruitment of the 60S subunit. Translational repression can also occur post-initiation. This mode of regulation is supported by polysome fractionation studies that do not detect changes in the levels of target transcripts in polysome

fractions, and also by studies that find miRNAs present in these fractions. While the mechanism is not understood, it is speculated that premature termination is involved or that translational elongation may be slowed down. There have also been suggestions that miRNPs recruit proteases that degrade nascent polypeptides [189].

Several studies have taken a genome-wide approach to study the effects that miRNAs have on the ribosomal loading of their targets. In one set of studies, miRNA levels are manipulated and SILAC (stable isotope labeling with amino acids in cell culture) with quantitative mass spectrometry is used to measure changes in the resulting protein levels [190,191]. These studies found that miRNAs act mostly by degradation of target transcripts and less so by repressing translation [190]. They also found that miRNAs generally have modest effects on protein levels [190,191], and that protein level effects are more pronounced if the target transcripts are degraded [190]. One caveat of these studies is that the use of mass spectrometry limits analysis of translation to the most abundant proteins [192].

In another set of studies, ribosomally loaded transcripts are used as a proxy for translation. While not measuring protein levels directly may be seen as a shortcoming, it could also be an advantage. The dynamics of protein and mRNA turnover are very different, making the two difficult to compare directly. The use of ribosomally loaded transcripts allows the comparison of two populations of mRNA, which is a more straightforward comparison with fewer confounding factors. Hendrickson et al. [2009] overexpressed miR-124 in HEK293T cells and then used polysome fractionation and microarrays to determine the ribosome occupancy (percent of transcript with ribosomes) and density (number of ribosomes per transcript) of target transcripts. They found that miR-124 acts to both decrease target levels as well as decrease the ribosomal

occupancy and density of targets. In another study, Guo et al. [2010] overexpressed different miRNAs in HeLa cells and used ribosomal footprinting and RNAseq to determine translational efficiency of targets. They found that transcript destabilization mostly accounts for the decrease in gene expression and that translational efficiency played a smaller role. These studies and others demonstrate that the mechanisms underlying miRNA regulation are complex and cannot be easily generalized.

Currently, the prevalent view is that both translational inhibition and transcript destabilization occur during miRNA regulation, and that the two processes are coupled [122]. The genome-wide studies described above have focused on steady state transcript and protein levels. Greater insight into the dynamics of miRNA regulation may be obtained by measuring transcript and protein levels at different time points. Also, the studies described above use chronic overexpression or knockdown of miRNAs. It will be interesting to see what acute, physiological changes in miRNA levels have on target translation, which is one of the areas of investigation of this study.

3.1.3.2 Stabilization by RNA binding proteins

RNA turnover is determined by an interplay between stabilization and destabilization. Sequences in the 3'UTR (*cis* elements) interact with *trans*-acting RNA binding proteins (RNABPs; e.g Hu proteins, hnRNPs) to enhance or decrease transcript stability [195].

3.1.3.3 Transcript localization

mRNA localization and local translation provide a means of spatially-restricting gene expression. Localization elements are most often found in the 3'UTR [74], and genes with

alternative 3'UTR isoforms may show different degrees of dendritic localization (e.g. importin b1 [196], BDNF [197]).

3.1.4 Translational regulation

In addition to new transcription, new translation is also required for long-term memory. The modification of translation factors and signaling pathways involved in translation can alter long-term memory formation [83,198,199]. For instance, the phosphorylation status of eIF2α can enhance or disrupt LTP [83]. Also, the mTOR signaling pathway regulates translation through phosphorylation of 4E-BPs and S6Ks, and activation of this pathway suppresses changes in synaptic strength [199].

Genetic mutations of translational regulators have been found in several monogenic causes of autism spectrum disorders [200-202]. One notable example is the fragile X mental retardation protein (FMRP). FMRP is an RNA binding protein that associates with a subset of mRNAs (i.e. those containing a G-quartet or kissing complex [203,204]) to regulate translation [92,205,206], transport [207], and degradation [208]. It associates with polysomes in the brain to repress translation, and this regulation is believed to occur at synapses and with transcripts encoding synaptic proteins [205,206].

3.1.4.1 Cis-regulatory elements influencing translational efficiency

There are several genes that are translated in a LTP/LTD-dependent manner (e.g. Camk2a, PKM, Arc, Map1b). However, not much is known about how these specific transcripts come to more actively translated. One *cis* regulatory element that has been identified in transcripts that are translated during long term memory is the 5' terminal oligopyrimidine tract (5'TOP) [209]. Interestingly, 5'TOP mRNAs have been found to be distally localized in mouse

and Aplysia neurons [210,211]. Another *cis* regulatory element that plays a role during activity-dependent translation is the cytoplasmic polyadenylation element (CPE) (see Section 3.1.4.2) [84].

As a demonstration of the importance of *cis* elements in regulating translation during synaptic plasticity, studies have found that alternative 3'UTR isoforms confer different translational efficiencies upon the same coding sequence. For instance, BDNF has two tandem 3'UTR isoforms that encode the same protein, but the longer 3'UTR contains regulatory sequences that are absent in the shorter 3'UTR. Translation of the longer 3'UTR is repressed under basal conditions, and this repression is alleviated by activity [212]. A similar observation has been made for GluA2, which also has short and long 3'UTR isoforms that are differentially translated upon activity [144].

3.1.4.2 Polyadenylation affecting translation

Most mRNAs acquire a long polyA tail (~200 -250 nucleotides) after cleavage and polyadenylation in the nucleus. In the cytoplasm, CPE-containing mRNAs interact with the CPE binding protein (CPEB), which dynamically regulates polyA tail length [84]. CPEB has many interacting partners. One of them is polyA ribonuclease (PARN), which shortens the polyA tail of CPE-containing mRNAs to ~20-40 nt. Phosphorylation of CPEB disrupts the interaction with PARN, and allows the polyA polymerase, germ-line-development factor 2 (Gld2), to lengthen the polyA tail [84,213]. Polyadenylation requires two *cis* elements in the 3'UTR: the hexanucleotide AAUAAA and the CPE (UUUUUAU and variants) [214]. PolyA binding proteins (PABP) bind along the lengthened tail to help initiate translation by recruiting eIF4G to eIF4E, which then recruits the 40S ribosomal subunit. PolyA tail length correlates with

ribosomal density (the number of ribosomes on a transcript) and consequently, how actively a transcript is translated [215]. Hence, CPEB regulates translation of a subset of mRNAs by altering the length of the polyA tail. (PolyA tail length does not correlate with mRNA decay rates, although deadenylation is required for decay [215,216])

In neurons, CPEB has been detected at synapses and is phosphorylated in an activity-dependent manner [85,213,217]. NMDAR activation leads to the phosphorylation of CPEB by Aurora kinase, and is correlated with an increase in the polyadenylation of Camk2α transcripts [217]. Visual stimulation of rats also leads to the polyadenylation and translation of Camk2α [85]. Studies using injected *Xenopus* oocytes have found that the polyadenylation of Camk2α is dependent upon the two CPEs in the Camk2α 3'UTR [85]. CPEB phosphorylation is also increased by Camk2α [218].

3.1.5 Our experimental paradigm

Long term potentiation (LTP) is a long-lasting form of synaptic plasticity that occurs between many types of synapses. It has been particularly well-characterized for the CA3-CA1 synaptic connections of the Schaffer collateral pathway in the rodent hippocampus (Figure 1-3). Late-phase LTP (L-LTP) at the CA3-CA1 synapses is transcription and translation-dependent, and also requires activation of NMDA receptors.

3.1.5.1 Acute hippocampal slices

We are interested in studying the synaptic connections between neurons, and have chosen an experimental model in which normal synaptic contacts are preserved. Furthermore, the neighboring, non-neuronal cells (i.e. glia) in acute slices also retain their native positions. However, it should be noted that since acute slices are an *ex vivo* preparation, the longer range

connections and neuromodulatory factors are naturally lost. By performing our study in acute slices, our results can hopefully be generalized to processes that occur in the brain. Although working with tissue brings greater physiological relevance to our study, the presence of multiple cell types causes reduced sensitivity to detect events that occur only in a subpopulation of cells.

3.1.5.2 Chemical LTP

In choosing a stimulation protocol to use, our main criteria were that (1) the synaptic effect produced is long-lasting and requires new transcription, (2) majority of the cells are affected, and (3) the signaling pathways involved are physiologically pertinent. Chemical LTP (chemLTP) meets these criteria. The potentiation produced by chemLTP lasts for at least 3 hours and is transcription dependent [219]. During chemLTP, the entire slice is bathed in the treatment solution, inducing potentiation at a maximum number of synapses. This is in contrast to the more traditional way of inducing LTP with electrical stimulation, which only affects a subset of synapses. Finally, chemLTP produces potentiation by activating the cAMP-PKA and CamK2α pathways [219], both of which are important for learning and memory in animals [220-222].

We would like to focus on transcriptional events that are specifically required for the establishment of long-lasting changes in synaptic strength, and have chosen to study chemically-induced LTP (chemLTP) in acute hippocampal slices as our experimental paradigm [219]. Since the potentiation achieved with this stimulation is long-lasting and transcription and translation dependent, the transcriptional changes induced should include the subset specifically required for long-term plasticity. With the chemLTP paradigm, we hope to identify the population of transcripts relevant to the maintenance of long-lasting forms of plasticity and also elucidate general mechanisms that come into play to regulate gene expression.

3.2 Methods

3.2.1 Sample preparation and sequencing

See Table 3-1.

3.2.1.1 Preparation of acute slices

Acute slices were prepared from 2-3 month old male C57BL/6 mice. Mice were first anesthetized with isofluorane and then sacrificed by cervical dislocation. The hippocampus was quickly isolated on ice, and then cut into 500 um slices with a tissue chopper. The slices were trimmed to remove the dentate gyrus, and then transferred to interface chambers where they were recovered at 30 ^{o}C with continuous ACSF perfusion. Unlike the CA1 and CA3 cell body layers that contain mostly pyramidal cells, the dentate gyrus has mostly granule cell bodies and is removed to reduce cell heterogeneity. Furthermore, the mossy fiber connections between the dentate gyrus and CA3 undergo a form of LTP that is not dependent on NMDARs [223]. The CA3 is retained as bursting from CA3 cells is required for chemLTP in the CA1 [219]. Furthermore, the CA3 region has recurrent collaterals that should undergo chemLTP with mechanisms similar to the CA1 neurons [224-228].

3.2.1.2 Elevated potassium treatment

Slices were recovered for two hours and treated with elevated potassium (8.4 mM KCl) for 40 minutes. The slices were collected by quick freezing on dry ice 3 hours after washout of the treatment solution. Untreated, time-matched controls were also collected.

3.2.1.3 ChemLTP, forskolin, and chemLTP with APV treatments

After two hour recovery periods, slices in separate chambers were treated with either DMSO only, the chemLTP cocktail, forskolin only, or the chemLTP cocktail with APV (see

Appendix, Protocol 2). The slices were collected by quick freezing on dry ice 3 hours after treatment. The experiment was performed three times. Two mice were used for each replicate, and yielded a total of 20-24 slices (5 or 6 slices per condition). For the pilot experiment, the same protocol was used except slices were recovered for 3 hours, only the control and chemLTP treatments were performed, and 10 mice were used for 10 replicates that were pooled.

3.2.1.4 RNA extraction

Frozen slices were transferred to a glass 0.2 mL micro grinder and homogenized in Qiazol. RNA was then extracted with the Qiagen microRNeasy kit, which is suitable for both mRNA and small RNAs. About 2.5 µg of total RNA can be recovered from 5-6 slices.

3.2.1.5 Library preparation

Libraries for regular RNA sequencing were prepared with the Illumina TruSeq Stranded Total RNA sample prep kit with RiboZero to remove ribosomal RNA. For each library, 1.1 µg of total RNA was used. Stranded libraries preserve the directionality of the fragments so that the sequencing reads can be unequivocally aligned to one strand of DNA (Figure 3-2). Libraries prepared with random hexamers usually have low coverage at the ends of transcripts because of an inherently reduced number of priming positions (Figure 3-3). Coverage at the very 3' end of transcripts is also low because for fragments to cover this region, reverse transcription should start in the polyA tail. In a truly random mix of hexamers, only 1/4096 hexamers can generate fragments that begin in the polyA tail. To enrich for reads at the 3' end, the reverse transcription step was spiked with dT_6 oligos to try increase priming events in the polyA tail. However, this did not seem to improve 3'UTR coverage (Figure 3-4). Libraries were multiplexed and sequenced with 50 bp paired-end reads.

Figure 3-2. Comparison between stranded and unstranded libraries.

(A) Stranded libraries preserve the directionality of the reads. The dUTP method of library preparation is depicted here [229].

(B) Unstranded libraries loose information about which strand of DNA the RNA was transcribed from.

A

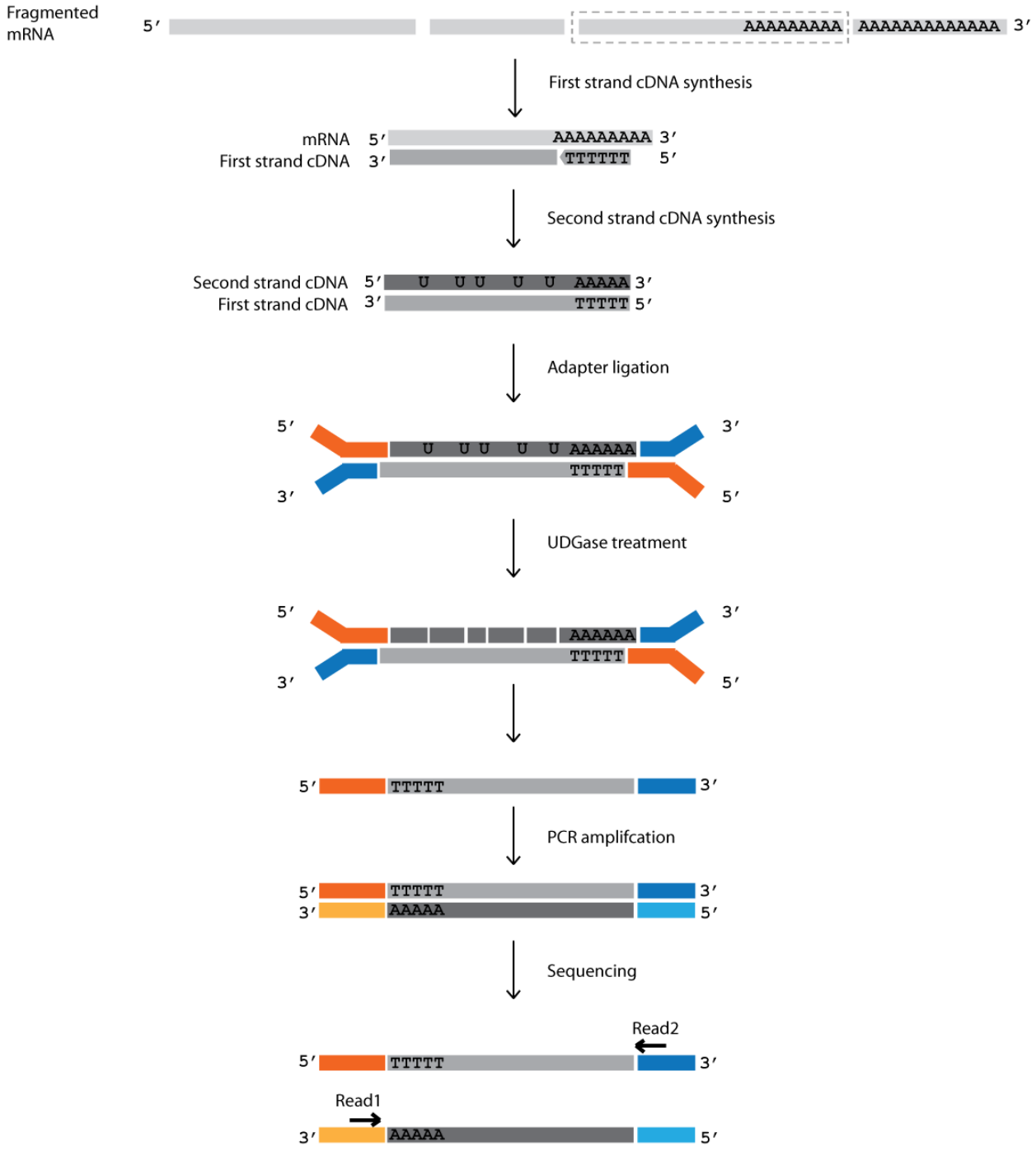
Fragmented mRNA
5′
AAAAAAAAA
AAAAAAAAAAAAA
3′
First strand cDNA synthesis
mRNA 5′ AAAAAAAAA 3′
First strand cDNA 3′ TTTTTT 5′
Second strand cDNA synthesis
Second strand cDNA 5′ U U U U U AAAAA 3′
First strand cDNA 3′ TTTTT 5′
Adapter ligation
5′ U U U U U AAAAA 3′
TTTTT
3′ 5′
UDGase treatment
5′ AAAAA 3′
TTTTT
3′ 5′
5′ TTTTT 3′
PCR amplifcation
5′ TTTTT 3′
3′ AAAAA 5′
Sequencing
Read2
5′ TTTTT 3′
Read1
3′ AAAAA 5′

B

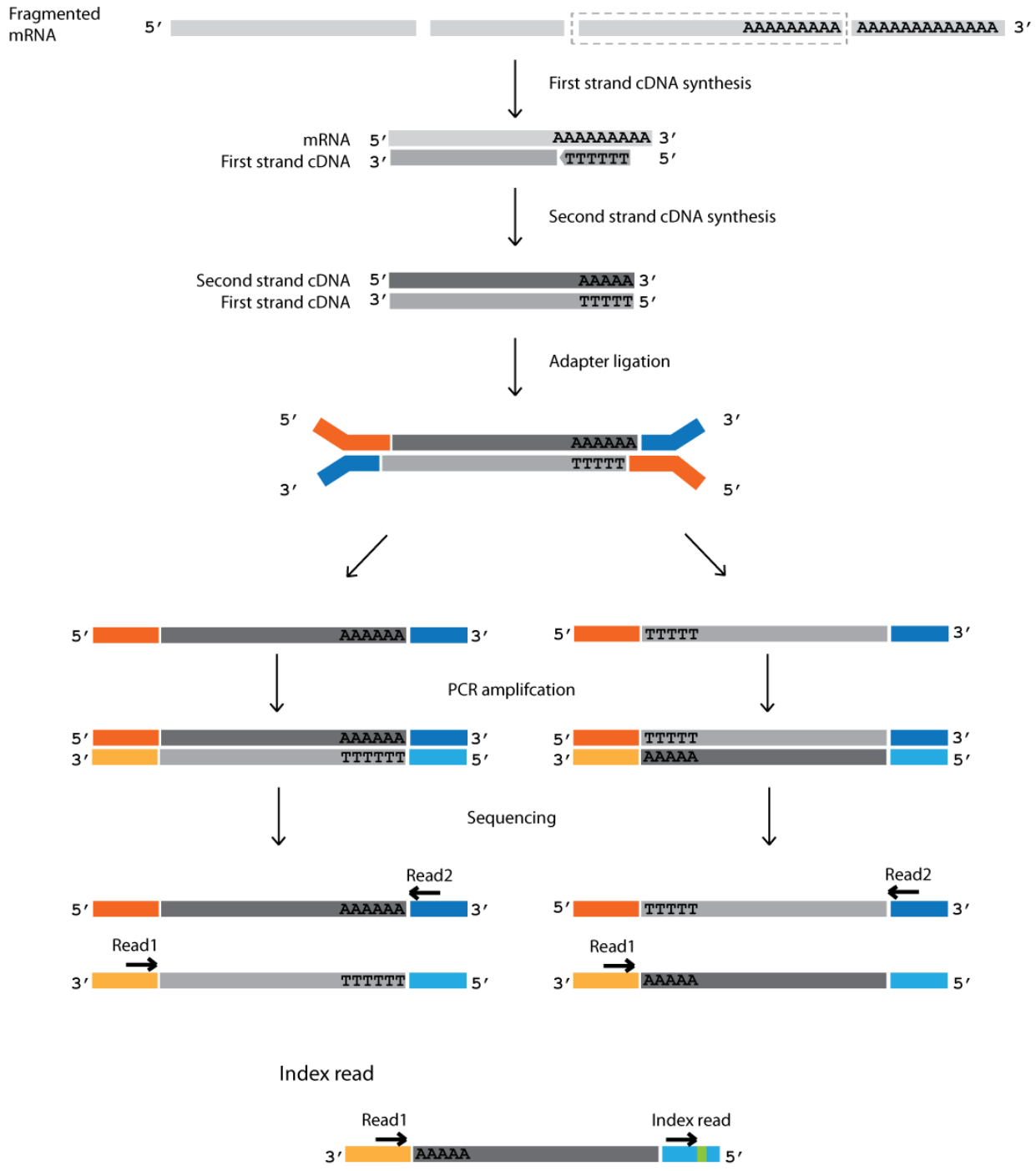
Fragmented mRNA
5′
AAAAAAAAA
AAAAAAAAAAAAA
3′
First strand cDNA synthesis
mRNA 5′ AAAAAAAAA 3′
First strand cDNA 3′ TTTTTT 5′
Second strand cDNA synthesis
Second strand cDNA 5′ AAAAA 3′
First strand cDNA 3′ TTTTT 5′
Adapter ligation
AAAAAA
TTTTT
PCR amplifcation
TTTTTT
Sequencing
Read2
Read1
Index read

Figure 3-3. Schema illustrating why coverage at both ends of transcrips are low.

Colored bars represent sequencing fragments, and arrowheads of the same color represent the a nucleotide they cover. For example,for the nucleotide indicated by the orange arrowhead, there is only one possible sequencing fragment that would cover it (assuming all fragments are the same length). The green nucleotide is more likely to be sequenced, since there are more fragments that can cover it. Coverage at the end of the 3'UTR requires sequencing fragments that arise from priming in the polyA tail. Reverse transcription with dT_6 hexamer primers may increase the number of fragments thatspan the polyA tail and 3'UTR.

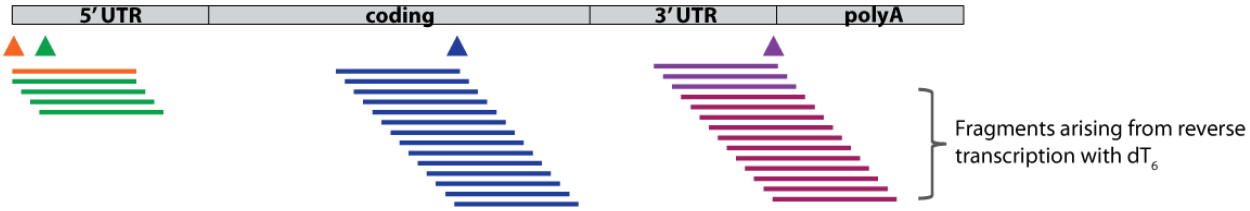

Figure 3-4. Transcript coverage at the 3' end was not improved by spiking in dT_6 hexamers during reverse transcription.

Top: Library preparation using the Illumina Truseq kit with oligodT purification and the dUTP modification [229]. Single end 100 bp sequencing.

Bottom: Library preparation with the Illumina TruSeq stranded kit with RiboZero purification. Only the first read of paired end 100 bp sequencing run was considered.

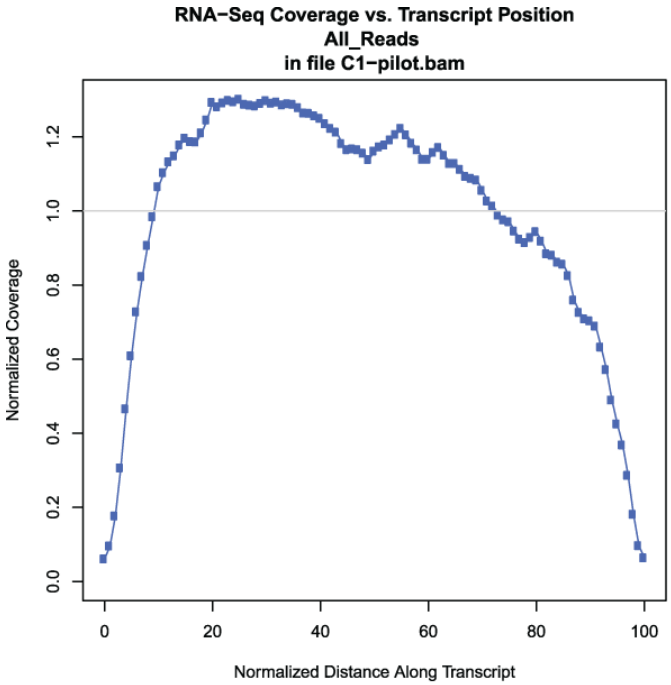
RNA−Seq Coverage vs. Transcript Position
All_Reads
in file C1−pilot.bam
Normalized Coverage
0.0
0.2
0.4
0.6
0.8
1.0
1.2
0
20
40
60
80
100
Normalized Distance Along Transcript

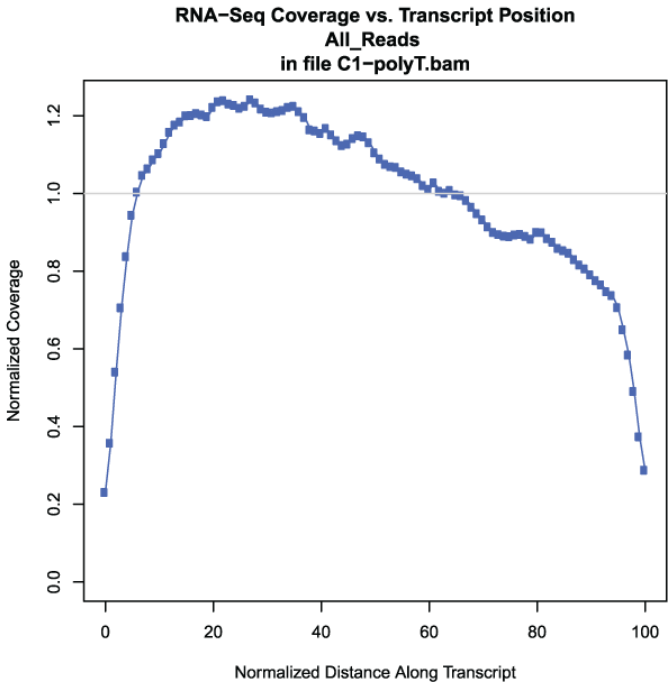
RNA−Seq Coverage vs. Transcript Position
All_Reads
in file C1−polyT.bam
Normalized Coverage
0.0
0.2
0.4
0.6
0.8
1.0
1.2
0
20
40
60
80
100
Normalized Distance Along Transcript

Libraries for small RNA sequencing were prepared with the Illumina TruSeq small RNA sample prep kit using 1.1 µg of total RNA from the same samples used for total RNA sequencing. Libraries were multiplexed and sequenced with 50 bp single end reads.

For the pilot experiment, Illumina TruSeq kit with polyA selection was used to make a library from 4 µg of total RNA. The Illumina protocol was modified with the dUTP modification to make the library strand specific. The resulting library was amplified and the 350-450 bp bands were gel purified for sequencing.

3.2.2 Bioinformatics

3.2.2.1 Preprocessing

Binary basecalls were filtered for chastity and converted to Sanger FASTQ format using CASAVA v.1.8.2 [230]. The resultant FASTQ files were then passed through FastQC-0.10.1 to verify that no considerable artifacts arose related to library generation or sequencing [231].

3.2.2.2 Alignment

A reference genome was created for the STAR Aligner-2.3.0.1 [232]. Ensembl release 72 was used as the annotation source for creation of the splice junction database [233]. Chromosome ordering and naming conventions were altered to make the annotation consistent with the UCSC mm10 assembly [234]. All samples were aligned using default parameters, and the resultant alignments were sorted and converted to the BAM alignment specification using SAMTools-0.1.14 [235].

3.2.2.3 Differential expression analysis

Differential expression analysis was carried out using the Cuffdiff program supplied with Cufflinks-2.1.1 [236]. The alignment files for each treatment were supplied as biological

replicates and Cuffdiff was run with the options for fragment bias and multi-read correction enabled (flags –b and –u, respectively).

3.2.2.4 Identification of end-tags

Reads that span the 3' end of transcripts and the polyA tail are considered "end-tags" as they provide information on the exact site of CPA. Unmapped reads with 7 or more leading 'A's or 'T's (read1 or read2, respectively) were trimmed of the homopolymer sequence and realigned with the same settings. The re-alignments were clustered into groups to identify putative CPA sites. Mates for low quality homopolymer reads were pulled, trimmed for As and realigned.

3.2.3 Validation experiments

3.2.3.1 RT-qPCR

Total RNA (100 ng) was reverse transcribed using random hexamers (50 ng/μL) and SuperScript III (Invitrogen) in a total reaction volume of 20 μL. The resulting cDNA was used for quantitative PCR with SYBR green and exon-spanning gene-specific primers. The efficiency of the primers were determined to all be within 100±10%.

3.2.3.2 Semi-quantitative end-point PCR

cDNA prepared from control and chemLTP treated slices was used for PCR using isoform specific primers. The number of cycles was kept low at 25 to avoid saturation of the reaction.

3.3 Results

3.3.1 Optimization of the treatment protocol

3.3.1.1 Effects of elevated potassium treatments on gene expression

Slices exhibit periods of high-frequency bursting while incubated in elevated potassium (8.4 mM KCl, compared to 2.5 mM in ACSF and 30 mM in high potassium solutions) (Figure 3-

5a). After washout, acute slices treated with elevated potassium continue to have persistent spontaneous bursting (approximates 2-3 bursts/min compared no bursting in control) (Figure 3-5b). The spontaneous bursting lasts at least two-hours in all the slices tested, and are attenuated over time by incubation in actinomycin D (Figure 3-5c). These results indicate that the activity induced by elevated potassium has long-lasting effects on synaptic connections, and that these effects are transcription-dependent.

Despite the increased levels of activity and potentiation of synaptic connections, we did not detect upregulation of the immediate early genes Arc, c-Fos, BDNF (fold change by RT-qPCR relative to time-matched controls were 0.79, 0.79, and 1.48 respectively). This unexpected observation led us to consider previous reports that slice preparation itself has significant effects on gene expression and test this phenomenon in our slices [237,238].

3.3.1.2 Slice preparation up-regulates gene expression

We extracted RNA from slices that were prepared and maintained on interface chambers but not treated with any stimulation. We also extracted RNA from hippocampi that were removed and frozen immediately without being sliced. RT-qPCR results show substantial upregulation of genes associated with neuronal activity (Figure 3-6). These results show the gene induction effects induced by the injury of cutting acute slices and incubating them in interface chambers.

The observation that slice preparation alters the transcriptional landscape of the neurons is consistent with previous findings that neuronal injury induces activity and engages plasticity mechanisms [239]. Additionally, previous studies have found that acute slice preparation alters post-translational modifications and protein levels [237,238]. DMSO alone tends to induce a

Figure 3-5. Electrophysiological effects seen with incubation of acute slices in increased potassium.

(A) Bursting induced by continuous application of increased K^+ ACSF (8.4 mM KCl) for 6 hours. Traces show approx. 11 minute-long recordings taken at the indicated time points from the same slice. Similar responses were seen in 4 other slices. Vertical scale bar is 5 mV, horizontal scale bar is 1 minute. (continued) (Data from T. J. O'Dell)

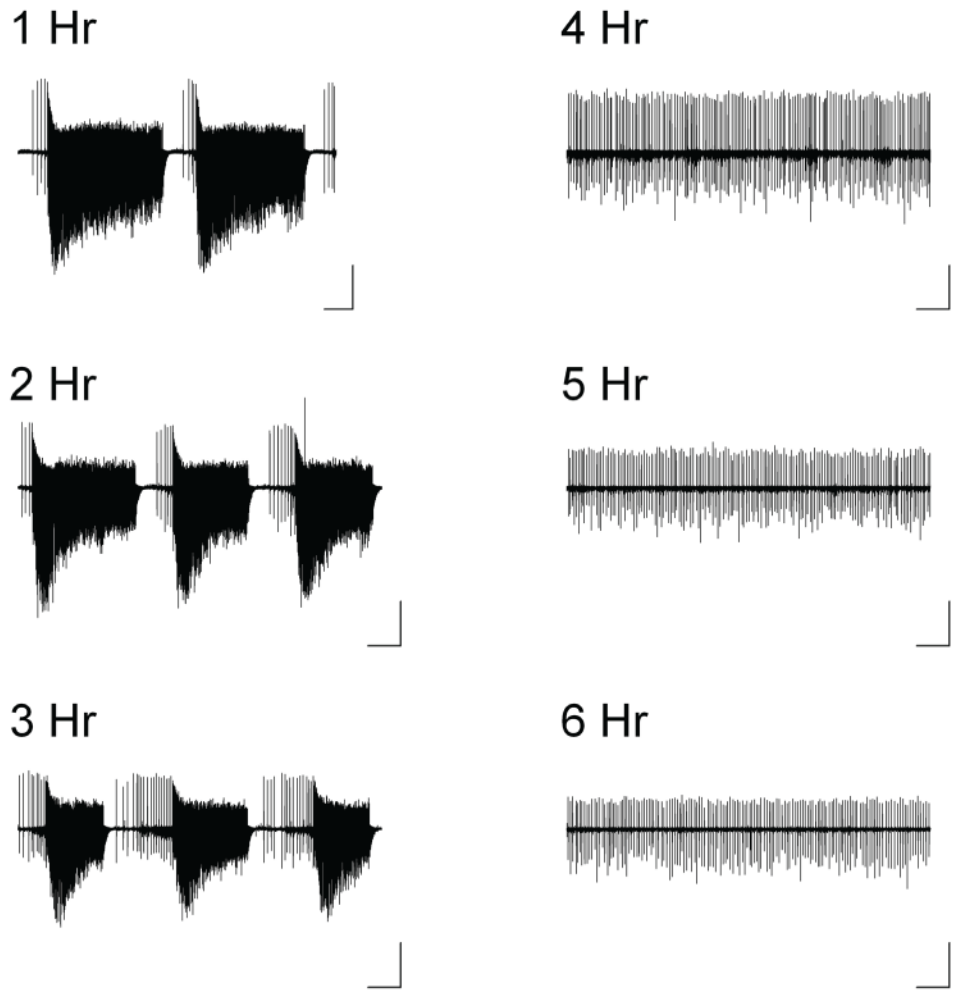

Figure 3-5 (continued). (B) Plots show spontaneous bursting induced by bath application of increased K^+ ACSF (8.4 mM) for either 20 (n = 8) or 40 minutes (n = 6). Although a 20 minute application of increased-K^+ ACSF does induce persistent bursting in some slices, the effect is much less reliable and robust compared to a 40 minute application of increased-K+ ACSF. (C) Blocking transcription suppresses the long-lasting spontaneous bursting induced by elevated potassium. Slices were incubated in 40 μM actinomycin D 30 min prior to increased K^+ treatment, during increased K^+, and for 1 hour after treatment. (Data from T. J. O'Dell)

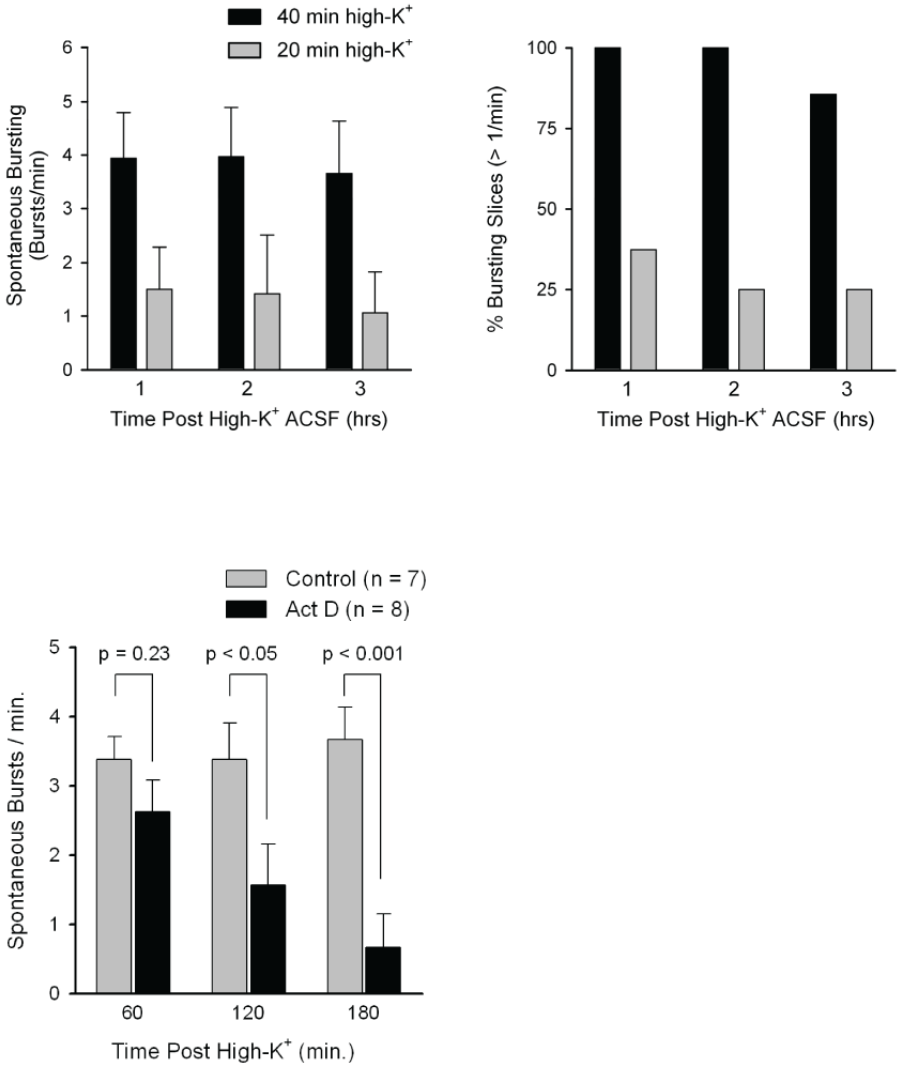

Figure 3-6. Slice preparation induces activity-dependent genes.

Hippocampus was dissected out and part of it was snap frozen immediately. Slices were cut from the other hippocampus and maintained in interface chambers for 30 min, 3 hr, or 5 hr. Error bars show standard deviation. N=2 for all except N=4 for c-Fos at 3 hours. Fold-change of several known activity-induced genes as measured by RT-qPCR. Slices treatments are indicated on the x-axis. The y-axis represents fold-change relative to control. Error bars show S.E.M.

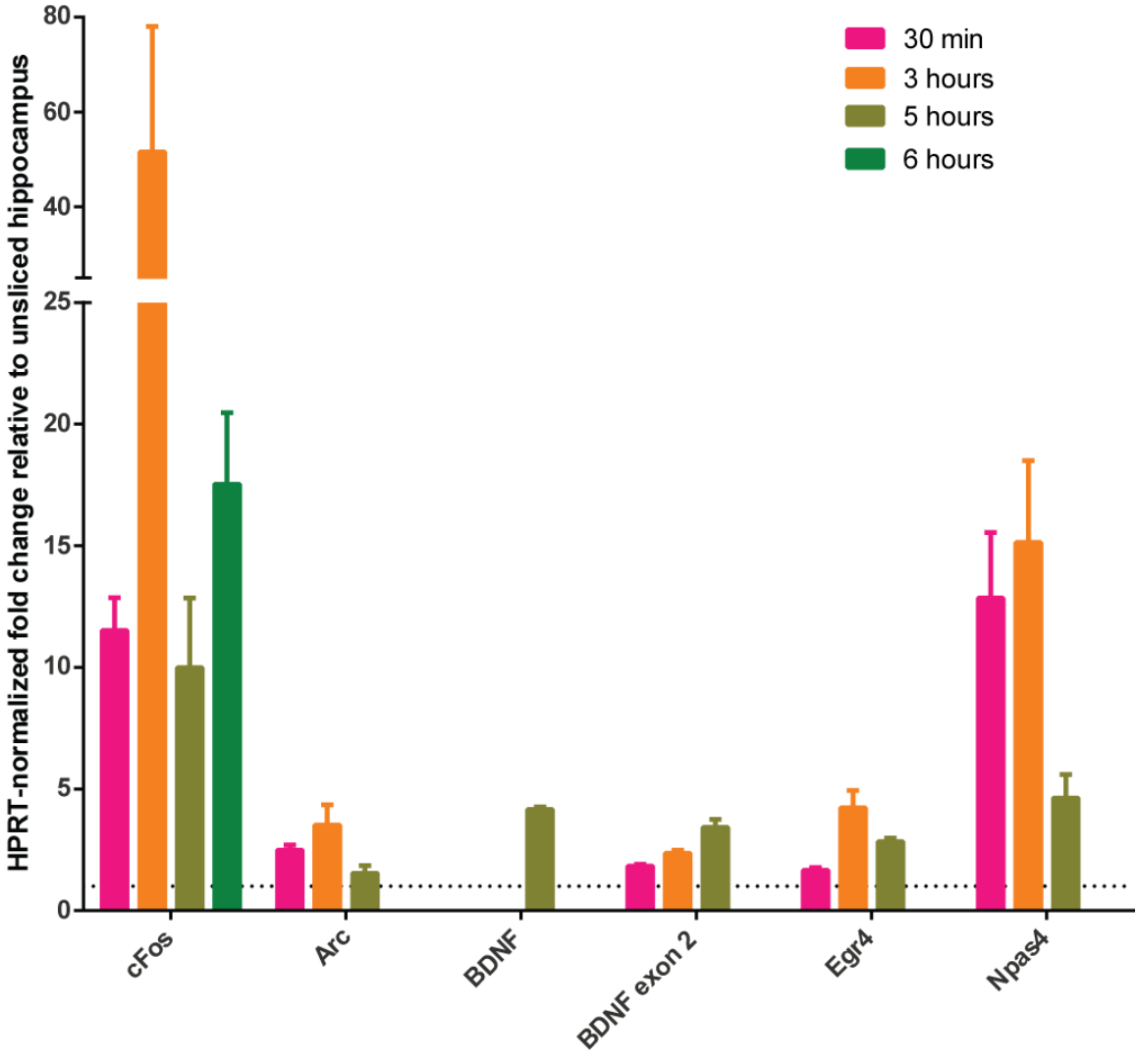

small degree of up-regulation in some genes (Figure 3-7). These finding highlight the importance of having controls that account for the slice preparation induced injury and the effects of vehicle application.

Although comparison to time-matched control slices will allow us to identify LTP-relevant transcripts amidst injury-induced transcription, the signaling pathways activated by slice preparation should still be minimized. Neurons may engage injury responses that interfere with normal LTP mechanisms, and the injury responses introduce a relatively unpredictable variable. To minimize injury effects, we tried modifying the ACSF as well as our slice preparation methods (Figure 3-8) [240]. However, these modifications did not attenuate the injury response, as determined by measuring changes in transcript levels. We decided that time is the best way to minimize the injury response, i.e. the recovery period after slicing, since the transcript levels begin to decrease by 5 hours (Figure 3-6).

While deciding on the parameters with which to induce chemLTP, we considered two factors: the injury effects associated with slice preparation and the health of the slice as it is maintained *in vitro*. We would like to apply the treatment with minimal interference from the injury effects, but cannot wait too long as slice health is equivocal beyond 8 hours after cutting. We performed some preliminary experiments varying the recovery period before treatment and the wash-out period after treatment (Figure 3-9), and decided on 2 and 3 hours for recovery and post-washout incubation, respectively. We compared a 2 or 3 hour recovery period and found that neither enhanced the detection of chemLTP-induced changes (Figure 3-9A). It seemed that the 3-hour recovery period may reduce the variability in fold change measured, however 2 hours would be more consistent with previous studies. We also compared harvesting slices at 30

Figure 3-7. Effects of DMSO on gene expression.

Slices were cut, recovered for 3 hours, treated with 0.2% DMSO, and harvested 3 hours after treatment washout. Expression of different genes was determined by RT-qPCR. Genes were normalized to HPRT mRNA and compared to time-matched, untreated control slices. Error bars show standard deviation.

N=2.

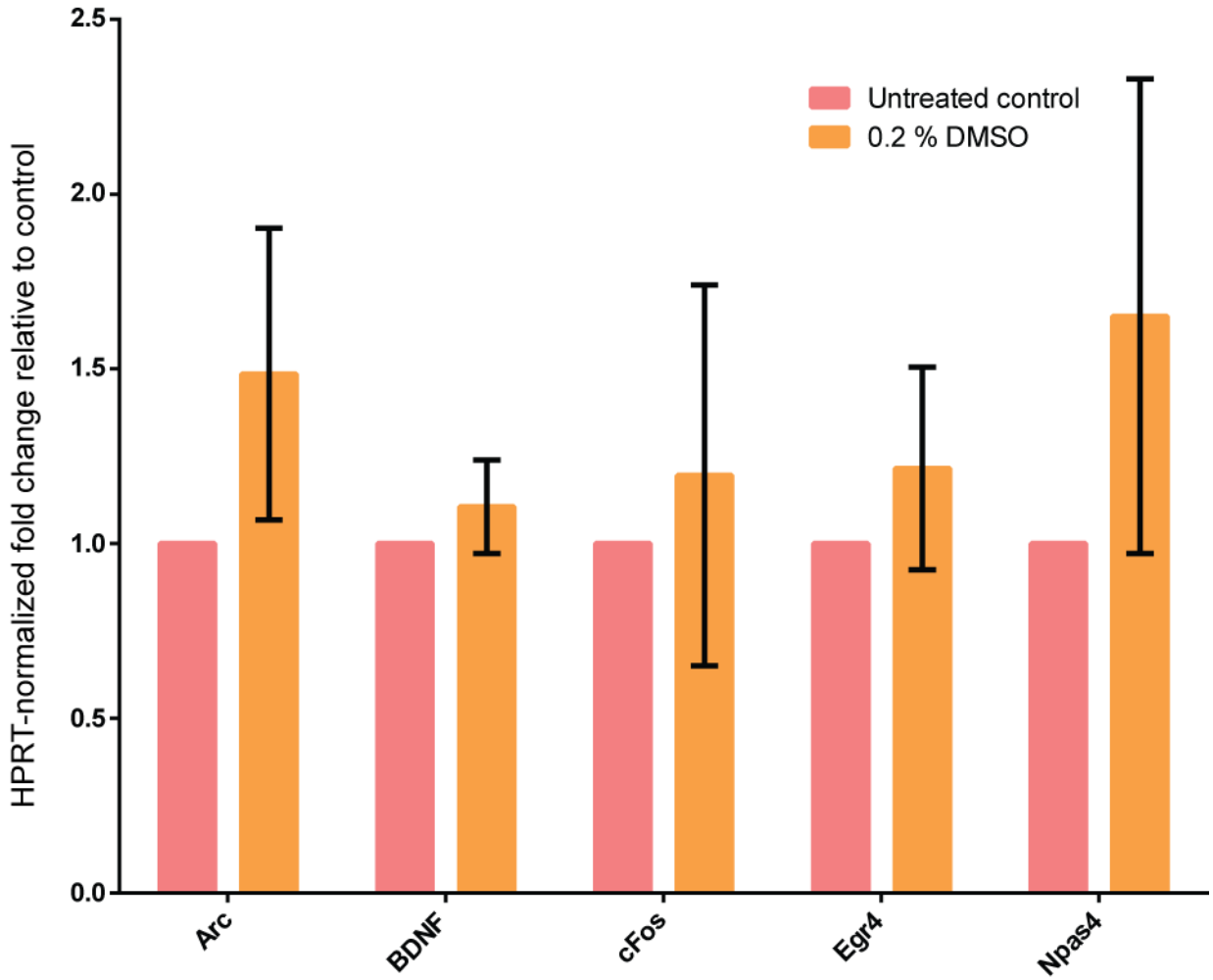

Figure 3-8. Attempts to minimize gene expression induced by slice preparation.

(A) Dissection and slice cutting were performed in a modified ACSF that contained no calcium and 10 mM Mg^{2+}. Slices were maintained in the modified ACSF for 30 minutes and either frozen or switched to normal ACSF. (B) Slices were cut and allowed to recover as described previously in Coba et al. (i.e. in a submerged chamber, among other differences). Error bars show standard deviation. N= 2.

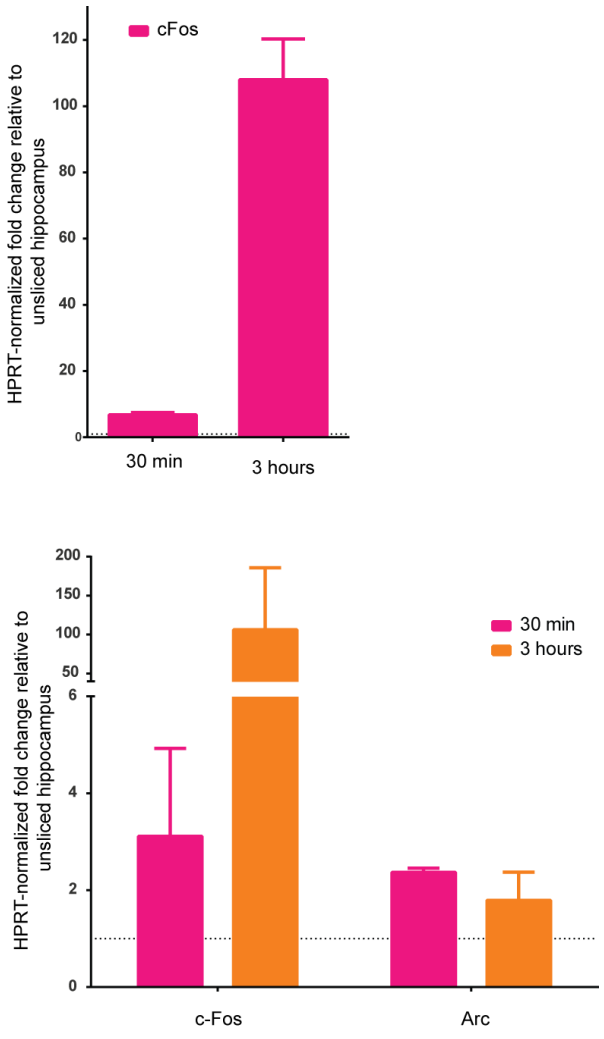

Figure 3-9. Changes in transcript levels at different time points.

Comparison of changes in transcript levels induced after different periods of recovery and post-washout incubation. (A) Slices were recovered for 2 (N = 4) or 3 hours (N = 2), treated to induce chemLTP, and then incubated for 3 hours after treatment washout. (B) Slices were recovered for 2 hours, treated to induce chemLTP, and then incubated for 30 min (N = 2) or 3 hours (N = 4) after treatment washout. (C) Slices were recovered for 3 hours, treated to induce chemLTP, and then incubated for 30 min or 3 hours (both N = 2) after treatment washout. Error bars show standard deviation.

(A) 3 hour washout after treatment

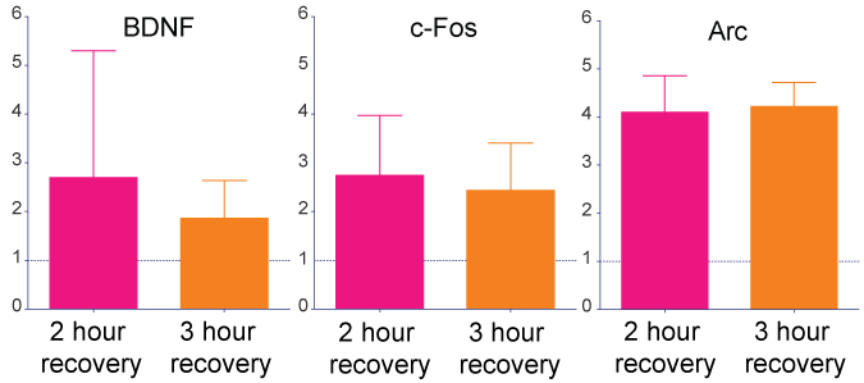

(B) 2 hour recovery before treatment

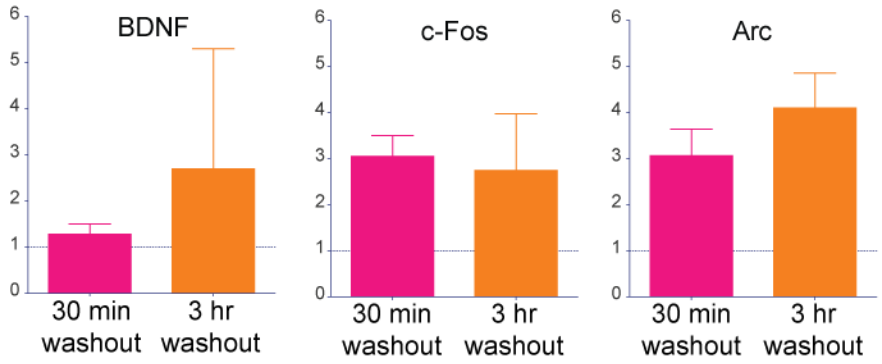

(C) 3 hour recovery before treatment

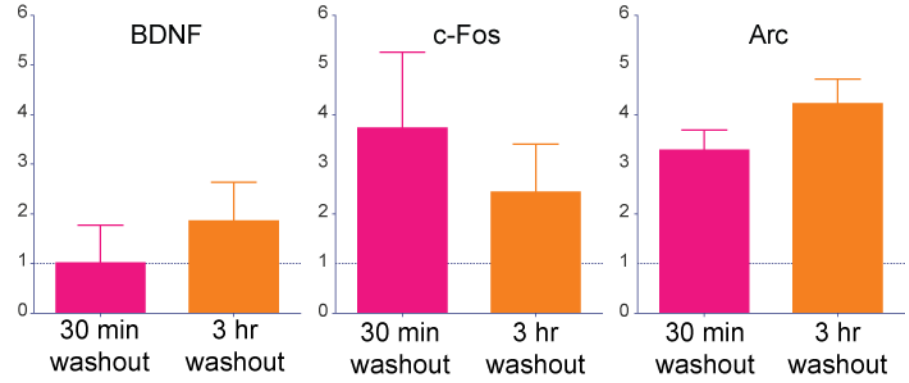

minutes or 3 hours after treatment washout, and found that BDNF and Arc both tended to be more up-regulated at 3 hours while cFos was more up-regulated at 30 minutes (Figure 3- 9B and C). Since cFos is a rapid immediate early gene (IEG), we decided that a 3 hour post-washout would allow us to detect transcript level changes that are not limited to the rapid IEGs. Preliminary tests indicate that these parameters will allow the detection of significant changes in chemLTP versus vehicle-treated slices (section 3.3.2.1).

3.3.2 Preliminary results

3.3.2.1 Activity-induced genes are up-regulated by chemLTP treatment

We used RT-qPCR to confirm upregulation of the known activity-induced genes – Arc, c-Fos, Egr4, and Npas4 [155,241] (Figure 3-10).

3.3.2.2 The short isoform of Homer1 is upregulated by chemLTP treatment

Slices treated with the chemLTP protocol showed an increase in the Homer1 isoform with the shorter 3'UTR (called Homer1a or Homer1S) while the isoforms with the longer 3'UTR (Homer1L and D) were unchanged (Figure 3-11). These results are consistent with previous reports of the activity-induction of Homer1a [160,181,183]. The Homer proteins are important post-synaptic scaffolding proteins. Homer1a arises from the use of an upstream polyadenylation signal that results in an isoform encoding a truncated protein. The truncated protein has the N-terminal PPXXF motif, which interacts with other post-synaptic proteins, but lacks the C-terminal coiled-coiled domain, which mediates dimerization with other Homer proteins. Homer1a acts as a dominant negative to full-length Homer1, and reduces spine size and synaptic transmission [180].

Figure 3-10. Fold change of known activity-induced genes as determined by RT-qPCR. Total RNA extracted from the slices sent for sequencing were used. Genes were normalized to HPRT mRNA, and then to control condition levels to determine fold induction.

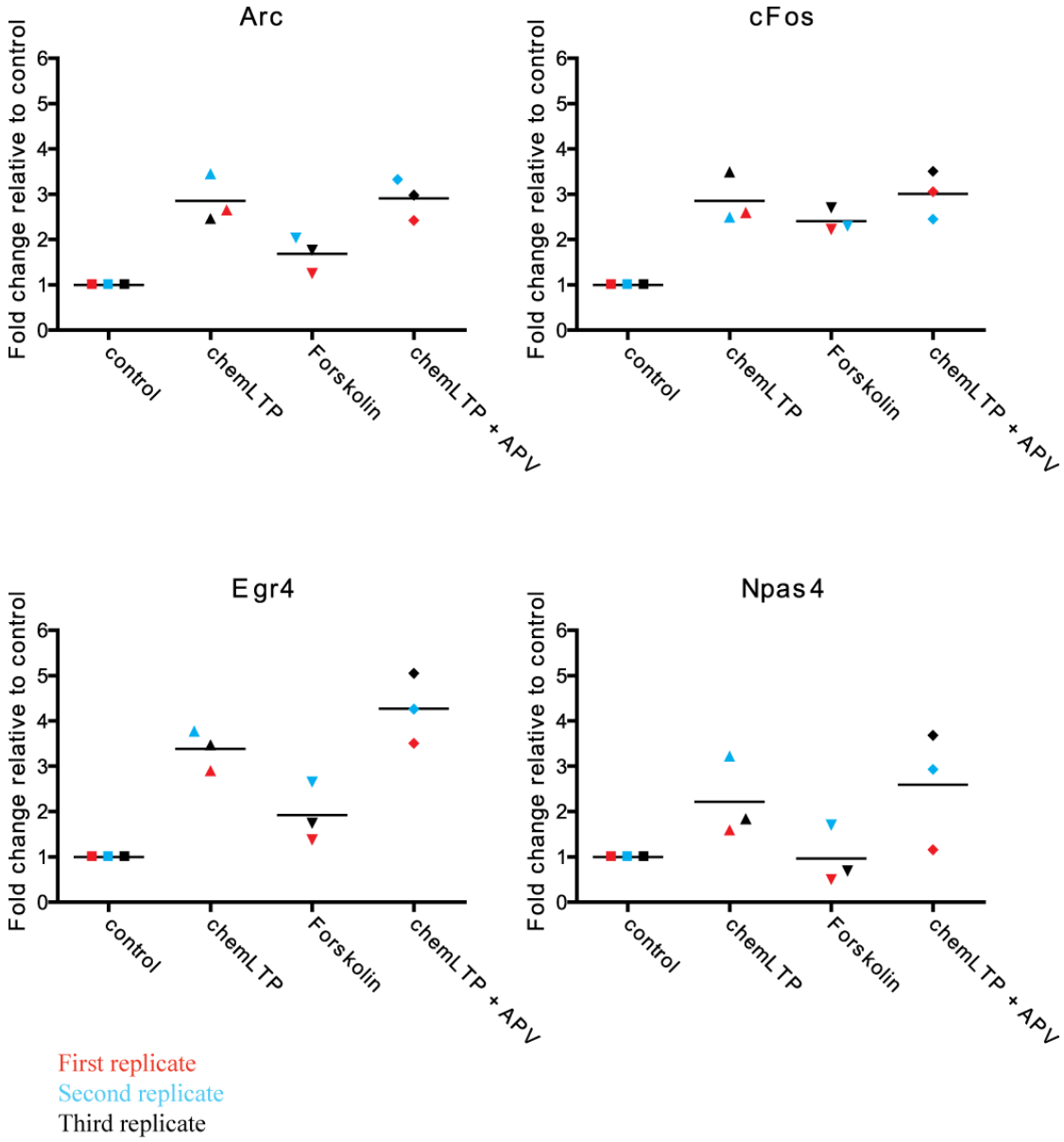

Figure 3-11. The short Homer1 isoform is preferentially up-regulated by chemLTP.

(A) Semi-quantitative end-point qPCR (25 amplification cycles) shows increase in the short:long ratio in chemLTP-treated slices compared to control. PCR with no reverse transcription ("No RT") confirm absence of genomic DNA in the RNA extracts. (B) Positions of the PCR primers.

(continued)

A

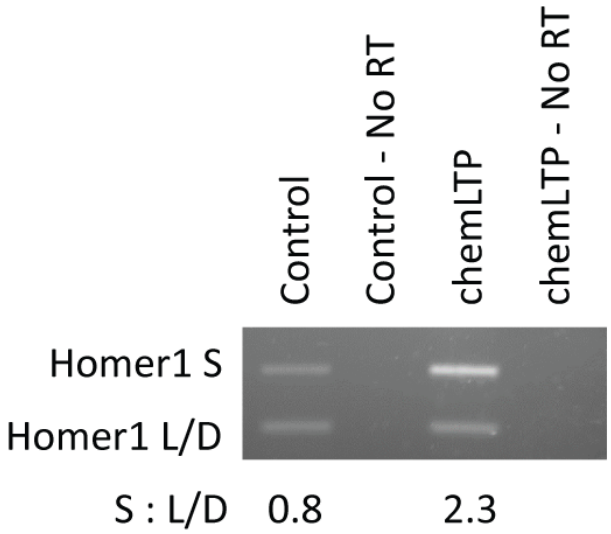
Control
Control - No RT
chemLTP
chemLTP - No RT
Homer1 S
Homer1 L/D
S : L/D
0.8
2.3

B

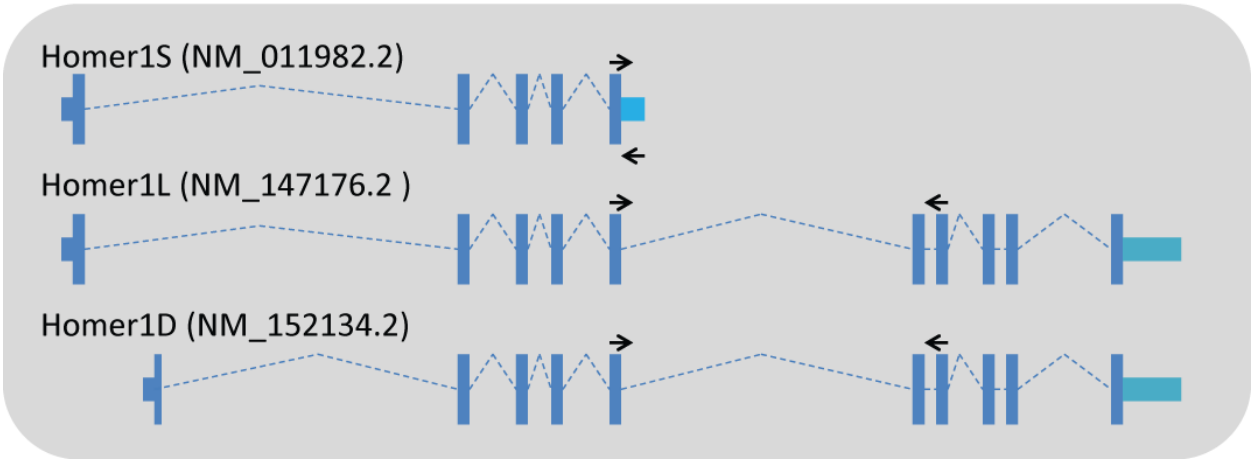
Homer1S (NM_011982.2)
Homer1L (NM_147176.2)
Homer1D (NM_152134.2)

Figure 3-11. (continued) (C) Normalized coverage of the short Homer1 isoform. The region shown correspondsto the 3'UTR of the short isoform (coordinates indicated are for UCSC mm10). The blue lines at the top show positions of annotated exons (thick bars) and introns (thin lines). The coverage indicates that 3'UTR of this isoform extends past the current annotation and probably has two polyadenylation signals. To normalize the coverage tracks for visual inspection, we applied a normalization method similar to that used by the R package DESeq (Anders, 2010). We first generated size-factors essentially as described, and then used this as a normalization quotient on all data points.

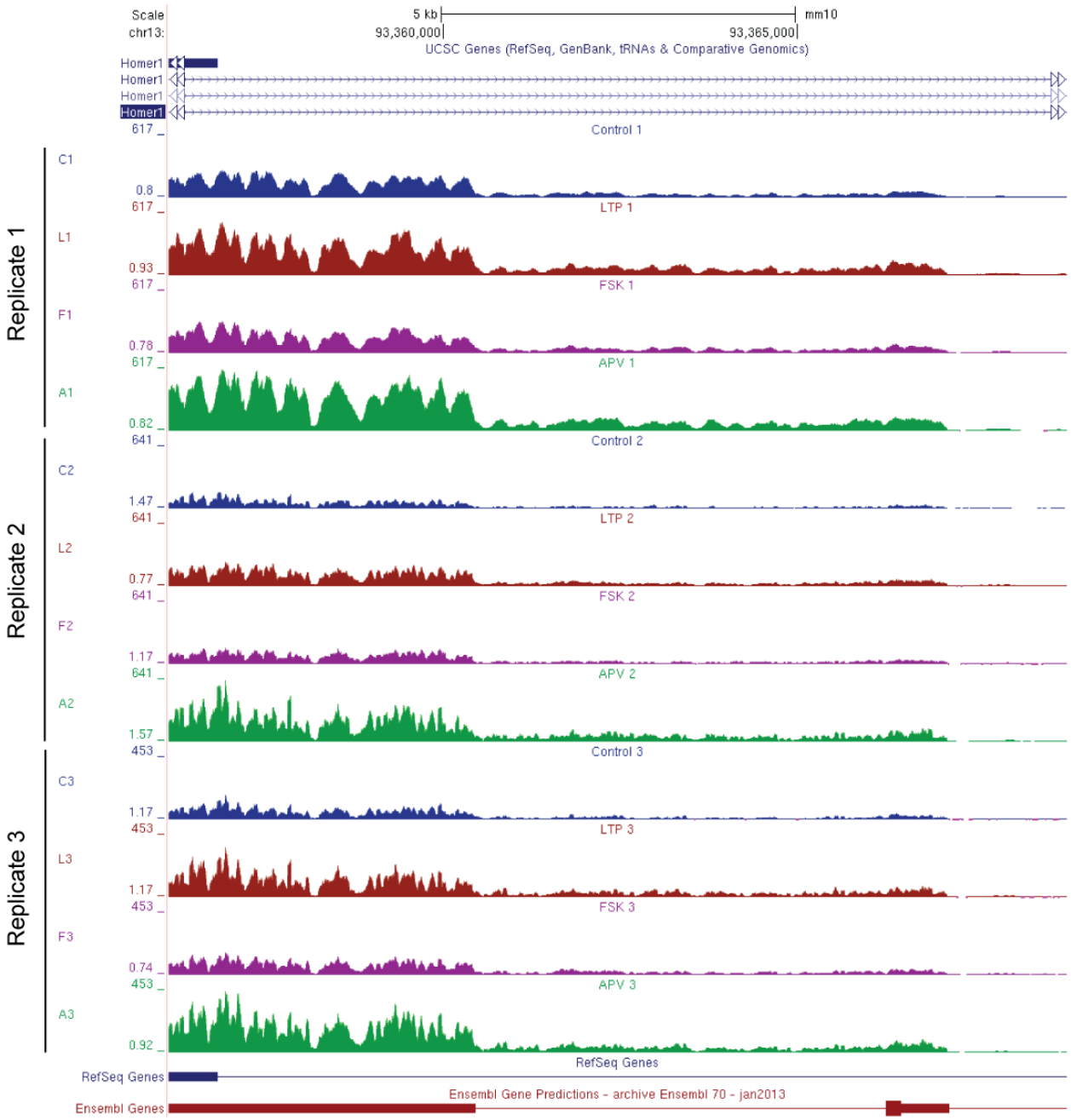
Scale
chr13:
5 kb
93,360,000
93,365,000
mm10
UCSC Genes (RefSeq, GenBank, tRNAs & Comparative Genomics)
Homer1
Homer1
Homer1
Homer1
617
Control 1
Replicate 1
C1
0.8
617
LTP 1
L1
0.93
617
FSK 1
F1
0.78
617
APV 1
A1
0.82
641
Control 2
Replicate 2
C2
1.47
641
LTP 2
L2
0.77
641
FSK 2
F2
1.17
641
APV 2
A2
1.57
453
Control 3
Replicate 3
C3
1.17
453
LTP 3
L3
1.17
453
FSK 3
F3
0.74
453
APV 3
A3
0.92
RefSeq Genes
RefSeq Genes
Ensembl Genes
Ensembl Gene Predictions - archive Ensembl 70 - jan2013

3.3.2.3 Sequencing statistics

Sequencing statistics are provided in Table 3-2.

3.3.2.4 End-tags can be used to identify CPA sites

Preliminary analysis of the end-tags identified in our sequencing data seem to lie mostly in the 3'UTR of annotated genes. They also appear to agree well with the Hoque et al. annotation of alternative 3'UTRs [175]. Some genes had many more end-tags than others, and this did not seem to correlate with expression level determined by the number total reads to that gene (Figure 3-12).

3.3.3 Differential expression analysis

New transcription is required for the maintenance of LTP [154,219,242], indicating an important role for the newly transcribed genes. To identify these induced genes, we use differential expression analysis between the four conditions. It should be noted that in our experiments, we are measuring the steady-state levels of transcripts at 3 hours after treatment. Hence, the abundance of a given transcript is determined by both transcription rates and transcript stability. Transcripts that are up-regulated may be due to transcriptional induction or enhanced transcript stability. LTP also leads to the downregulation of transcripts, although the significance of downregulation is not clear. It may be that these transcripts are simply not required in the new cell state, or that the protein products of these transcripts are inhibitory to the maintenance of LTP. As before, the downregulation of transcripts may be a result of transcriptional repression or decreased transcript stability.

Differential expression analysis of our sequences results are shown in Tables 3-3 and 3-4. Briefly, compared to control, chemLTP treatment up-regulated 163 genes and down-regulated 16

Figure 3-12. Reads that span the 3'UTR / polyA tail junction can be used to identify site of cleavage and polyadenylation (CPA).

These reads contain terminal untemplated 'A's (or 'T's depending on direction) are called "end-tags". The 3'UTR of BDNF contains two polyA signals and shown here is the CPA site for the upstream polyA signal. Gray bars represent reads, colored nucleotides represent mismatches, the sequence panel shows the genomic sequence, and the RefSeq panel shows annotation for the BDNF 3'UTR. VH1, VH2, and VH3 refer to the control, chemLTP, and forskolin only samples from replicate 1.

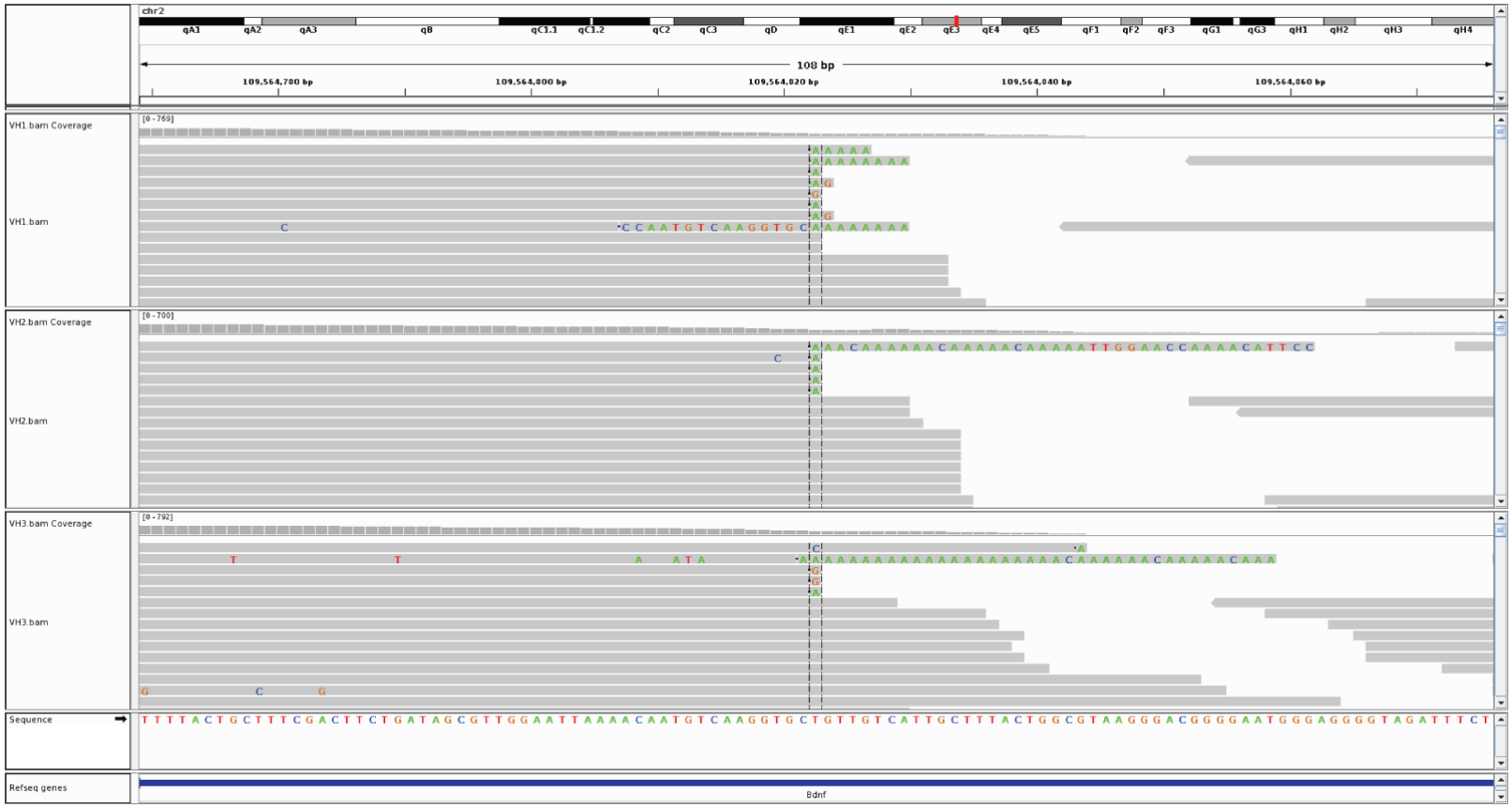
chr2
qA1 qA2 qA3 qB qC1.1 qC1.2 qC2 qC3 qD qE1 qE2 qE3 qE4 qE5 qF1 qF2 qF3 qG1 qG3 qH1 qH2 qH3 qH4
108 bp
109,564,780 bp
109,564,800 bp
109,564,820 bp
109,564,840 bp
109,564,860 bp
VH1.bam Coverage
[0 - 769]
VH1.bam
VH2.bam Coverage
[0 - 700]
VH2.bam
VH3.bam Coverage
[0 - 792]
VH3.bam
Sequence
Refseq genes
Bdnf

genes, forksolin treatment up-regulated 63 genes and down-regulated 4 genes, and chemLTP in the presence of NMDAR block up-regulated 118 genes and down-regulated 7 genes. Across the conditions, the mean upregulation was 2.20-fold and median upregulation is 1.86-fold. These changes are modest compared to other RNAseq studies, and may be due to several related factors. First, the plasticity-related gene induction is occurring in the presence of injury-related gene induction that occurs from slice preparation. Although the effects of injury are common in all the treatment conditions and can be accounted for with the vehicle-treated control, the injury causes substantial gene induction that may dampen the fold change induced by chemLTP. Second, our protocol induces synaptic strengthening, which is a relatively mild change in cell state compared to differentiation or transformation. Third, many of the transcripts that are up-regulated in our samples are transcripts that were already being expressed. Even seemingly small two or three fold increases in these transcripts can actually represent substantial changes in transcription. For comparison, when a transcript goes from not being expressed to being expressed at one copy, its fold change is infinite (i.e 1 divided by 0) even though it has only undergone one additional round of transcription. On the other hand, a transcript that is initially present at 100 copies and increases to 150 copies is measured as having a 1.5 fold increase. Fourth, the brain slices used are a heterogeneous mix of many cell types that probably respond differently to chemLTP. Finally, a study using KCl depolarization of cultured neurons found similarly modest levels of gene up-regulation of MEF2 targets: mean 2.92 and median 2.22 [160]. Hence, even though the fold changes detected in the slices seem modest, they should not be viewed with less confidence.

3.3.3.1 Dissecting the signaling pathways involved in chemLTP

The chemLTP protocol has two main components: (1) activation of the cAMP signaling pathway by forskolin, and (2) global depolarization by high potassium. During depolarization, both ligand-gated and voltage-gated ion channels are activated to allow the influx of calcium and activation of calcium signaling pathways. In particular, concurrent pre- and post-synaptic depolarization leads to glutamate release and relief of the magnesium block from NMDA receptors (NMDARs) and their subsequent activation. NMDAR activation is necessary for LTP at CA3-CA1 synapses, as blocking their activity blocks the maintenance of potentiation [219,243].

Individually, neither depolarization nor forskolin treatment results in LTP. While the cAMP and calcium signaling pathways have overlapping targets, their downstream effects are sometimes antagonistic. To elucidate the roles of the different pathways, we treated slices with forskolin only so that the changes in gene expression due to cAMP signaling could be determined separately. We also treated slices with chemLTP in the presence of APV to block NMDARs. This condition allows us to examine the effect of activating this very specific class of glutamate receptors. We do not have a depolarization-only condition and will rely on published databases for gene expression changes due to calcium signaling [160].

To delineate the effects of the different pathways, we determined the differential expression for each condition compared to control and compared the list of genes to see where they overlap (Table 3-4 and Figure 3-13). We were interested to see if there were any genes that were up-regulated in one condition while down-regulated in another, but did not observe this happening. However, there was one instance of two genes from the same family that were altered in opposite directions (Col6a1 and Col6a3).

Figure 3-13. Overlapping differential expression (DE) between the conditions tested. Cuffdiff was used to determine DE between the conditions shown and control. Results from the three replicate experiments were considered ($q<0.05$). The number of DE genes in each group are indicated.

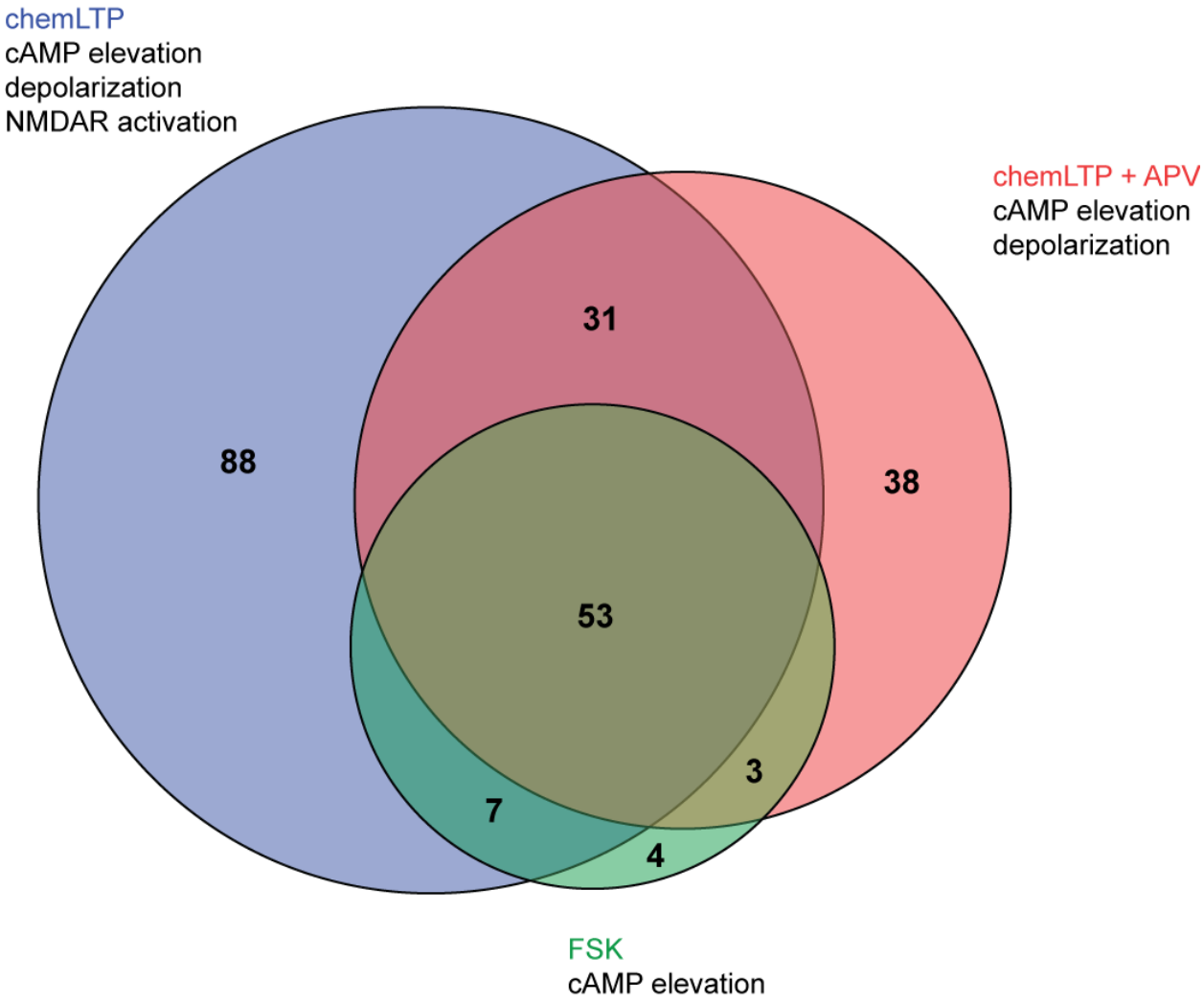

We also made direct comparisons between the conditions and report the DE in Table 3-3. There is some degree of agreement between the direct comparisons and the comparisons with respect to control; both lists should be considered when identifying genes that are differentially regulated in one condition but not another.

3.3.3.1.1 Genes differentially expressed by LTP only (88 genes)

The differential expression of these genes is a result of the synergistic effects of cAMP, depolarization, and NMDAR activation acting together. They are only induced when all three components are present.

3.3.3.1.2 Genes differentially expressed by LTP with APV only (38 genes)

This list was unexpectedly long. These genes are only differentially expressed when cAMP is elevated, neurons are depolarized, but NMDAR are blocked. The implication is that NMDAR activation suppresses these genes during depolarization and cAMP elevation (genes in this list are all upregulated). Somehow, calcium influx through NMDAR decreases transcription or transcript stability of this population.

3.3.3.1.3 Genes differentially expressed by forskolin only (4 genes)

This list is short, indicating that most genes that are induced by cAMP elevation are generally not antagonized by calcium elevation. Most genes that are activated in the presence of forskolin remain activated in the presence of depolarization.

3.3.3.1.4 Genes that are differentially expressed whenever there is cAMP elevation (53 genes)

These genes are DE in the presence of cAMP elevation, regardless of whether there is depolarization or NMDAR activity. Most of the forskolin-induced genes fall into this category. This subset includes 14 of the previously identified 49 immediate early genes (IEGs) [241].

3.3.3.1.5 *Genes that are differentially expressed when there is cAMP elevation and depolarization (31 genes)*

These genes are differentially expressed by cAMP signaling only if there is also calcium signaling, regardless of NMDAR activity. This may also contain the subset of genes activated by depolarization alone, but that condition has not been explored yet.

3.3.3.2 BDNF is not induced in our slice treatments

A gene that is notably absent from our DE lists is BDNF, which has been found by several studies to be an activity-induced gene [160,241,244]. One possible explanation of why it is not up-regulated in any of our conditions is that the time point we look at is too early. BDNF is considered a delayed IEG and in cultured neurons, its expression ramps up between 1 and 3 hours [241,245]. Another possibility is that since BDNF was already induced by slice preparation (Figure 3-6), chemLTP treatment was not able to induce it further. Finally, it is possible that cAMP signaling antagonizes the pathway that up-regulates BDNF during activity. Calcium influx during depolarization activates CREB, which then up-regulates BDNF transcription [245]. In addition to the CREB binding site, there is another calcium-dependent element in the BDNF promoter that is hypothesized to be responsible for the delayed kinetics of BDNF induction [245]. Regulation via this second element may be inhibited in a cAMP-dependent manner, an effect which would be exaggerated in our forskolin-treated slices. An example of a transcription factor that is activated by calcium but repressed by cAMP is MEF2 [168], which targets BDNF [160]. To explore the possibility that cAMP plays a role in suppressing calcium-induced BDNF expression, it would be informative to repeat the depolarization studies performed in cultures in the presence or absence of forskolin to see how

BDNF expression is modified. We did not do a depolarization only condition so cannot address this possibility with our dataset.

3.3.3.3 Gene ontology analysis of differentially expressed transcripts between LTP and control

The genes that were DE in LTP compared to control were organized into functional groups (Table 3-5). These groups can help identify interesting candidates for follow-up.

3.4 Discussion and future directions

3.4.1 Dissecting processes responsible for changes in transcript level

The steady-state level of a transcript is determined by how actively it is being transcribed and by factors that stabilize and destabilize the transcript. To determine the relative contribution of these processes and whether there are global mechanisms acting to regulate a large number of transcripts, we will examine genomic sequences for promoters and 3'UTRs for motifs affecting stability. Correlation of gene expression with *cis* regulatory elements and promoter usage will allow us to determine whether changes in transcript levels are due to altered stability or transcription.

3.4.1.1 Promoter usage

The proximal promoter region of differentially expressed genes will be scanned for known promoter elements, histone positions, and enriched motifs. Expression patterns that correlate well with promoter usage would suggest that transcriptional regulation is a likely mechanism of gene regulation for those transcripts. For example, if there is a group of up-regulated transcripts that have a promoter element in common, these transcripts are likely to be up-regulated because of increased transcription (which may or may not be accompanied by increases in transcript stability). This interpretation can be tested in cultured neurons using

transcriptional inhibitors and pharmacologically-induced activity (e.g. TTX withdrawal or bicuculline treatment).

3.4.1.2 Transcript stability

Transcript stability is influenced by *cis* elements, most of which are expected in the untranslated regions, especially the 3' UTR which is typically longer than the 5' UTR (800 and 200 nucleotides on average, respectively [246]).

3.4.1.2.1 Motif analysis

The 5' and 3' UTRs of differentially expressed transcripts will be scanned for enriched motifs that may influence transcript stability. Motifs that correlate well with changes in transcript levels would suggest that transcript stability is being regulated. For example, a motif that is enriched in up-regulated transcripts may be playing a role in stabilizing the transcripts. The degree of conservation of the motifs will also be considered.

The polyadenylation signal usage between conditions will also be characterized.

3.4.1.2.2 Length of the polyA tail

The fragments that arise from reverse transcription priming in the polyA tail may provide information on polyA tail length (read types 2, 3, and 4 in Figure 3-14), since a longer polyA tail has more opportunities for primer binding. This can be tested with ligation-mediated polyadenylation tests.

3.4.2 Differential expression of glia-enriched genes

3.4.2.1 Astrocyte genes

Several astrocyte-enriched genes were significantly up-regulated by chemLTP treatment. These include thrombospondin, which is important for synapse formation [247], and glypican4,

Figure 3-14. Types of reads from paired-end sequencing.

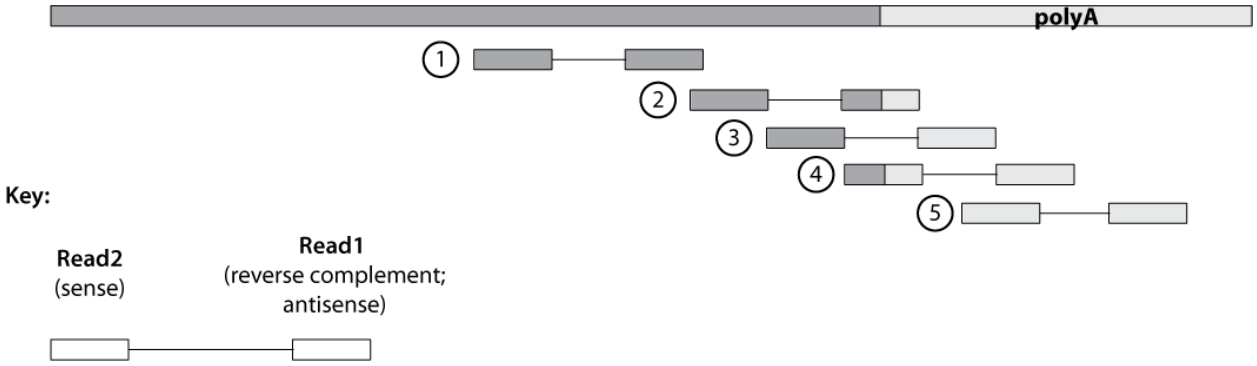

	Read1	Read2
1	5′- NNNN....NNNN -3′	5′- NNNN....NNNN -3′
2	5′- TTTT....NNNN -3′	5′- NNNN....NNNN -3′
3	5′- TTTT....TTTT -3′	5′- NNNN....NNNN -3′
4	5′- TTTT....TTTT -3′	5′- NNNN....AAAA -3′
5	5′- TTTT....TTTT -3′	5′- AAAA....AAAA -3′

which is important for the formation of functional synapses [248]. It is tempting to speculate from these results that astrocytes play a role in synaptic strengthening during LTP. In order for this to occur, there should be a way to signal to astrocytes which synapses are active and should be strengthened. An alternative explanation could be that the forskolin and depolarization during chemLTP treatment have direct effects on astrocytes, causing them to up-regulate thrombospondin and glypican4 whether or not there is synaptic activity. One way to distinguish between these two possibilities would be induce LTP using electrical stimulation and determining whether these astrocyte genes are again up-regulated. This question may also be addressed in culture by using bicuculline to increase synaptic activity, and then measuring glypican4. However, because the *in vivo* contacts between astrocytes and neurons are not preserved in dissociated culture, a negative result from culture studies would not be conclusive.

3.4.2.2 Microglia genes

Microglia-enriched genes were also differentially expressed with chemLTP treatment, which was an unexpected result. A possible role for microglia during synaptic plasticity could be to eliminate inactive synapses [249]. Potentiation at Schaffer collateral synapses during chemLTP is dependent upon bursting of the CA3 cells [219]. Although many of the connections between CA3-CA1 neurons are intact, some will invariably be lost as axons project out of the slice. Synapses on neurons downstream of the lost connections will not be potentiated because of the lack of synaptic activity. While intact CA3-CA1 connections are strengthened, synapses from severed connections may be weakened and selected for elimination. Consistent with the idea of synapse weakening and elimination with activity is the activity-induced expression of Arc, which accelerates AMPAR endocytosis [250], and the short isoform of Homer1, which weakens

synapses [180]. To explore the role of microglia in synapse elimination, one possible experiment could be to treat and stain for activated glia and assess the number of synapses on adjacent neurons.

3.4.3 Sequencing the translationally active population of mRNAs

3.4.3.1 Polysome fractionation

An mRNA transcript that is undergoing translation typically has many ribosomes bound to it and is called a polyribosome, or polysome. In polysomes, each ribosome may be engaged in translation so multiple nascent polypeptides may be synthesized simultaneously. Actively translating mRNAs can be separated from free mRNA by ultracentrifuging polysome lysates on a sucrose gradient. Light, free mRNA stays at the top of the gradient, while mRNA with heavy ribosomes bound will travel at a faster rate through the gradient. The sucrose gradient can then be fractionated with continuous UV monitoring to identify which fractions contain polysomes (Figure 3-15). RNA extracted from these fractions can be used for sequencing. Measuring transcripts in polysomes fractions is a proxy for measuring newly translated proteins. *Cis* elements in transcripts from the free and polysomal fractions will be compared to identify motifs that influence translation.

In addition to sequencing the entire polysome fraction, the individual polysome peaks can be collected separately and used for RT-qPCR studies. This will allow us to determine how many polysomes are bound to an mRNA, which provides a measure of how actively it is being translated.

Figure 3-15. Example of a brain polysome profile.

Polysome profile obtained from forebrain homogenate that was centrifuged on a 20-50 % sucrose gradient. This lysate for this profile was obtained from a 3 month old mouse without the addition of detergents in the lysis buffer.

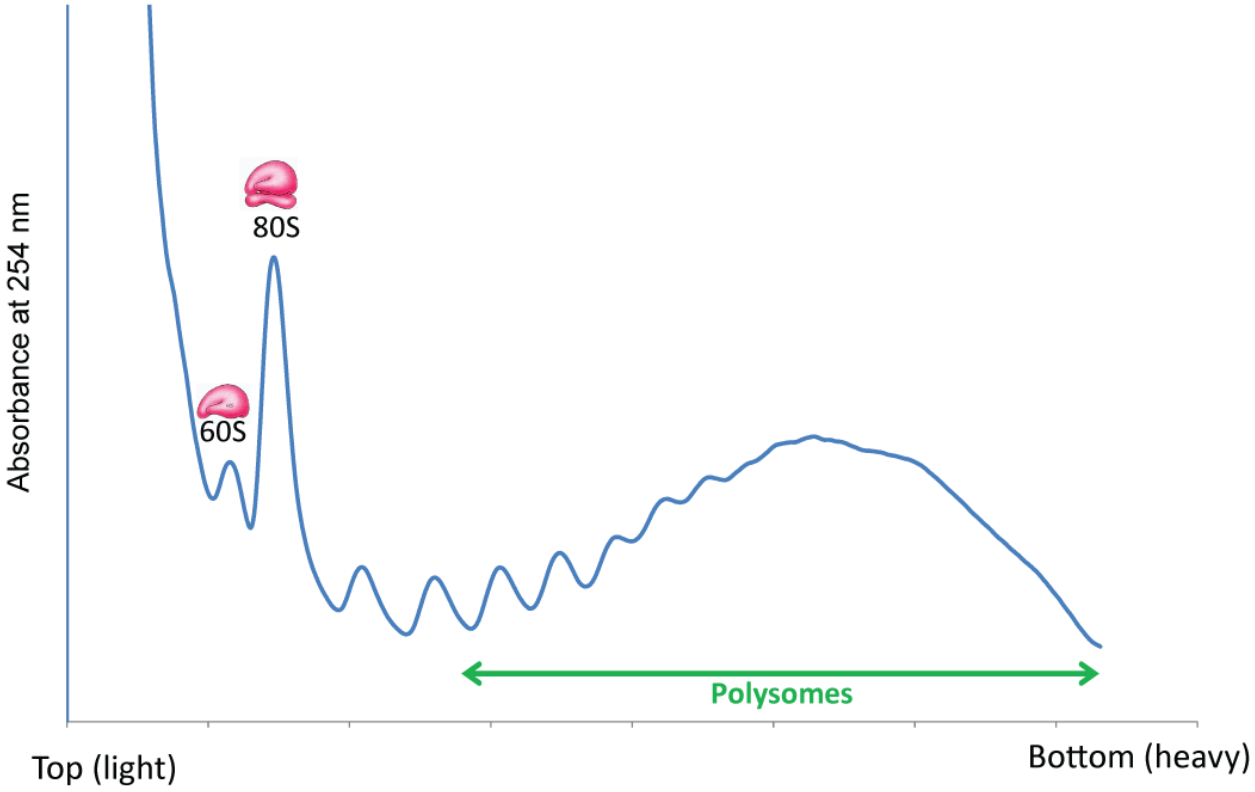

3.4.3.2 Advantages and disadvantages of polysome fractionation

Examining changes in mRNA levels alone provides an incomplete picture of gene expression, since mRNA levels are not well-correlated with protein levels [251]. One of the reasons for this discrepancy is the abundance of post-transcriptional mechanisms that regulate mRNA translation. Another reason for the discrepancy between mRNA and protein levels is the different dynamics that regulate the synthesis and degradation of these two very different macromolecules. Proteins and mRNAs are not easily compared as they have very different half-lives and do not exist on the same time scale [251]. One of the advantages of polysome fractionation over proteomic assays (e.g. mass spectrometry) is that it allows us to compare total transcripts with ribosomally-loaded transcripts. By comparing two populations of mRNAs, we do not need to worry about preexisting proteins or rates of protein degradation confounding our analysis. An advantage of polysome fractionation over ribosome pull-down assays is that fractionation allows the separation of monosomes, which are generally considered inactive, from polysomes, which are more active. Polysome fractionation is also preferred over ribosomal footprinting for this study, since we are interested in identifying *cis* regulatory elements, which are abundant in the untranslated regions of transcripts where ribosomes are not expected to bind. Another advantage of polysome fractionation is that the integrity of the polysome complexes can confirmed by UV monitoring the fractions.

A disadvantage of using polysome fractions is that not all transcripts with multiple ribosomes are being translated. A subset of polysomes may be stalled, for example by FMRP [205]. Also, it is not clear how quantitative measuring mRNA levels in polysomes will be for assessing increases or decreases in translation. A transcript with 3 ribosomes or 12 ribosomes

would be counted as one, even though the latter is probably undergoing much more active translation than the former.

3.4.3.3 Enriching for reads a the 3' end

Since spiking in dT_6 hexamers did not improve coverage of 3'UTRs, we could try published protocols that are designed to sequence exclusively from the 3' end of transcripts (e.g. 3'T-Fill [252]). This would allow us to precisely identify CPA sites and what 3'UTR isoforms are being loaded onto ribosomes.

3.4.3.4 microRNA-mRNA interactions

With sequencing data from total mRNA, miRNA, and ribosomally-loaded mRNA, we can study the correlation between miRNA expression and transcript abundance, as well as translational efficiency. This would provide information on how miRNAs regulate targets during synaptic plasticity.

3.5 Conclusions

This study will generate three main datasets (total RNA, small RNA, and polysomal RNA) that will provide genome-wide information on how gene expression changes during LTP and during activation of different signaling cascades. One of the most common applications of high-throughput sequencing is use differential expression analysis to identify genes that are up- and down-regulated under different conditions. In addition to determining differential expression in the three datasets, this study will address general mechanisms of gene regulation that are employed during LTP. We will have a lot of data to work with and will take a systematic approach to make sense of it by classifying the data (based on e.g. motifs, expression patterns, etc.) and trying to make connections between observations.

Table 1. Sequencing project details.

Sample name		Experiment cate	Sample details	condition	concentration	A 260/280	RIN	Fold change by qPCR				Library details	Sequencing details	miRNA		mRNA	
								Arc	cFos	Egr4	Npas4			Project ID	Run ID	Project ID	Run ID
Pilot		7.11	- Slices were recovered for 3 hours, and then harvested 3 hours after treatment - Slices from 10 mice treated over 5 days: 7/2, 7/5, 7/6, 7/9, 7/10/12 - Slices were pooled and RNA was extracted on 7/11	control	1060.40		7.9	1.00	1.00	1.00	1.00	- Library prepared with Illumina TruSeq kit (polyA purification) with dUTP modification for strand specificity (Parkhomchuk, NAR 2009) - Elute/prime/fragmentation performed for 4 minutes - Gel purified 350-450 bp band for sequencing.	Libraries were multiplexed into one lane and sequenced for single-end 50 bp.	-	-	Sequenced through the stem cell facility	
VH1	C1	12.19	- Slices were recovered for 2 hours, and then harvested 3 hours after treatment - For each replicate, slices from 2 mice treated on the same day were used.	control	108.66	2.06		1.00	1.00	1.00	1.00	- Total RNA library prepared by the UNGC with Illumina strand specific TruSeq kit with RiboZero purification. Replicate from 12/19 was prepared first, separately from the other two replicates - Small RNA library prepared by the UNGC with Illumina small RNA TruSeq kit	- Total RNA libraries multiplexed (4 conditions from each replicate / lane) - Replicate from 12/19 was sequenced first with paired-end 100 bp - Replicates from 12/20 and 1/18 were sequenced later with the Rapid Run format, single end 50 bp - Small RNA libraries were pooled into a single lane and sequenced single end 50 bp	2013-056 (3/5/13)		2012-361	2013-067
VH2	L1			LTP	103.90	2.13		2.65	2.60	2.90	1.59						
VH3	F1			FSK	108.84	2.12		1.25	2.22	1.38	0.50						
VH4	A1			APV	75.53	2.14		2.42	3.06	3.51	1.16						
VH5	C2	12.20		control	134.80	1.94		1.00	1.00	1.00	1.00					2013-057 (3/5/13)	
VH6	L2			LTP	150.55	2.1		3.45	2.45	3.78	3.22						
VH7	F2			FSK	156.65	2.07		2.04	2.30	2.65	1.70						
VH8	A2			APV	156.83	2.06		3.33	2.45	4.26	2.93						
VH9	C3	1.18		control	113.00			1.00	1.00	1.00	1.00						
VH10	L3			LTP	92.90			2.46	3.49	3.47	1.84						
VH11	F3			FSK	110.00			1.77	2.70	1.74	0.69						
VH12	A3			APV	86.30			2.98	3.51	5.05	3.68						

Table 2. Alignment statistics.

Alignment statistics for the sequencing runs for all 3 sets of replicates C, control; L, chemLTP; F, forskolin only; A, chemLTP + APV.

SAMPLE	C1	L1	F1	A1	C2	L2	F2	A2	C3	L3	F3	A3
Number of input reads	53744935	53391420	57093572	59934169	40781767	56113828	46740197	45539090	35818142	52984314	56639099	44447084
Average input read length	100	100	100	100	100	100	100	100	100	100	100	100
UNIQUE READS:												
Uniquely mapped reads number	38792253	38895977	41484776	41253710	29018411	42790321	33343433	32460675	27475107	37743816	43225923	34210198
Uniquely mapped reads %	72.18%	72.85%	72.66%	68.83%	71.16%	76.26%	71.34%	71.28%	76.71%	71.24%	76.32%	76.97%
Average mapped length	99.53	99.47	99.49	99.38	99.35	99.62	99.33	99.31	99.6	99.3	99.62	99.63
Number of splices: Total	8579876	7248342	8438596	8378047	4949267	9164974	6025085	4546726	6026736	6191553	9464932	7650246
Number of splices: Annotated (sjdb)	8452609	7132365	8304095	8248479	4869022	9024844	5929116	4461706	5938249	6090624	9327508	7534760
Number of splices: GT/AG	8477648	7159745	8335471	8276449	4884324	9056993	5946460	4478828	5953073	6110520	9352043	7557885
Number of splices: GC/AG	80421	67529	80346	78662	45270	83545	56166	41913	56762	56365	87977	72583
Number of splices: AT/AC	10180	8687	9878	9710	5872	10408	7222	5324	7402	7386	11306	8995
Number of splices: Non-canonical	11627	12381	12901	13226	13801	14028	15237	20661	9499	17282	13606	10783
Mismatch rate per base, %	0.28%	0.31%	0.30%	0.35%	0.35%	0.24%	0.36%	0.37%	0.36%	0.51%	0.37%	0.36%
Deletion rate per base	0.00%	0.01%	0.01%	0.01%	0.03%	0.01%	0.03%	0.04%	0.01%	0.03%	0.00%	0.00%
Deletion average length	1.86	2.4	2.15	2.45	4.28	2.09	4.17	4.7	2.66	4.35	1.72	1.72
Insertion rate per base	0.01%	0.01%	0.01%	0.01%	0.02%	0.01%	0.01%	0.02%	0.01%	0.02%	0.00%	0.00%
Insertion average length	1.25	1.34	1.32	1.32	1.26	1.2	1.29	1.27	1.18	1.27	1.17	1.17
MULTI-MAPPING READS:												
Number of reads mapped to multiple loci	8995303	6969150	8534678	9623438	4619650	7403839	5557400	4800697	4860479	5656112	7976710	6334856
% of reads mapped to multiple loci	16.74%	13.05%	14.95%	16.06%	11.33%	13.19%	11.89%	10.54%	13.57%	10.68%	14.08%	14.25%
Number of reads mapped to too many loci	216937	169951	176217	194107	113433	216822	136021	118104	123674	140471	215652	170021
% of reads mapped to too many loci	0.40%	0.32%	0.31%	0.32%	0.28%	0.39%	0.29%	0.26%	0.35%	0.27%	0.38%	0.38%
UNMAPPED READS:												
% of reads unmapped: too many mismatche	0.00%	0.00%	0.00%	0.00%	0.00%	0.00%	0.00%	0.00%	0.00%	0.00%	0.00%	0.00%
% of reads unmapped: too short	10.34%	13.34%	11.71%	14.46%	17.04%	9.78%	16.20%	17.68%	9.13%	17.59%	8.86%	8.07%
% of reads unmapped: other	0.35%	0.44%	0.37%	0.32%	0.19%	0.38%	0.28%	0.24%	0.25%	0.23%	0.36%	0.33%

Table 3. Differential expression between treatment conditions as determined by Cuffdiff. Cellular location and type of protein provided by Ingenuity Pathways Analysis software.

Gene ID	Description	Normalized FPKM		Fold change (2/1)	q value	Cellular location	Type of protein
		Sample 1	Sample 2				
Control vs. LTP (179 genes)							
Has1	Hyaluronan synthase1	0.145925	1.05738	7.246076314	0.0124402	Plasma Membrane	enzyme
Trh	Thyrotropin releasing hormone	1.20911	8.32476	6.88506369	0.0124402	Extracellular Space	other
Ccr7	Chemokine (C-C motif) receptor 7	0.298029	1.25953	4.226167652	0.0124402	Plasma Membrane	G-protein coupled receptor
Thbs1	Thrombospondin 1	3.13313	12.1784	3.88698085	0.0124402	Extracellular Space	other
Egr4	Early growth response 4	7.9458	29.3352	3.691916695	0.0124402	Nucleus	transcription regulator
Esm1	Endothelial cell-specific molecule 1	0.204663	0.705059	3.44496661	0.0464016	Extracellular Space	growth factor
Il12b	Interleukin 12b	2.27201	7.67096	3.376292745	0.0124402	Extracellular Space	cytokine
Inhba	Inhibin beta-A	4.30587	14.526	3.373555742	0.0124402	Extracellular Space	growth factor
Klf4	Kruppel-like factor 4 (gut)	3.6239	12.0448	3.323722649	0.0124402	Nucleus	transcription regulator
Cyr61	Cysteine rich protein 61	6.21073	20.3972	3.284172714	0.0124402	Extracellular Space	other
Ppp1r3g	Protein phosphatase 1, regulatory (inhibitor) subunit 3G	2.11439	6.65617	3.14803155	0.0124402	Cytoplasm	other
Arc	Activity regulated cytoskeletal-associated protein	61.8026	189.486	3.065983642	0.0124402	Cytoplasm	other
Rasl11a	RAS-like, family 11, member A	15.8113	48.4323	3.063137226	0.0124402	Nucleus	other
3930402G23Rik	RIKEN cDNA 3930402G23	0.295745	0.900712	3.045565221	0.0124402	unknown	other
Sik1	Salt inducible kinase 1	3.20985	9.29046	2.894351222	0.0124402	Cytoplasm	kinase
Fos	FBJ osteosarcoma oncogene	104.082	300.459	2.88673765	0.0124402	Nucleus	transcription regulator
Tinf2	Terf1 (TRF1)-interacting nuclear factor 2	11.1058	31.8618	2.868924496	0.0124402	Nucleus	other
Col6a3	Collagen, type VI, alpha 3	0.46462	1.26853	2.730244209	0.0124402	Extracellular Space	other
Gem	GTP binding protein (gene overexpressed in skeletal muscle)	20.0825	54.8241	2.729941432	0.0124402	Plasma Membrane	enzyme
Fosb	FBJ osteosarcoma oncogene B	11.0894	28.3375	2.555366106	0.0124402	Nucleus	transcription regulator
Gja4	Gap junction protein, alpha 4	0.725493	1.85101	2.551383911	0.0124402	Plasma Membrane	transporter
Egr1	Early growth response 1	9.96789	25.3788	2.546048674	0.0124402	Nucleus	transcription regulator
Arl4d	ADP-ribosylation factor-like 4D	11.5731	29.4388	2.543720221	0.0124402	Nucleus	enzyme
Btg2	B-cell translocation gene 2, anti-proliferative	15.1533	38.2818	2.526307056	0.0124402	Nucleus	transcription regulator
Zic2	Zic finger protein of the cerebellum 2	1.22075	3.0817	2.524434071	0.0124402	Nucleus	transcription regulator
Il10	Interleukin 10	0.615259	1.55045	2.519993478	0.0124402	Extracellular Space	cytokine
Hist1h4a	Histone cluster 1, H4a	51.0824	125.832	2.463313077	0.0124402	Nucleus	other
Igfbpl1	Insulin-like growth factor binding protein-like 1	0.47245	1.15018	2.434507593	0.0124402	unknown	other
Bmf	Bcl2 modifying factor	0.408524	0.984943	2.410980529	0.0124402	Cytoplasm	other
Atoh8	Atonal homolog 8 (Drosophila)	0.365986	0.879602	2.40337205	0.0225306	unknown	other
Ccrl2	Chemokine (C-C motif) receptor-like 2	2.24667	5.38835	2.398379571	0.0124402	Plasma Membrane	G-protein coupled receptor
Nr4a1	Nuclear receptor subfamily 4, group A, member 1	14.5828	34.8614	2.390578864	0.0124402	Nucleus	ligand-dependent nuclear receptor
Neat1	Nuclear paraspeckle assembly transcript 1	9.28607	21.6874	2.335481472	0.0124402	Nucleus	other
4930523C07Rik	RIKEN cDNA 4930523C07 gene	1.64527	3.83933	2.333572031	0.0124402	uknown	other
Tnfaip2	Tumor necrosis factor, alpha-induced protein 2	4.8495	11.0136	2.271098061	0.0124402	Extracellular Space	other
Egr2	Early growth response 2	3.5251	7.98169	2.264244887	0.0124402	Nucleus	transcription regulator
Trmt61b	tRNA methyltransferase 61 homolog B	10.672	24.0398	2.252598199	0.0124402	unknown	other
Il1b	Interleukin 1 beta	21.3488	48.0293	2.249742682	0.0124402	Extracellular Space	cytokine
Cartpt	CART prepropeptide	1.56793	3.52705	2.249493191	0.0388086	Extracellular Space	other
Rnf217	Ring finger protein 217	8.29902	18.5481	2.234977024	0.0124402	unknown	enzyme
Zic1	Zinc finger protein of the cerebellum 1	1.25028	2.78708	2.229159736	0.0124402	Nucleus	transcription regulator
Espl1	Extra spindle poles-like 1 (S. cerevisiae)	0.267412	0.595055	2.225238544	0.0124402	Nucleus	peptidase
Dom3z	DOM-3 homolog Z (C. elegans)	4.88464	10.8535	2.221971019	0.0124402	unknown	other
Foxc1	Forkhead box C1	0.677113	1.50242	2.218846707	0.0124402	Nucleus	transcription regulator
Satb2	Special AT-rich sequence binding protein 2	0.871555	1.89228	2.1711509	0.0124402	Nucleus	transcription regulator
Gjb2	Gap junction protein, beta 2	0.933745	2.02629	2.170067623	0.0124402	Plasma Membrane	transporter
Cyp1b1	Cytochrome P450, family 1, subfamily b, polypeptide 1	1.36252	2.94746	2.163249396	0.0124402	Cytoplasm	enzyme
Rab20	RAB20, member RAS oncogene family	3.54401	7.66622	2.163144437	0.0124402	Cytoplasm	enzyme
Fam163b	Family with sequence similarity 163, member B	4.60065	9.88032	2.147592096	0.0124402	unknown	other
Gadd45g	Growth arrest and DNA-damage-inducible 45 gamma	38.9467	82.3454	2.114299858	0.0124402	Nucleus	other
Tpbg	Trophoblast glycoprotein	4.03427	8.49878	2.10664906	0.0124402	Plasma Membrane	other
Il6	Interleukin 6	15.0086	31.5671	2.103264077	0.0124402	Extracellular Space	cytokine
Niacr1	Niacin receptor 1	2.03419	4.21681	2.072971095	0.0124402	Plasma Membrane	G-protein coupled receptor
Npas4	Neuronal PAS domain protein 4	8.41951	17.0605	2.02630311	0.0124402	Nucleus	transcription regulator
Ccnl1	Cyclin L1	26.5044	53.6779	2.025249989	0.0124402	Nucleus	other
Nr4a2	Nuclear receptor subfamily 4, group A, member 2	8.33552	16.6923	2.002552409	0.0124402	Nucleus	ligand-dependent nuclear receptor
Nfkbie	Nuclear factor of kappa light polypeptide gene enhancer in B-cells inhibitor, epsilon	2.89311	5.62842	1.945458223	0.0124402	Nucleus	transcription regulator
Arrdc3	Arrestin domain containing 3	17.9833	34.9372	1.942761767	0.0124402	Plasma Membrane	other
Vps37b	Vacuolar protein sorting 37B (yeast)	9.60922	18.6017	1.935814886	0.0124402	Cytoplasm	other
Procr	Protein C receptor, endothelial	2.43194	4.66529	1.918342073	0.0225306	Plasma Membrane	other
Gpr63	G protein-coupled receptor 63	4.03189	7.66605	1.901356422	0.0124402	Plasma Membrane	G-protein coupled receptor
Bag3	Bcl2-associated athanogene 3	3.11515	5.90584	1.895846291	0.0124402	Cytoplasm	other
Kcne4	Potassium voltage-gated channel, Isk-related subfamily, gene 4	2.29907	4.33693	1.886382187	0.0124402	Plasma Membrane	ion channel
Kdm6b	KDM1 lysine (K)-specific demethylase 6B	1.81754	3.42787	1.885989965	0.0124402	Extracellular Space	other
Pax6	Paired box gene 6	4.07291	7.66306	1.881470931	0.0124402	Nucleus	transcription regulator

Ghsr	Growth hormone secretagogue receptor	0.969501	1.80067	1.857318197	0.0225306	Plasma Membrane	G-protein coupled receptor
Sox11	SRY-box containing gene 11	3.11506	5.77913	1.855222214	0.0124402	Nucleus	transcription regulator
Klf2	Kruppel-like factor 2 (lung)	1.57287	2.91767	1.854989473	0.0388086	Nucleus	transcription regulator
Ier2	Immediate early response 2	12.5639	23.2304	1.848975361	0.0124402	Cytoplasm	other
Junb	Jun-B oncogene	110.789	204.47	1.845582207	0.0124402	Nucleus	transcription regulator
Tet3	Tet methylcytosine dioxygenase 3	3.87407	7.10299	1.83346789	0.0124402	Nucleus	other
Wipf3	WAS/WASL interacting protein family, member 3	31.9066	58.484	1.832973591	0.0124402	Plasma Membrane	other
Ppp1r15a	Protein phosphatase 1, regulatory (inhibitor) subunit 15A	20.2024	36.9414	1.828565113	0.0124402	Cytoplasm	other
Irs2	Insulin receptor substrate 2	11.9626	21.8267	1.824574425	0.0124402	Cytoplasm	enzyme
Zfhx4	Zinc finger homeodomain 4	1.05489	1.91868	1.818849282	0.0124402	Extracellular Space	other
Atf3	Activating transcription factor 3	26.7836	48.5411	1.812347997	0.0124402	Nucleus	transcription regulator
Il1rn	Interleukin 1 receptor antagonist	4.29139	7.77309	1.811319441	0.0124402	Extracellular Space	cytokine
Ak7	Adenylate kinase 7	1.38547	2.50761	1.80994016	0.0225306	Cytoplasm	kinase
Cd14	CD14 antigen	32.225	58.2805	1.808549393	0.0124402	Plasma Membrane	transmembrane receptor
Il11	Interleukin 11	1.83095	3.28256	1.792815466	0.0388086	Extracellular Space	cytokine
Ttn	Titin	0.31577	0.565256	1.790084884	0.0124402	unknown	kinase
Nrarp	Notch-regulated ankyrin repeat protein	2.70508	4.83116	1.785955334	0.0225306	Nucleus	transcription regulator
Rnf122	Ring finger protein 122	1.70215	3.03882	1.78528574	0.0225306	unknown	other
Lrrc32	Leucine rich repeat containing 32	1.00367	1.78675	1.780219333	0.0307235	Plasma Membrane	other
Gm13889	Predicted gene 13889	42.5227	75.4709	1.774837573	0.0124402	unknown	other
Fstl4	Follistatin-like 4	4.4257	7.85415	1.77466904	0.0124402	unknown	other
Csmp1	Cysteine-serine-rich nuclear protein 1	18.0467	31.8958	1.767402953	0.0124402	Nucleus	transcription regulator
Dusp1	Dual specificity phosphatase 1	13.102	23.0889	1.762243153	0.0124402	Nucleus	phosphatase
Lcmt2	Leucine carboxyl methyltransferase 2	5.08249	8.94468	1.759900665	0.0124402	unknown	enzyme
Cwc25	CWC25 spliceosome-associated protein homolog	12.6848	22.243	1.753510416	0.0124402	unknown	other
Doc2b	Double C2, beta	8.21059	14.2829	1.739569115	0.0124402	Cytoplasm	transporter
Maff	V-maf musculoaponeurotic fibrosarcoma oncogene family, protein F (avian)	21.3883	37.1484	1.736853415	0.0124402	Nucleus	transcription regulator
Wfs1	Wolfram syndrome 1 homolog (human)	15.032	26.1052	1.736637931	0.0124402	Cytoplasm	enzyme
Dusp5	Dual specificity phosphatase 5	8.68065	15.0493	1.733658811	0.0307235	Nucleus	phosphatase
Inf2	Inverted formin, FH2 and WH2 domain containing	9.91076	17.1681	1.732272626	0.0124402	unknown	other
Dgkh	Diacylglycerol kinase, eta	18.0494	31.2405	1.730829962	0.0124402	Cytoplasm	kinase
Tiparp	TCDD-inducible poly(ADP-ribose) polymerase	25.483	44.0828	1.729890836	0.0124402	unknown	other
Lct	Lactase	5.24767	9.07122	1.728619091	0.0124402	Plasma Membrane	enzyme
Kcnh7	Potassium voltage-gated channel, subfamily H (eag-related), member 7	9.30062	16.0269	1.723205787	0.0124402	Plasma Membrane	ion channel
Apold1	Apolipoprotein L domain containing 1	10.5025	18.0628	1.719852691	0.0124402	unknown	other
Sipa1l3	Signal-induced proliferation-associated 1 like 3	8.62413	14.8148	1.717827295	0.0124402	unknown	other
6430411K18Rik	RIKEN cDNA 6430411K18 gene, non-coding RNA	4.74648	8.13546	1.71399987	0.0124402	unknown	other
Cxcl10	Chemokine (C-X-C motif) ligand 10	28.8546	49.0808	1.700970358	0.0124402	Extracellular Space	cytokine
Cdkn1a	Cyclin-dependent kinase inhibitor 1A (P21)	6.49421	11.0082	1.695083098	0.0124402	Nucleus	kinase
Igsf9b	Immunoglobulin superfamily, member 9B	2.49586	4.22986	1.694748272	0.0307235	unknown	other
Aff1	AF4/FMR2 family, member 1	3.57581	6.05272	1.692683217	0.0124402	Nucleus	transcription regulator
Grin2b	Glutamate receptor, ionotropic, NMDA2B (epsilon 2)	55.286	93.2179	1.686104555	0.0124402	Plasma Membrane	ion channel
Hr	Hairless	1.19878	2.01611	1.681806819	0.0307235	Nucleus	transcription regulator
Iqsec2	IQ motif and Sec7 domain 2	13.8502	23.2826	1.681025955	0.0124402	Cytoplasm	other
Dsp	Desmoplakin	4.43602	7.44933	1.679282558	0.0124402	Plasma Membrane	other
Zfhx2	Zinc finger homeobox 2	1.37119	2.30084	1.677987537	0.0225306	Nucleus	other
Dyrk1b	Dual-specificity tyrosine-(Y)-phosphorylation regulated kinase 1b	3.56228	5.97322	1.676799277	0.0124402	Nucleus	kinase
Fam65a	Family with sequence similarity 65, member A	5.76374	9.57649	1.661507724	0.0124402	Cytoplasm	other
Pim1	Proviral integration site 1	11.3869	18.9171	1.661296982	0.0225306	Cytoplasm	kinase
Hs6st3	Heparan sulfate 6-O-sulfotransferase 3	9.45639	15.6935	1.659570595	0.0225306	unknown	enzyme
Slc2a1	Solute carrier family 2 (facilitated glucose transporter), member 1	19.0634	31.5498	1.654991721	0.0124402	Plasma Membrane	transporter
Soga2	SOGA family member 2, coiled-coil domain-containing protein 165	4.57473	7.53402	1.646877218	0.0124402	unknown	other
Nfil3	Nuclear factor, interleukin 3, regulated	16.8631	27.7442	1.645257046	0.0124402	Nucleus	transcription regulator
Egr3	Early growth response 3	9.10872	14.9516	1.641465013	0.0307235	Nucleus	transcription regulator
Sema5b	Sema domain, seven thrombospondin repeats (type 1 and type 1-like), transmembrane domain (TM) and short cytoplasmic domain, (semaphorin) 5B	1.83477	2.999	1.634538093	0.0307235	Plasma Membrane	other
Rph3a	Rabphilin 3A	24.3221	39.6359	1.629627239	0.0124402	Plasma Membrane	transporter
Gm2115	Predicted gene 2115	21.8874	35.6562	1.629071584	0.0124402	unknown	other
Mast4	Microtubule associated serine/threonine kinase family member 4	5.40195	8.78573	1.626400992	0.0124402	unknown	kinase
Tac1	Tachykinin 1	9.02419	14.6732	1.625986185	0.0307235	Extracellular Space	other
Shank1	SH3/ankyrin domain gene 1	21.9651	35.7094	1.625732619	0.0124402	Cytoplasm	other
Map3k13	Mitogen-activated protein kinase kinase kinase 13	2.28316	3.70695	1.623607602	0.0388086	Cytoplasm	kinase
Ncor2	Nuclear receptor co-repressor 2	6.26093	10.1565	1.622201462	0.0124402	Nucleus	transcription regulator
Gpc4	Glypican 4	6.0968	9.8734	1.619438858	0.0124402	Plasma Membrane	transmembrane receptor
Shisa7	Shisa homolog 7	7.80255	12.6101	1.616145401	0.0124402	unknown	other

Kcnq3	Potassium voltage-gated channel, subfamily Q, member 3	23.9148	38.6472	1.616038983	0.0124402	Plasma Membrane	ion channel
AI414108	Expressed sequence AI414108	2.10251	3.39368	1.614106755	0.0464016	unknown	other
Nfkb1	Nuclear factor of kappa light chain gene enhancer in B-cells 1, p105	15.1769	24.351	1.604477991	0.0225306	Nucleus	transcription regulator
Per1	Period homolog 1 (Drosophila)	7.26696	11.6375	1.601420301	0.0307235	Nucleus	other
Fat4	FAT tumor suppressor homolog 4 (Drosophila)	4.04595	6.46438	1.597740379	0.0225306	unknown	other
Elmsan1	ELM2 and Myb/SANT-like domain containing 1	3.02368	4.81953	1.593927489	0.0307235	Nucleus	other
Sema5a	Sema domain, seven thrombospondin repeats (type 1 and type 1-like), transmembrane domain (TM) and short cytoplasmic domain, (semaphorin) 5A	8.28422	13.1702	1.589788669	0.0124402	Plasma Membrane	transmembrane receptor
Mdga1	MAM domain containing glycosylphosphatidylinositol anchor 1	5.68312	9.03217	1.589298373	0.0225306	Plasma Membrane	other
Ankrd13a	Ankyrin repeat domain 13a	15.667	24.8852	1.588389798	0.0225306	Plasma Membrane	other
Mll2	Myeloid/lymphoid or mixed-lineage leukemia 2	3.95437	6.27065	1.585750723	0.0124402	Nucleus	transcription regulator
Siah2	Seven in absentia 2	7.80205	12.3562	1.583713094	0.0388086	Nucleus	transcription regulator
Nr4a3	Nuclear receptor subfamily 4, group A, member 3	13.4583	21.313	1.58362857	0.0225306	Nucleus	ligand-dependent nuclear receptor
Mn1	Meningioma 1	4.35686	6.89478	1.582512615	0.0307235	Nucleus	other
Eif2c2	Eukaryotic translation initiation factor 2C, 2	6.95175	10.9573	1.576188412	0.0307235	Cytoplasm	Other
Zbtb20	Zinc finger and BTB domain containing 20	23.0167	36.2526	1.575060232	0.0225306	Nucleus	other
Epha6	Eph receptor A6	63.6171	100.197	1.575001279	0.0464016	Plasma Membrane	kinase
Camta2	Calmodulin binding transcription activator 2	20.8301	32.782	1.573780132	0.0124402	Nucleus	other
Zmiz1	Zinc finger, MIZ-type containing 1	2.54128	3.98924	1.569777406	0.0307235	Nucleus	other
Fam107b	Family with sequence similarity 107, member B	19.5676	30.6773	1.567758129	0.0225306	unknown	other
Gpr19	G protein-coupled receptor 19	15.098	23.65	1.566437274	0.0464016	Plasma Membrane	G-protein coupled receptor
Sez6	Seizure related gene 6	17.5049	27.4139	1.566070326	0.0225306	Extracellular Space	other
Crem	CAMP responsive element modulator	13.6105	21.202	1.557769741	0.0388086	Nucleus	transcription regulator
Cebpb	CCAAT/enhancer binding protein (C/EBP), beta	12.4953	19.458	1.557222397	0.0464016	Nucleus	transcription regulator
Prkcd	Protein kinase C, delta	10.7477	16.7331	1.55689322	0.0225306	Cytoplasm	kinase
Arid1a	AT rich interactive domain 1A (Swi1 like)	5.21877	8.10715	1.553459899	0.0307235	Nucleus	transcription regulator
Grin2a	Glutamate receptor, ionotropic, NMDA2A (epsilon 1)	51.877	80.0349	1.542782835	0.0307235	Plasma Membrane	ion channel
Cacna1e	Calcium channel, voltage-dependent, R type, alpha 1E subunit	36.8218	56.5444	1.535621857	0.0307235	Plasma Membrane	ion channel
Crtc1	CREB regulated transcription coactivator 1	11.9256	18.235	1.529072698	0.0388086	Nucleus	transcription regulator
9830001H06Rik	RIKEN cDNA 9830001H06 gene	2.98005	4.5559	1.528800335	0.0307235	uknown	other
Adamts4	A disintegrin-like and metallopeptidase (reprolysin type) with thrombospondin type 1 motif, 4	15.0069	22.9266	1.527732547	0.0388086	Extracellular Space	peptidase
Fosl2	Fos-like antigen 2	11.1496	16.961	1.521219144	0.0464016	Nucleus	transcription regulator
Pcdh8	Protocadherin 8	25.0617	37.8404	1.509888484	0.0464016	Plasma Membrane	other
Celsr2	Cadherin EGF LAG seven-pass G-type receptor 2	16.8974	25.4704	1.507362075	0.0124402	Plasma Membrane	G-protein coupled receptor
R3hdm2	R3H domain containing 2	10.0863	15.1986	1.506844976	0.0464016	Nucleus	other
Nov	Nephroblastoma overexpressed gene	103.661	66.7471	0.643898413	0.0307235	Extracellular Space	growth factor
Crym	Crystallin, mu	264.877	167.842	0.633660504	0.0307235	Cytoplasm	enzyme
Nnat	Neuronatin	259.761	161.172	0.620462963	0.0307235	Plasma Membrane	transporter
Ccl9	Chemokine (C-C motif) ligand 9	35.8664	21.2817	0.593360584	0.0124402	Extracellular Space	cytokine
Cpne2	Copine II	6.48767	3.82828	0.590085536	0.0124402	unknown	other
Cpne7	Copine VII	130.922	71.153	0.543474782	0.0124402	unknown	transporter
Itgbl1	Integrin, beta-like 1	6.05808	3.15987	0.521595381	0.0124402	unknown	other
Scml4	Sex comb on midleg-like 4 (Drosophila)	1.3238	0.661393	0.499615451	0.0124402	unknown	other
Trhr	Thyrotropin releasing hormone receptor	0.897154	0.437655	0.487826488	0.0464016	Plasma Membrane	G-protein coupled receptor
Grp	Gastrin releasing peptide	18.5518	8.76831	0.472638809	0.0124402	Extracellular Space	growth factor
Fibin	Fin bud initiation factor homolog	1.70272	0.784839	0.460933331	0.0225306	unknown	other
Angptl4	Angiopoietin-like 4	30.0529	13.4086	0.446168325	0.0124402	Extracellular Space	other
Col6a1	Collagen, type VI, alpha 1	2.5136	1.06723	0.424580495	0.0124402	Extracellular Space	other
Dcn	Decorin	17.1931	6.00561	0.349305194	0.0124402	Extracellular Space	other
Ccl17	Chemokine (C-C motif) ligand 17	3.5803	1.01126	0.282450508	0.0307235	Extracellular Space	cytokine
Ttr	Transthyretin	3.99007	0.819246	0.205321982	0.0124402	Extracellular Space	transporter
Control vs. LTP with APV (125 genes)							
Xlr3b	X-linked lymphocyte-regulated 3B	0.154514	1.81916	11.7734889	0.0124402	Nucleus	other
Has1	Hyaluronan synthase1	0.145925	1.22684	8.407343391	0.0124402	Plasma Membrane	enzyme
Trh	Thyrotropin releasing hormone	1.20911	9.62441	7.959953484	0.0124402	Extracellular Space	other
Egr2	Early growth response 2	3.5251	19.4602	5.520465791	0.0124402	Nucleus	transcription regulator
Esm1	Endothelial cell-specific molecule 1	0.204663	0.953682	4.659774047	0.0124402	Extracellular Space	growth factor
Inhba	Inhibin beta-A	4.30587	19.4424	4.515325524	0.0124402	Extracellular Space	growth factor
Thbs1	Thrombospondin 1	3.13313	12.2732	3.917219578	0.0124402	Extracellular Space	other
Egr4	Early growth response 4	7.9458	30.8467	3.882134225	0.0124402	Nucleus	transcription regulator
Areg	Amphiregulin	0.397247	1.48012	3.725928527	0.0124402	Extracellular Space	growth factor
Arc	Activity regulated cytoskeletal-associated protein	61.8026	203.101	3.286267683	0.0124402	Cytoplasm	other
Fos	FBJ osteosarcoma oncogene	104.082	339.196	3.258911106	0.0124402	Nucleus	transcription regulator
Klf4	Kruppel-like factor 4 (gut)	3.6239	11.5158	3.1777376	0.0124402	Nucleus	transcription regulator
Sik1	Salt inducible kinase 1	3.20985	10.1293	3.155677994	0.0124402	Cytoplasm	kinase
Rasl11a	RAS-like, family 11, member A	15.8113	49.3388	3.120462772	0.0124402	Nucleus	other
Tinf2	Terf1 (TRF1)-interacting nuclear factor 2	11.1058	33.0469	2.975640008	0.0124402	Nucleus	other

Btg2	B-cell translocation gene 2, anti-proliferative	15.1533	44.6641	2.947475865	0.0124402	Nucleus	transcription regulator
Cyr61	Cysteine rich protein 61	6.21073	18.0732	2.910001708	0.0124402	Extracellular Space	other
Gem	GTP binding protein (gene overexpressed in skeletal muscle)	20.0825	58.2425	2.900154984	0.0124402	Plasma Membrane	enzyme
Nr4a1	Nuclear receptor subfamily 4, group A, member 1	14.5828	40.6345	2.786453349	0.0124402	Nucleus	ligand-dependent nuclear receptor
Ghsr	Growth hormone secretagogue receptor	0.969501	2.66125	2.744969273	0.0124402	Plasma Membrane	G-protein coupled receptor
Espl1	Extra spindle poles-like 1 (S. cerevisiae)	0.267412	0.732568	2.739476067	0.0124402	Nucleus	peptidase
Junb	Jun-B oncogene	110.789	298.779	2.696840129	0.0124402	Nucleus	transcription regulator
3930402G23Rik	RIKEN cDNA 3930402G23 gene	0.295745	0.791488	2.676263188	0.0124402	unknown	other
Cenpa	Centromere protein A	3.02543	7.80359	2.579336501	0.0124402	Nucleus	other
Fosb	FBJ osteosarcoma oncogene B	11.0894	28.5279	2.572533742	0.0124402	Nucleus	transcription regulator
Egr1	Early growth response 1	9.96789	24.6276	2.470700266	0.0124402	Nucleus	transcription regulator
Hist1h4a	Histone cluster 1, H4a	51.0824	123.008	2.408024382	0.0124402	Nucleus	other
Ppp1r3g	Protein phosphatase 1, regulatory (inhibitor) subunit 3G	2.11439	5.07707	2.401190724	0.0124402	Cytoplasm	other
Gja4	Gap junction protein, alpha 4	0.725493	1.73601	2.392866649	0.0124402	Plasma Membrane	transporter
Trmt61b	tRNA methyltransferase 61B	10.672	25.4018	2.380228372	0.0124402	unknown	other
Dom3z	DOM-3 homolog Z (C. elegans)	4.88464	11.4136	2.336631126	0.0124402	unknown	other
Gm13889	Predicted gene 13889	42.5227	99.0353	2.328998968	0.0124402	unknown	other
Gm129	Gene model 129, (NCBI)	7.00864	16.2007	2.311533066	0.0124402	unknown	other
4930523C07Rik	RIKEN cDNA 4930523C07 gene	1.64527	3.76342	2.287417958	0.0124402	unknown	other
Aldh1a3	Aldehyde dehydrogenase family 1, subfamily A3	0.753424	1.69429	2.248791647	0.0124402	Cytoplasm	enzyme
Kcne4	Potassium voltage-gated channel, Isk-related subfamily, gene 4	2.29907	5.14783	2.239086091	0.0124402	Plasma Membrane	ion channel
Tpbg	Trophoblast glycoprotein	4.03427	8.99308	2.229175187	0.0124402	Plasma Membrane	other
Npas4	Neuronal PAS domain protein 4	8.41951	18.4472	2.191000783	0.0124402	Nucleus	transcription regulator
Arl4d	ADP-ribosylation factor-like 4D	11.5731	25.17	2.174871254	0.0124402	Nucleus	enzyme
Cartpt	CART prepropeptide	1.56793	3.39806	2.167226591	0.0464016	Extracellular Space	other
Aim1	Absent in melanoma 1	0.331929	0.709099	2.136293694	0.0124402	Extracellular Space	other
Foxc1	Forkhead box C1	0.677113	1.44628	2.135953145	0.0124402	Nucleus	transcription regulator
Nrarp	Notch-regulated ankyrin repeat protein	2.70508	5.75612	2.127884729	0.0124402	Nucleus	transcription regulator
Errfi1	ERBB receptor feedback inhibitor 1	56.1768	118.764	2.114124003	0.0124402	Cytoplasm	other
Ier2	Immediate early response 2	12.5639	26.466	2.106503043	0.0124402	Cytoplasm	other
Bmf	Bcl2 modifying factor	0.408524	0.857623	2.099316953	0.0225306	Cytoplasm	other
Dusp1	Dual specificity phosphatase 1	13.102	27.504	2.099215096	0.0124402	Nucleus	phosphatase
Ccnl1	Cyclin L1	26.5044	55.503	2.094114026	0.0124402	Nucleus	other
Cwc25	CWC25 spliceosome-associated protein homolog	12.6848	26.4455	2.084815912	0.0124402	unknown	other
Ppp1r15a	Protein phosphatase 1, regulatory (inhibitor) subunit 15A	20.2024	41.768	2.067475166	0.0124402	Cytoplasm	other
Gpr19	G protein-coupled receptor 19	15.098	30.8176	2.041175174	0.0124402	Plasma Membrane	G-protein coupled receptor
Nr4a2	Nuclear receptor subfamily 4, group A, member 2	8.33552	17.0065	2.040255738	0.0124402	Nucleus	ligand-dependent nuclear receptor
Tiparp	TCDD-inducible poly(ADP-ribose) polymerase	25.483	51.845	2.034493964	0.0124402	unknown	other
Gjb2	Gap junction protein, beta 2	0.933745	1.89877	2.033492965	0.0307235	Plasma Membrane	transporter
Il12b	Interleukin 12b	2.27201	4.56982	2.011358155	0.0124402	Extracellular Space	cytokine
Dusp6	Dual specificity phosphatase 6	55.2217	110.556	2.002038891	0.0124402	Cytoplasm	phosphatase
Sox11	SRY-box containing gene 11	3.11506	6.22382	1.997977034	0.0124402	Nucleus	transcription regulator
Nptx2	Neuronal pentraxin 2	47.933	95.0478	1.98292897	0.0124402	Extracellular Space	other
Gpr3	G-protein coupled receptor 3	3.78124	7.42551	1.96377821	0.0124402	Plasma Membrane	G-protein coupled receptor
Rfx4	Regulatory factor X, 4 (influences HLA class II expression)	1.00393	1.96062	1.952935091	0.0124402	Nucleus	transcription regulator
Kdm6b	KDM1 lysine (K)-specific demethylase 6B	1.81754	3.54298	1.949324131	0.0124402	Extracellular Space	other
Nfil3	Nuclear factor, interleukin 3, regulated	16.8631	32.7973	1.944910813	0.0124402	Nucleus	transcription regulator
Il6	Interleukin 6	15.0086	29.045	1.935219216	0.0124402	Extracellular Space	cytokine
Ccrl2	Chemokine (C-C motif) receptor-like 2	2.24667	4.33	1.927294447	0.0124402	Plasma Membrane	G-protein coupled receptor
Cyp1b1	Cytochrome P450, family 1, subfamily b, polypeptide 1	1.36252	2.62043	1.923232259	0.0124402	Cytoplasm	enzyme
Pax6	Paired box gene 6	4.07291	7.8241	1.921009961	0.0124402	Nucleus	transcription regulator
Ak7	Adenylate kinase 7	1.38547	2.6197	1.890840931	0.0124402	Cytoplasm	kinase
Klf2	Kruppel-like factor 2 (lung)	1.57287	2.95168	1.876612786	0.0307235	Nucleus	transcription regulator
Homer1	Homer homolog 1 (Drosophila)	100.354	187.929	1.87265093	0.0124402	Plasma Membrane	other
Arl5b	ADP-ribosylation factor-like 5B	10.9664	20.3091	1.851942107	0.0124402	unknown	enzyme
Rnf217	Ring finger protein 217	8.29902	15.2522	1.837827041	0.0124402	unknown	enzyme
Csrnp1	Cysteine-serine-rich nuclear protein 1	18.0467	33.0304	1.830275722	0.0124402	Nucleus	transcription regulator
Il11	Interleukin 11	1.83095	3.33588	1.821936907	0.0307235	Extracellular Space	cytokine
Rnf122	Ring finger protein 122	1.70215	3.06627	1.80141053	0.0124402	unknown	other
Apold1	Apolipoprotein L domain containing 1	10.5025	18.9146	1.800959827	0.0124402	unknown	other
Plk3	Polo-like kinase 3 (Drosophila)	5.48893	9.85727	1.795846449	0.0124402	Nucleus	kinase
Per1	Period homolog 1 (Drosophila)	7.26696	12.967	1.784376434	0.0124402	Nucleus	other
Maff	V-maf musculoaponeurotic fibrosarcoma oncogene family, protein F (avian)	21.3883	38.0332	1.778221449	0.0124402	Nucleus	transcription regulator
Bag3	Bcl2-associated athanogene 3	3.11515	5.50618	1.767551193	0.0307235	Cytoplasm	other
Rgs4	Regulator of G-protein signaling 4	159.739	282.233	1.76684196	0.0124402	Cytoplasm	other
Fosl2	Fos-like antigen 2	11.1496	19.6916	1.766131788	0.0124402	Nucleus	transcription regulator
Rrad	Ras-related associated with diabetes	2.65355	4.68272	1.764702513	0.0225306	Cytoplasm	enzyme
Trib1	Tribbles homolog 1 (Drosophila)	5.18027	9.05974	1.748894181	0.0124402	Cytoplasm	kinase

Vps37b	Vacuolar protein sorting 37B (yeast)	9.60922	16.6934	1.73722305	0.0124402	Cytoplasm	other
Neat1	Nuclear paraspeckle assembly transcript 1	9.28607	16.0726	1.730823963	0.0124402	Nucleus	other
Lmbr1l	Limb region 1 like	2.9887	5.15936	1.72628899	0.0388086	Plasma Membrane	other
Dusp5	Dual specificity phosphatase 5	8.68065	14.9339	1.720371337	0.0388086	Nucleus	phosphatase
Gadd45g	Growth arrest and DNA-damage-inducible 45 gamma	38.9467	66.9749	1.71965362	0.0124402	Nucleus	other
Bhlhe40	Basic helix-loop-helix family, member e40	29.4365	50.2916	1.708479575	0.0124402	Nucleus	transcription regulator
Frmd6	FERM domain containing 6	11.5625	19.7062	1.704324443	0.0124402	Cytoplasm	other
Tac1	Tachykinin 1	9.02419	15.2729	1.692435673	0.0307235	Extracellular Space	other
Siah2	Seven in absentia 2	7.80205	13.1781	1.689056982	0.0124402	Nucleus	transcription regulator
Nfkbie	Nuclear factor of kappa light polypeptide gene enhancer in B-cells inhibitor, epsilon	2.89311	4.86203	1.680556446	0.0464016	Nucleus	transcription regulator
Pvr	Poliovirus receptor	4.72537	7.84977	1.661197954	0.0225306	Plasma Membrane	other
Irs2	Insulin receptor substrate 2	11.9626	19.6774	1.644910399	0.0124402	Cytoplasm	enzyme
Nfkb1	Nuclear factor of kappa light chain gene enhancer in B-cells 1, p105	15.1769	24.9487	1.643859503	0.0124402	Nucleus	transcription regulator
Ptgs2	Prostaglandin-endoperoxide synthase 2	60.02	98.4376	1.640080923	0.0124402	Cytoplasm	enzyme
Stk40	Serine/threonine kinase 40	8.63235	14.1102	1.634575482	0.0124402	Cytoplasm	kinase
Arrdc3	Arrestin domain containing 3	17.9833	29.3852	1.634028334	0.0124402	Plasma Membrane	other
Crem	CAMP responsive element modulator	13.6105	22.0388	1.619248042	0.0225306	Nucleus	transcription regulator
Spry2	Sprouty homolog 2 (Drosophila)	32.5639	52.6299	1.616201413	0.0124402	Plasma Membrane	other
Aff1	AF4/FMR2 family, member 1	3.57581	5.75597	1.609694602	0.0307235	Nucleus	transcription regulator
Cd24a	CD24a antigen	7.35762	11.8119	1.605390205	0.0307235	Plasma Membrane	other
Tet3	Tet methylcytosine dioxygenase 3	3.87407	6.18293	1.595974942	0.0124402	Nucleus	other
Fam107b	Family with sequence similarity 107, member B	19.5676	31.2042	1.594682264	0.0225306	unknown	other
Mirg	MiRNA containing gene	8.26192	13.1612	1.592989768	0.0225306	unknown	other
Elmsan1	ELM2 and Myb/SANT-like domain containing 1	3.02368	4.81395	1.592083497	0.0388086	Nucleus	other
1190002N15Rik	RIKEN cDNA 1190002N15 gene	13.9153	22.0972	1.587981384	0.0124402	Cytoplasm	other
Rasl11b	RAS-like, family 11, member B	26.0711	40.7386	1.562592939	0.0225306	unknown	enzyme
Cdk11b	Cyclin-dependent kinase 11B	19.5217	30.395	1.556988188	0.0307235	Nucleus	kinase
Dnajb5	DnaJ (Hsp40) homolog, subfamily B, member 5	48.5464	74.8859	1.542563629	0.0124402	Cytoplasm	other
Gadd45b	Growth arrest and DNA-damage-inducible 45 beta	92.4912	141.63	1.531280946	0.0307235	Cytoplasm	other
Pqlc1	PQ loop repeat containing 1	18.4737	28.0537	1.518576934	0.0388086	unknown	other
Ifrd1	Interferon-related developmental regulator 1	59.7856	90.7734	1.518316965	0.0388086	Nucleus	other
Jund	Jun proto-oncogene related gene d	55.8745	83.9123	1.501800316	0.0464016	Nucleus	transcription regulator
Dnajb1	DnaJ (Hsp40) homolog, subfamily B, member 1	36.3227	54.506	1.500602638	0.0388086	Nucleus	other
Slc2a1	Solute carrier family 2 (facilitated glucose transporter), member 1	19.0634	28.5639	1.498359698	0.0388086	Plasma Membrane	transporter
Eprs	Glutamyl-prolyl-tRNA synthetase	48.7692	72.8437	1.493641585	0.0464016	Cytoplasm	enzyme
Il1a	Interleukin 1 alpha	86.7899	57.4984	0.662500753	0.0464016	Extracellular Space	cytokine
Ccl3	Chemokine (C-C motif) ligand 3	197.289	128.159	0.649601559	0.0225306	Extracellular Space	cytokine
Ccl9	Chemokine (C-C motif) ligand 9	35.8664	21.5112	0.599758665	0.0124402	Extracellular Space	cytokine
Zfp273	Zinc finger protein 273	5.45411	3.02355	0.554361895	0.0225306	Nucleus	other
Sele	Selectin, endothelial cell	2.88161	1.17007	0.406047384	0.0124402	Plasma Membrane	transmembrane receptor
Mmp13	Matrix metallopeptidase 13	0.645794	0.20649	0.319746395	0.0307235	Extracellular Space	peptidase
Angptl4	Angiopoietin-like 4	30.0529	8.10918	0.269831372	0.0124402	Extracellular Space	other
Control vs. forskolin (67 genes)							
Xlr3b	X-linked lymphocyte-regulated 3B	0.154514	1.71126	11.07511673	0.0124402	Nucleus	other
Trh	Thyrotropin releasing hormone	1.20911	11.1759	9.243120556	0.0124402	Extracellular Space	other
Has1	Hyaluronan synthase1	0.145925	1.10279	7.557242933	0.0124402	Plasma Membrane	enzyme
Thbs1	Thrombospondin 1	3.13313	11.3223	3.613733208	0.0124402	Extracellular Space	other
Tinf2	Terf1 (TRF1)-interacting nuclear factor 2	11.1058	32.0195	2.883138215	0.0124402	Nucleus	other
Espl1	Extra spindle poles-like 1 (S. cerevisiae)	0.267412	0.762848	2.852703884	0.0124402	Nucleus	peptidase
Gja4	Gap junction protein, alpha 4	0.725493	2.04283	2.815790502	0.0124402	Plasma Membrane	transporter
Sptssb	Serine palmitoyltransferase, small subunit	0.491788	1.384	2.814210023	0.0124402	Cytoplasm	other
3930402G23Rik	RIKEN cDNA 3930402G23 gene	0.295745	0.820929	2.775812268	0.0124402	unknown	other
Gem	GTP binding protein (gene overexpressed in skeletal muscle)	20.0825	54.5182	2.714713594	0.0124402	Plasma Membrane	enzyme
Cyr61	Cysteine rich protein 61	6.21073	16.8442	2.712118095	0.0124402	Extracellular Space	other
Sik1	Salt inducible kinase 1	3.20985	8.64936	2.694635249	0.0124402	Cytoplasm	kinase
Cartpt	CART prepropeptide	1.56793	4.16088	2.653745464	0.0124402	Extracellular Space	other
Il12b	Interleukin 12b	2.27201	5.93568	2.61251623	0.0124402	Extracellular Space	cytokine
Klf4	Kruppel-like factor 4 (gut)	3.6239	9.45911	2.61019936	0.0124402	Nucleus	transcription regulator
Ppp1r3g	Protein phosphatase 1, regulatory (inhibitor) subunit 3G	2.11439	5.4444	2.574924266	0.0124402	Cytoplasm	other
Rasl11a	RAS-like, family 11, member A	15.8113	39.1288	2.474728059	0.0124402	Nucleus	other
Fos	FBJ osteosarcoma oncogene	104.082	252.204	2.423110169	0.0124402	Nucleus	transcription regulator
Inhba	Inhibin beta-A	4.30587	9.96417	2.31408202	0.0124402	Extracellular Space	growth factor
Trmt61b	tRNA methyltransferase 61B	10.672	24.4176	2.288004675	0.0124402	unknown	other
Egr2	Early growth response 2	3.5251	7.90626	2.242845123	0.0124402	Nucleus	transcription regulator
Rab20	RAB20, member RAS oncogene family	3.54401	7.8821	2.224066615	0.0124402	Cytoplasm	enzyme
Hist1h4a	Histone cluster 1, H4a	51.0824	113.598	2.223819972	0.0124402	Nucleus	other
Bmf	Bcl2 modifying factor	0.408524	0.895813	2.192808765	0.0124402	Cytoplasm	other
Dom3z	DOM-3 homolog Z (C. elegans)	4.88464	10.5425	2.158306865	0.0124402	unknown	other
4930523C07Rik	RIKEN cDNA 4930523C07 gene	1.64527	3.5298	2.145419843	0.0124402	unknown	other

Kcne4	Potassium voltage-gated channel, Isk-related subfamily, gene 4	2.29907	4.92816	2.143546925	0.0124402	Plasma Membrane	ion channel
Zic2	Zic finger protein of the cerebellum 2	1.22075	2.54586	2.085480756	0.0124402	Nucleus	transcription regulator
Foxc1	Forkhead box C1	0.677113	1.40506	2.075069993	0.0124402	Nucleus	transcription regulator
Il11	Interleukin 11	1.83095	3.67821	2.008905917	0.0124402	Extracellular Space	cytokine
Slc16a3	Solute carrier family 16 (monocarboxylic acid transporters), member 3	0.666323	1.327	1.991526946	0.0388086	Plasma Membrane	transporter
Tpbg	Trophoblast glycoprotein	4.03427	8.0246	1.98910578	0.0124402	Plasma Membrane	other
Pax6	Paired box gene 6	4.07291	8.05847	1.978553395	0.0124402	Nucleus	transcription regulator
Gjb2	Gap junction protein, beta 2	0.933745	1.83127	1.961215407	0.0225306	Plasma Membrane	transporter
Btg2	B-cell translocation gene 2, anti-proliferative	15.1533	29.5762	1.951801044	0.0124402	Nucleus	transcription regulator
Nrarp	Notch-regulated ankyrin repeat protein	2.70508	5.23362	1.934735034	0.0124402	Nucleus	transcription regulator
Ccnl1	Cyclin L1	26.5044	49.3476	1.861868265	0.0124402	Nucleus	other
Ccrl2	Chemokine (C-C motif) receptor-like 2	2.24667	4.17512	1.858356127	0.0124402	Plasma Membrane	G-protein coupled receptor
Nfkbie	Nuclear factor of kappa light polypeptide gene enhancer in B-cells inhibitor, epsilon	2.89311	5.33813	1.845119172	0.0124402	Nucleus	transcription regulator
Kcnj8	Potassium inwardly-rectifying channel, subfamily J, member 8	1.37025	2.52424	1.842173571	0.0388086	Plasma Membrane	ion channel
Arl4d	ADP-ribosylation factor-like 4D	11.5731	21.2861	1.839272194	0.0124402	Nucleus	enzyme
Tnfaip2	Tumor necrosis factor, alpha-induced protein 2	4.8495	8.79041	1.812643233	0.0124402	Extracellular Space	other
Il6	Interleukin 6	15.0086	26.9754	1.797328355	0.0124402	Extracellular Space	cytokine
Apold1	Apolipoprotein L domain containing 1	10.5025	18.5785	1.768957025	0.0124402	unknown	other
Sphk1	Sphingosine kinase 1	4.65885	8.21756	1.763861153	0.0124402	Cytoplasm	kinase
Fam163b	Family with sequence similarity 163, member B	4.60065	8.11007	1.762810017	0.0124402	unknown	other
Egr4	Early growth response 4	7.9458	13.5805	1.709136947	0.0124402	Nucleus	transcription regulator
Cwc25	CWC25 spliceosome-associated protein homolog	12.6848	21.6125	1.703802368	0.0124402	unknown	other
Maff	V-maf musculoaponeurotic fibrosarcoma oncogene family, protein F (avian)	21.3883	36.3427	1.699181543	0.0124402	Nucleus	transcription regulator
Arc	Activity regulated cytoskeletal-associated protein	61.8026	104.172	1.685555346	0.0124402	Cytoplasm	other
Junb	Jun-B oncogene	110.789	184.81	1.668122225	0.0124402	Nucleus	transcription regulator
Ier2	Immediate early response 2	12.5639	20.8142	1.656662819	0.0124402	Cytoplasm	other
Sox11	SRY-box containing gene 11	3.11506	5.132	1.647481197	0.0124402	Nucleus	transcription regulator
Neat1	Nuclear paraspeckle assembly transcript 1	9.28607	14.9458	1.609481507	0.0124402	Nucleus	other
Vps37b	Vacuolar protein sorting 37B (yeast)	9.60922	15.3488	1.597295238	0.0124402	Cytoplasm	other
Pqlc1	PQ loop repeat containing 1	18.4737	29.3421	1.588321538	0.0124402	unknown	other
Tiparp	TCDD-inducible poly(ADP-ribose) polymerase	25.483	40.3389	1.58297558	0.0124402	unknown	other
Lcmt2	Leucine carboxyl methyltransferase 2	5.08249	7.99305	1.572663486	0.0307235	unknown	enzyme
Egr1	Early growth response 1	9.96789	15.4849	1.553479281	0.0307235	Nucleus	transcription regulator
Gadd45g	Growth arrest and DNA-damage-inducible 45 gamma	38.9467	60.2779	1.547700158	0.0225306	Nucleus	other
Ppp1r15a	Protein phosphatase 1, regulatory (inhibitor) subunit 15A	20.2024	31.2318	1.545945007	0.0307235	Cytoplasm	other
Arrdc3	Arrestin domain containing 3	17.9833	27.7063	1.540671196	0.0307235	Plasma Membrane	other
Slc2a1	Solute carrier family 2 (facilitated glucose transporter), member 1	19.0634	28.5112	1.495595463	0.0464016	Plasma Membrane	transporter
Dcn	Decorin	17.1931	10.9026	0.634127567	0.0388086	Extracellular Space	other
Grp	Gastrin releasing peptide	18.5518	11.4224	0.615704919	0.0464016	Extracellular Space	growth factor
Sele	Selectin, endothelial cell	2.88161	1.52564	0.529442164	0.0124402	Plasma Membrane	transmembrane receptor
Angptl4	Angiopoietin-like 4	30.0529	8.62501	0.286995496	0.0124402	Extracellular Space	other
LTP with APV vs. LTP (24 genes)							
Col6a3	Collagen, type VI, alpha 3	0.401061	1.26853	3.162935314	0.0124402	Extracellular Space	other
Il10	Interleukin 10	0.631201	1.55045	2.456349087	0.0464016	Extracellular Space	cytokine
Sele	Selectin, endothelial cell	1.17007	2.60349	2.225072004	0.0124402	Plasma Membrane	transmembrane receptor
Zic1	Zinc finger protein of the cerebellum 1	1.28209	2.78708	2.17385675	0.0124402	Nucleus	transcription regulator
Ano2	Anoctamin 2	0.607397	1.32013	2.173421996	0.0124402	Plasma Membrane	ion channel
Col23a1	Collagen, type XXIII, alpha 1	0.348567	0.711228	2.04043412	0.0225306	Plasma Membrane	other
Satb2	Special AT-rich sequence binding protein 2	0.978791	1.89228	1.933282999	0.0124402	Nucleus	transcription regulator
Cxcl2	Chemokine (C-X-C motif) ligand 2	27.1032	49.8186	1.838107677	0.0124402	Extracellular Space	cytokine
Il1b	Interleukin 1 beta	27.6107	48.0293	1.739517651	0.0124402	Extracellular Space	cytokine
Il1a	Interleukin 1 alpha	57.4984	95.655	1.663611509	0.0124402	Extracellular Space	cytokine
Angptl4	Angiopoietin-like 4	8.10918	13.4086	1.653508739	0.0225306	Extracellular Space	other
Wipf3	WAS/WASL interacting protein family, member 3	37.5678	58.484	1.556758714	0.0124402	Plasma Membrane	other
Sez6	Seizure related gene 6	17.6208	27.4139	1.555769318	0.0225306	Extracellular Space	other
Shank1	SH3/ankyrin domain gene 1	23.5436	35.7094	1.516734909	0.0464016	Cytoplasm	other
Cpne7	Copine VII	109.54	71.153	0.649561804	0.0307235	unknown	transporter
Rgs4	Regulator of G-protein signaling 4	282.233	172.699	0.611902223	0.0124402	Cytoplasm	other
Errfi1	ERBB receptor feedback inhibitor 1	118.764	71.886	0.60528443	0.0124402	Cytoplasm	other
Dcn	Decorin	11.5481	6.00561	0.520051783	0.0124402	Extracellular Space	other
Gm129	Gene model 129, (NCBI)	16.2007	8.23754	0.508468153	0.0124402	unknown	other
Col6a1	Collagen, type VI, alpha 1	2.43247	1.06723	0.438743335	0.0124402	Extracellular Space	other
Egr2	Early growth response 2	19.4602	7.98169	0.410154572	0.0124402	Nucleus	transcription regulator
Clca1	Chloride channel calcium activated 1	0.759641	0.285465	0.375789353	0.0124402	Plasma Membrane	ion channel
Ttr	Transthyretin	5.46587	0.819246	0.149883916	0.0124402	Extracellular Space	transporter
Xlr3b	X-linked lymphocyte-regulated 3B	1.81916	0.169736	0.093304602	0.0124402	Nucleus	other
Forskolin vs. LTP (18 genes)							
Npas4	Neuronal PAS domain protein 4	5.64827	17.0605	3.020482378	0.0124402	Nucleus	transcription regulator

Fosb	FBJ osteosarcoma oncogene B	12.6997	28.3375	2.231351922	0.0124402	Nucleus	transcription regulator
Egr4	Early growth response 4	13.5805	29.3352	2.160097198	0.0124402	Nucleus	transcription regulator
Col6a3	Collagen, type VI, alpha 3	0.590885	1.26853	2.146830602	0.0124402	Extracellular Space	other
Satb2	Special AT-rich sequence binding protein 2	0.989159	1.89228	1.913019039	0.0307235	Nucleus	transcription regulator
Arc	Activity regulated cytoskeletal-associated protein	104.172	189.486	1.818972469	0.0124402	Cytoplasm	other
Col22a1	Collagen, type XXII, alpha 1	0.570378	1.00934	1.769598407	0.0388086	Extracellular Space	other
Sele	Selectin, endothelial cell	1.52564	2.60349	1.706490391	0.0388086	Plasma Membrane	transmembrane receptor
Egr1	Early growth response 1	15.4849	25.3788	1.638938579	0.0124402	Nucleus	transcription regulator
Nr4a1	Nuclear receptor subfamily 4, group A, member 1	21.7041	34.8614	1.606212651	0.0124402	Nucleus	ligand-dependent nuclear receptor
Cxcl2	Chemokine (C-X-C motif) ligand 2	31.1211	49.8186	1.600798172	0.0124402	Extracellular Space	cytokine
Pim1	Proviral integration site 1	11.8806	18.9171	1.592268067	0.0124402	Cytoplasm	kinase
Wipf3	WAS/WASL interacting protein family, member 3	37.187	58.484	1.572700137	0.0124402	Plasma Membrane	other
Dcn	Decorin	10.9026	6.00561	0.550842001	0.0124402	Extracellular Space	other
Col6a1	Collagen, type VI, alpha 1	2.17234	1.06723	0.491281291	0.0124402	Extracellular Space	other
C2cd4a	C2 calcium-dependent domain containing 4A	1.6789	0.583804	0.347730061	0.0124402	unknown	other
Ttr	Transthyretin	2.76076	0.819246	0.296746548	0.0124402	Extracellular Space	transporter
Xlr3b	X-linked lymphocyte-regulated 3B	1.71126	0.169736	0.099187733	0.0124402	Nucleus	other
LTP with APV vs. forskolin (24 genes)							
Ece1	Endothelin converting enzyme-like 1	0.216979	0.642666	2.961873448	0.0388086	Plasma Membrane	peptidase
Pld5	Phospholipase D family, member 5	0.306339	0.859188	2.804687434	0.0124402	unknown	other
Btg2	B-cell translocation gene 2, anti-proliferative	44.6641	29.5762	0.662193613	0.0464016	Nucleus	transcription regulator
Fbxo33	F-box protein 33	67.8535	44.6603	0.658186801	0.0388086	unknown	other
1190002N15Rik	RIKEN cDNA 1190002N15 gene	22.0972	14.3243	0.648240921	0.0124402	Cytoplasm	other
Egr1	Early growth response 1	24.6276	15.4849	0.628762029	0.0124402	Nucleus	transcription regulator
Dusp1	Dual specificity phosphatase 1	27.504	17.1622	0.62398835	0.0124402	Nucleus	phosphatase
Ptgs2	Prostaglandin-endoperoxide synthase 2	98.4376	61.3528	0.623266035	0.0124402	Cytoplasm	enzyme
Junb	Jun-B oncogene	298.779	184.81	0.618549089	0.0124402	Nucleus	transcription regulator
Errfi1	ERBB receptor feedback inhibitor 1	118.764	71.1491	0.5990781	0.0124402	Cytoplasm	other
Rgs4	Regulator of G-protein signaling 4	282.233	161.537	0.572355336	0.0124402	Cytoplasm	other
Gm13889	Predicted gene 13889	99.0353	56.4404	0.569902095	0.0124402	unknown	other
Homer1	Homer homolog 1 (Drosophila)	187.929	104.766	0.557477313	0.0124402	Plasma Membrane	other
Gm129	Gene model 129, (NCBI)	16.2007	8.89097	0.548800614	0.0124402	unknown	other
Nptx2	Neuronal pentraxin 2	95.0478	51.2848	0.539568488	0.0124402	Extracellular Space	other
Nr4a1	Nuclear receptor subfamily 4, group A, member 1	40.6345	21.7041	0.534129325	0.0124402	Nucleus	ligand-dependent nuclear receptor
Arc	Activity regulated cytoskeletal-associated protein	203.101	104.172	0.512906941	0.0124402	Cytoplasm	other
Inhba	Inhibin beta-A	19.4424	9.96417	0.512495769	0.0124402	Extracellular Space	growth factor
Ghsr	Growth hormone secretagogue receptor	2.66125	1.31057	0.492463942	0.0124402	Plasma Membrane	G-protein coupled receptor
Fosb	FBJ osteosarcoma oncogene B	28.5279	12.6997	0.445167446	0.0124402	Nucleus	transcription regulator
Egr4	Early growth response 4	30.8467	13.5805	0.440257657	0.0124402	Nucleus	transcription regulator
Egr2	Early growth response 2	19.4602	7.90626	0.406278239	0.0124402	Nucleus	transcription regulator
Npas4	Neuronal PAS domain protein 4	18.4472	5.64827	0.306185952	0.0124402	Nucleus	transcription regulator
Lars2	Leucyl-tRNA synthetase, mitochondrial	881.882	164.575	0.186617993	0.0225306	Cytoplasm	enzyme

Table 4. List of genes shown in the different regions of the Venn diagram in Figure 3-13

Upregulated genes in black, downregulated genes in blue.

Gene ID	Description	Location	Type
LTP only (88 genes)			
Crym	crystallin, mu	Cytoplasm	enzyme
Wfs1	Wolfram syndrome 1 (wolframin)	Cytoplasm	enzyme
Dgkh	diacylglycerol kinase, eta	Cytoplasm	kinase
Map3k13	mitogen-activated protein kinase kinase kinase 13	Cytoplasm	kinase
Pim1	pim-1 oncogene	Cytoplasm	kinase
Prkcd	protein kinase C, delta	Cytoplasm	kinase
Fam65a	family with sequence similarity 65, member A	Cytoplasm	other
Iqsec2	IQ motif and Sec7 domain 2	Cytoplasm	other
Shank1	SH3 and multiple ankyrin repeat domains 1	Cytoplasm	other
Eif2c2	Eukaryotic translation initiation factor 2C, 2	Cytoplasm	other
Doc2b	double C2-like domains, beta	Cytoplasm	transporter
Ccl17	chemokine (C-C motif) ligand 17	Extracellular Space	cytokine
Cxcl10	chemokine (C-X-C motif) ligand 10	Extracellular Space	cytokine
Il10	interleukin 10	Extracellular Space	cytokine
Il1b	interleukin 1, beta	Extracellular Space	cytokine
Il1rn	interleukin 1 receptor antagonist	Extracellular Space	cytokine
Nov	nephroblastoma overexpressed	Extracellular Space	growth factor
Col6a1	collagen, type VI, alpha 1	Extracellular Space	other
Col6a3	collagen, type VI, alpha 3	Extracellular Space	other
Sez6	seizure related 6 homolog (mouse)	Extracellular Space	other
Zfhx4	zinc finger homeobox 4	Extracellular Space	other
Adamts4	ADAM metallopeptidase with thrombospondin type 1 motif, 4	Extracellular Space	peptidase
Ttr	transthyretin	Extracellular Space	transporter
Cdkn1a	cyclin-dependent kinase inhibitor 1A (p21, Cip1)	Nucleus	kinase
Dyrk1b	dual-specificity tyrosine-(Y)-phosphorylation regulated kinase 1B	Nucleus	kinase
Nr4a3	nuclear receptor subfamily 4, group A, member 3	Nucleus	ligand-dependent nuclear receptor
Camta2	calmodulin binding transcription activator 2	Nucleus	other
Mn1	meningioma (disrupted in balanced translocation) 1	Nucleus	other
R3hdm2	R3H domain containing 2	Nucleus	other
Zbtb20	zinc finger and BTB domain containing 20	Nucleus	other
Zfhx2	zinc finger homeobox 2	Nucleus	other
Zmiz1	zinc finger, MIZ-type containing 1	Nucleus	other
Arid1a	AT rich interactive domain 1A (SWI-like)	Nucleus	transcription regulator
Atf3	activating transcription factor 3	Nucleus	transcription regulator
Cebpb	CCAAT/enhancer binding protein (C/EBP), beta	Nucleus	transcription regulator
Crtc1	CREB regulated transcription coactivator 1	Nucleus	transcription regulator
Egr3	early growth response 3	Nucleus	transcription regulator
Hr	hair growth associated	Nucleus	transcription regulator
Mll2	myeloid/lymphoid or mixed-lineage leukemia 2	Nucleus	transcription regulator
Ncor2	nuclear receptor corepressor 2	Nucleus	transcription regulator
Satb2	SATB homeobox 2	Nucleus	transcription regulator
Zic1	Zic family member 1	Nucleus	transcription regulator
Lct	lactase	Plasma Membrane	enzyme
Ccr7	chemokine (C-C motif) receptor 7	Plasma Membrane	G-protein coupled receptor
Celsr2	cadherin, EGF LAG seven-pass G-type receptor 2	Plasma Membrane	G-protein coupled receptor
Gpr63	G protein-coupled receptor 63	Plasma Membrane	G-protein coupled receptor
Niacr1	hydroxycarboxylic acid receptor 2	Plasma Membrane	G-protein coupled receptor
Trhr	thyrotropin-releasing hormone receptor	Plasma Membrane	G-protein coupled receptor
Cacna1e	calcium channel, voltage-dependent, R type, alpha 1E subunit	Plasma Membrane	ion channel
Grin2a	glutamate receptor, ionotropic, N-methyl D-aspartate 2A	Plasma Membrane	ion channel
Grin2b	glutamate receptor, ionotropic, N-methyl D-aspartate 2B	Plasma Membrane	ion channel

Kcnh7	potassium voltage-gated channel, subfamily H (eag-related), member 7	Plasma Membrane	ion channel
Kcnq3	potassium voltage-gated channel, KQT-like subfamily, member 3	Plasma Membrane	ion channel
Epha6	EPH receptor A6	Plasma Membrane	kinase
Ankrd13a	ankyrin repeat domain 13A	Plasma Membrane	other
Dsp	desmoplakin	Plasma Membrane	other
Lrrc32	leucine rich repeat containing 32	Plasma Membrane	other
Mdga1	MAM domain containing glycosylphosphatidylinositol anchor 1	Plasma Membrane	other
Pcdh8	protocadherin 8	Plasma Membrane	other
Procr	protein C receptor, endothelial	Plasma Membrane	other
Sema5b	sema domain, seven thrombospondin repeats (type 1 and type 1-like), transmembrane domain (TM) and short cytoplasmic domain, (semaphorin) 5B	Plasma Membrane	other
Wipf3	WAS/WASL interacting protein family, member 3	Plasma Membrane	other
Cd14	CD14 molecule	Plasma Membrane	transmembrane receptor
Gpc4	glypican 4	Plasma Membrane	transmembrane receptor
Sema5a	sema domain, seven thrombospondin repeats (type 1 and type 1-like), transmembrane domain (TM) and short cytoplasmic domain, (semaphorin) 5A	Plasma Membrane	transmembrane receptor
Nnat	neuronatin	Plasma Membrane	transporter
Rph3a	rabphilin 3A homolog (mouse)	Plasma Membrane	transporter
Hs6st3	heparan sulfate 6-O-sulfotransferase 3	unknown	enzyme
Mast4	microtubule associated serine/threonine kinase family member 4	unknown	kinase
Ttn	titin	unknown	kinase
6430411K18Rik	RIKEN cDNA 6430411K18 gen	unknown	other
AI414108	expressed sequence AI414108	unknown	other
Atoh8	atonal homolog 8 (Drosophila)	unknown	other
Cpne2	copine II	unknown	other
Fat4	FAT tumor suppressor homolog 4 (Drosophila)	unknown	other
Fibin	fin bud initiation factor homolog (zebrafish)	unknown	other
Fstl4	follistatin-like 4	unknown	other
Gm2115	predicted gene 2115	unknown	other
Igfbpl1	insulin-like growth factor binding protein-like 1	unknown	other
Igsf9b	immunoglobulin superfamily, member 9B	unknown	other
Inf2	inverted formin, FH2 and WH2 domain containing	unknown	other
Itgbl1	integrin, beta-like 1 (with EGF-like repeat domains)	unknown	other
Scml4	sex comb on midleg-like 4 (Drosophila)	unknown	other
Shisa7	shisa homolog 7 (Xenopus laevis)	unknown	other
Sipa1l3	signal-induced proliferation-associated 1 like 3	unknown	other
Soga2	SOGA family member 2	unknown	other
9830001H06Rik	RIKEN cDNA 9830001H06 gene	unknown	other
Cpne7	copine VII	unknown	transporter
APV only (38 genes)			
Aldh1a3	aldehyde dehydrogenase 1 family, member A3	Cytoplasm	enzyme
Eprs	glutamyl-prolyl-tRNA synthetase	Cytoplasm	enzyme
Ptgs2	prostaglandin-endoperoxide synthase 2 (prostaglandin G/H synthase and cyclooxygenase)	Cytoplasm	enzyme
Rrad	Ras-related associated with diabetes	Cytoplasm	enzyme
Stk40	serine/threonine kinase 40	Cytoplasm	kinase
Trib1	tribbles homolog 1 (Drosophila)	Cytoplasm	kinase
1190002N15Rik	chromosome 3 open reading frame 58	Cytoplasm	other
Dnajb5	DnaJ (Hsp40) homolog, subfamily B, member 5	Cytoplasm	other
Errfi1	ERBB receptor feedback inhibitor 1	Cytoplasm	other
Frmd6	FERM domain containing 6	Cytoplasm	other
Gadd45b	growth arrest and DNA-damage-inducible, beta	Cytoplasm	other
Rgs4	regulator of G-protein signaling 4	Cytoplasm	other
Dusp6	dual specificity phosphatase 6	Cytoplasm	phosphatase

Ccl3	chemokine (C-C motif) ligand 3-like 1	Extracellular Space	cytokine
Il1a	interleukin 1, alpha	Extracellular Space	cytokine
Areg	amphiregulin	Extracellular Space	growth factor
Aim1	absent in melanoma 1	Extracellular Space	other
Nptx2	neuronal pentraxin II	Extracellular Space	other
Mmp13	matrix metallopeptidase 13 (collagenase 3)	Extracellular Space	peptidase
Cdk11b	cyclin-dependent kinase 11B	Nucleus	kinase
Plk3	polo-like kinase 3	Nucleus	kinase
Cenpa	centromere protein A	Nucleus	other
Dnajb1	DnaJ (Hsp40) homolog, subfamily B, member 1	Nucleus	other
Ifrd1	interferon-related developmental regulator 1	Nucleus	other
Zfp273	zinc finger protein 708	Nucleus	other
Bhlhe40	basic helix-loop-helix family, member e40	Nucleus	transcription regulator
Jund	jun D proto-oncogene	Nucleus	transcription regulator
Rfx4	regulatory factor X, 4 (influences HLA class II expression)	Nucleus	transcription regulator
Gpr3	G protein-coupled receptor 3	Plasma Membrane	G-protein coupled receptor
Cd24a	CD24a antigen	Plasma Membrane	other
Homer1	homer homolog 1 (Drosophila)	Plasma Membrane	other
Lmbr1l	limb region 1 homolog (mouse)-like	Plasma Membrane	other
Pvr	poliovirus receptor	Plasma Membrane	other
Spry2	sprouty homolog 2 (Drosophila)	Plasma Membrane	other
Arl5b	ADP-ribosylation factor-like 5B	unknown	enzyme
Rasl11b	RAS-like, family 11, member B	unknown	enzyme
Gm129	chromosome 1 open reading frame 51	unknown	other
Mirg	miRNA containing gene	unknown	other
FSK only (4 genes)			
Sphk1	sphingosine kinase 1	Cytoplasm	kinase
Sptssb	serine palmitoyltransferase, small subunit B	Cytoplasm	other
Kcnj8	potassium inwardly-rectifying channel, subfamily J, member 8	Plasma Membrane	ion channel
Slc16a3	solute carrier family 16, member 3 (monocarboxylic acid transporter 4)	Plasma Membrane	transporter
LTP and FSK (7 genes)			
Rab20	RAB20, member RAS oncogene family	Cytoplasm	enzyme
Grp	gastrin-releasing peptide	Extracellular Space	growth factor
Dcn	decorin	Extracellular Space	other
Tnfaip2	tumor necrosis factor, alpha-induced protein 2	Extracellular Space	other
Zic2	Zic family member 2	Nucleus	transcription regulator
Lcmt2	leucine carboxyl methyltransferase 2	unknown	enzyme
Fam163b	family with sequence similarity 163, member B	unknown	other
LTP and APV (31 genes)			
Cyp1b1	cytochrome P450, family 1, subfamily B, polypeptide 1	Cytoplasm	enzyme
Irs2	insulin receptor substrate 2	Cytoplasm	enzyme
Ak7	adenylate kinase 7	Cytoplasm	kinase
Bag3	BCL2-associated athanogene 3	Cytoplasm	other
Ccl9	chemokine (C-C motif) ligand 9	Extracellular Space	cytokine
Esm1	endothelial cell-specific molecule 1	Extracellular Space	growth factor
Kdm6b	lysine (K)-specific demethylase 6B	Extracellular Space	other
Tac1	tachykinin, precursor 1	Extracellular Space	other
Nr4a1	nuclear receptor subfamily 4, group A, member 1	Nucleus	ligand-dependent nuclear receptor
Nr4a2	nuclear receptor subfamily 4, group A, member 2	Nucleus	ligand-dependent nuclear receptor
Elmsan1	ELM2 and Myb/SANT-like domain containing 1	Nucleus	other
Per1	period circadian clock 1	Nucleus	other
Tet3	tet methylcytosine dioxygenase 3	Nucleus	other
Dusp1	dual specificity phosphatase 1	Nucleus	phosphatase
Dusp5	dual specificity phosphatase 5	Nucleus	phosphatase
Aff1	AF4/FMR2 family, member 1	Nucleus	transcription regulator

Crem	cAMP responsive element modulator	Nucleus	transcription regulator
Csrnp1	cysteine-serine-rich nuclear protein 1	Nucleus	transcription regulator
Fosb	FBJ murine osteosarcoma viral oncogene homolog B	Nucleus	transcription regulator
Fosl2	FOS-like antigen 2	Nucleus	transcription regulator
Klf2	Kruppel-like factor 2 (lung)	Nucleus	transcription regulator
Nfil3	nuclear factor, interleukin 3 regulated	Nucleus	transcription regulator
Nfkb1	nuclear factor of kappa light polypeptide gene enhancer in B-cells 1	Nucleus	transcription regulator
Npas4	neuronal PAS domain protein 4	Nucleus	transcription regulator
Siah2	siah E3 ubiquitin protein ligase 2	Nucleus	transcription regulator
Ghsr	growth hormone secretagogue receptor	Plasma Membrane	G-protein coupled receptor
Gpr19	G protein-coupled receptor 19	Plasma Membrane	G-protein coupled receptor
Rnf217	ring finger protein 217	unknown	enzyme
Fam107b	family with sequence similarity 107, member B	unknown	other
Gm13889	chromosome 11 open reading frame 96	unknown	other
Rnf122	ring finger protein 122	unknown	other
APV and FSK (3 genes)			
Xlr3b	X-linked lymphocyte-regulated 3C	Nucleus	other
Sele	selectin E	Plasma Membrane	transmembrane receptor
Pqlc1	PQ loop repeat containing 1	unknown	other
All three lists (53 genes)			
Trmt61b	tRNA methyltransferase 61 homolog B (S. cerevisiae)	Cytoplasm	enzyme
Sik1	salt-inducible kinase 1	Cytoplasm	kinase
Arc	activity-regulated cytoskeleton-associated protein	Cytoplasm	other
Bmf	Bcl2 modifying factor	Cytoplasm	other
Ier2	immediate early response 2	Cytoplasm	other
Ppp1r15a	protein phosphatase 1, regulatory subunit 15A	Cytoplasm	other
Ppp1r3g	protein phosphatase 1, regulatory subunit 3G	Cytoplasm	other
Vps37b	vacuolar protein sorting 37 homolog B (S. cerevisiae)	Cytoplasm	other
Il11	interleukin 11	Extracellular Space	cytokine
Il12b	interleukin 12B (natural killer cell stimulatory factor 2, cytotoxic lymph	Extracellular Space	cytokine
Il6	interleukin 6 (interferon, beta 2)	Extracellular Space	cytokine
Inhba	inhibin, beta A	Extracellular Space	growth factor
Angptl4	angiopoietin-like 4	Extracellular Space	other
Cartpt	CART prepropeptide	Extracellular Space	other
Cyr61	cysteine-rich, angiogenic inducer, 61	Extracellular Space	other
Thbs1	thrombospondin 1	Extracellular Space	other
Trh	thyrotropin-releasing hormone	Extracellular Space	other
Arl4d	ADP-ribosylation factor-like 4D	Nucleus	enzyme
Ccnl1	cyclin L1	Nucleus	other
Gadd45g	growth arrest and DNA-damage-inducible, gamma	Nucleus	other
Hist1h4a	histone cluster 2, H4	Nucleus	other
Neat1	nuclear paraspeckle assembly transcript 1 (non-protein coding)	Nucleus	other
Rasl11a	RAS-like, family 11, member A	Nucleus	other
Tinf2	TERF1 (TRF1) - interacting nuclear factor 2	Nucleus	other
Espl1	extra spindle pole bodies homolog 1 (S. cerevisiae)	Nucleus	peptidase
Btg2	BTG family, member 2	Nucleus	transcription regulator
Egr1	early growth response 1	Nucleus	transcription regulator
Egr2	early growth response 2	Nucleus	transcription regulator
Egr4	early growth response 4	Nucleus	transcription regulator
Fos	FBJ murine osteosarcoma viral oncogene homolog	Nucleus	transcription regulator
Foxc1	forkhead box C1	Nucleus	transcription regulator
Junb	jun B proto-oncogene	Nucleus	transcription regulator
Klf4	Kruppel-like factor 4 (gut)	Nucleus	transcription regulator
Maff	v-maf musculoaponeurotic fibrosarcoma oncogene homolog F (avian	Nucleus	transcription regulator
Nfkbie	nuclear factor of kappa light polypeptide gene enhancer in B-cells inh	Nucleus	transcription regulator
Nrarp	NOTCH-regulated ankyrin repeat protein	Nucleus	transcription regulator

Pax6	paired box 6	Nucleus	transcription regulator
Sox11	SRY (sex determining region Y)-box 11	Nucleus	transcription regulator
Gem	GTP binding protein overexpressed in skeletal muscle	Plasma Membrane	enzyme
Has1	hyaluronan synthase 1	Plasma Membrane	enzyme
Ccrl2	chemokine (C-C motif) receptor-like 2	Plasma Membrane	G-protein coupled receptor
Kcne4	potassium voltage-gated channel, Isk-related family, member 4	Plasma Membrane	ion channel
Arrdc3	arrestin domain containing 3	Plasma Membrane	other
Tpbg	trophoblast glycoprotein	Plasma Membrane	other
Gja4	gap junction protein, alpha 4, 37kDa	Plasma Membrane	transporter
Gjb2	gap junction protein, beta 2, 26kDa	Plasma Membrane	transporter
Slc2a1	solute carrier family 2 (facilitated glucose transporter), member 1	Plasma Membrane	transporter
3930402G23Rik	RIKEN cDNA 3930402G23 gene	unknown	other
4930523C07Rik	KIAA0040	unknown	other
Apold1	apolipoprotein L domain containing 1	unknown	other
Cwc25	CWC25 spliceosome-associated protein homolog (S. cerevisiae)	unknown	other
Dom3z	dom-3 homolog Z (C. elegans)	unknown	other
Tiparp	TCDD-inducible poly(ADP-ribose) polymerase	unknown	other

Table 5. Functional categories of differentially expressed genes.

A select list of functional categories containing genes that were differentially regulated between LTP and control. Ingenuity Pathway Analysis was used for this anlaysis. The p-values reported are a measure of likelihood that the association between a dataset of genes and a given process or function is due to random chance. It is calculated by considering the number of genes in the dataset that participate in the process and the total number of genes that are known to be associated with the process. The Benjamini-Hochberg method was used to correct for multiple testing.

Category	Function	Function Annotation	B-H p-value	# Molecules	Molecules
Gene Expression	transcription	transcription of RNA	3.06E-11	56	AFF1, ARID1A, ATF3, BTG2, CAMTA2, CDKN1A, CEBPB, CELSR2, CREM, CRTC1, CRYM, CSRNP1, DUSP1, DUSP5, DYRK1B, EGR1, EGR2, EGR4, FOS, FOSB, FOSL2, FOXC1, GADD45G, GEM, HR, IL10, IL11, IL1B, IL6, INHBA, JUNB, KDM6B, KLF2, KLF4, MAFF, MLL2, MN1, NCOR2, NFIL3, NFKB1, NPAS4, NR4A1, NR4A2, NR4A3, NRARP, PAX6, PER1, PRKCD, SATB2, SIK1, SOX11, TRH, ZBTB20, ZIC1, ZIC2, ZMIZ1
Behavior	behavior	behavior	9.75E-11	39	ARC, CACNA1E, CARTPT, CDKN1A, CREM, CYR61, DUSP1, EGR1, EGR2, EGR3, EPHA6, FOS, FOSB, GHSR, GRIN2A, GRIN2B, GRP, IL10, IL1B, IL1RN, IL6, JUNB, KLF4, MN1, NFKB1, NOV, NPAS4, NR4A2, NR4A3, PAX6, PCDH8, PER1, SEZ6, SHANK1, TAC1, TRH, TRHR, TTR, ZIC1
Behavior	learning	learning	2.80E-07	20	ARC, CACNA1E, CREM, EGR1, EPHA6, FOS, GRIN2A, GRIN2B, GRP, IL1B, IL1RN, IL6, JUNB, NR4A2, PAX6, PCDH8, SEZ6, SHANK1, TAC1, TTR
Behavior	long-term memory	long-term memory	2.25E-06	8	ARC, CREM, EGR1, GRP, IL6, PCDH8, SHANK1, TAC1
Behavior	memory	memory	1.40E-05	13	ARC, CREM, EGR1, GRIN2A, GRIN2B, GRP, IL1B, IL1RN, IL6, PAX6, PCDH8, SHANK1, TAC1
Behavior	spatial learning	spatial learning	9.34E-04	9	ARC, CACNA1E, EPHA6, FOS, GRIN2A, IL6, SEZ6, SHANK1, TTR
Behavior	long-term recognition memory	long-term recognition memory	2.76E-03	3	ARC, EGR1, IL6
Behavior	conditioning	conditioning	3.64E-03	8	ARC, CARTPT, CREM, EPHA6, GHSR, GRIN2A, IL1RN, PER1
Nervous System Development and Function	long-term memory	long-term memory	2.25E-06	8	ARC, CREM, EGR1, GRP, IL6, PCDH8, SHANK1, TAC1
Nervous System Development and Function	memory	memory	1.40E-05	13	ARC, CREM, EGR1, GRIN2A, GRIN2B, GRP, IL1B, IL1RN, IL6, PAX6, PCDH8, SHANK1, TAC1
Nervous System Development and Function	proliferation	proliferation of brain cells	1.49E-05	9	CDKN1A, IL1B, IL1RN, IL6, INHBA, NCOR2, PAX6, ZIC1, ZIC2
Nervous System Development and Function	loss	loss of neurons	1.35E-04	9	CEBPB, IL10, IL1RN, IL6, NFKB1, NR4A2, PPP1R15A, TAC1, TTR
Nervous System Development and Function	morphology	morphology of nervous system	9.59E-04	22	ADAMTS4, CELSR2, DUSP1, EGR1, EGR2, EGR3, GRIN2B, IL1B, IL1RN, IL6, NCOR2, NFKB1, NPAS4, NR4A2, NRARP, PAX6, SEMA5A, SEMA5B, SEZ6, SHANK1, TAC1, ZIC1
Nervous System Development and Function	morphology	morphology of dendrites	2.01E-03	5	DUSP1, SEMA5A, SEMA5B, SEZ6, TAC1
Nervous System Development and Function	excitatory postsynaptic potential	excitatory postsynaptic potential	1.23E-03	7	ARC, DOC2B, EGR3, GRIN2A, GRIN2B, IL1B, SEZ6
Nervous System Development and Function	development	development of central nervous system	1.68E-03	17	CXCL10, EGR1, EGR2, FOXC1, IL11, IL1B, IL6, IRS2, MDGA1, NCOR2, NR4A2, NR4A3, PAX6, THBS1, ZBTB20, ZIC1, ZIC2
Nervous System Development and Function	development	development of brain	2.83E-03	14	EGR1, EGR2, FOXC1, IL6, IRS2, MDGA1, NCOR2, NR4A2, NR4A3, PAX6, THBS1, ZBTB20, ZIC1, ZIC2
Nervous System Development and Function	firing	firing of histaminergic neurons	1.27E-03	2	TRH, TRHR
Nervous System Development and Function	long-term recognition memory	long-term recognition memory	2.76E-03	3	ARC, EGR1, IL6
Nervous System Development and Function	action potential	action potential of nervous tissue	2.87E-03	5	EGR3, GRIN2B, IL1B, NFKB1, SEZ6
Nervous System Development and Function	NMDA-mediated synaptic current	NMDA-mediated synaptic current	3.79E-03	3	FOSB, GRIN2A, GRIN2B
Cell-To-Cell Signaling and Interaction	induction	induction of cells	4.37E-06	8	GRP, IL10, IL12B, IL1B, IL1RN, IL6, INHBA, TRH

Cell-To-Cell Signaling and Interaction	activation	activation of cells	3.70E-05	25	ATF3, CARTPT, Ccl9, CCR7, CD14, CDKN1A, CEBPB, DUSP1, EGR2, EGR3, GHSR, GJA4, IL10, IL11, IL12B, IL1B, IL1RN, IL6, KLF2, NCOR2, NFKB1, PRKCD, PROCR, TAC1, THBS1
Cell-To-Cell Signaling and Interaction	activation	activation of central nervous system cells	4.86E-04	5	CDKN1A, CEBPB, IL1B, IL1RN, IL6
Cell-To-Cell Signaling and Interaction	activation	activation of astrocytes	1.18E-03	4	CEBPB, IL1B, IL1RN, IL6
Cell-To-Cell Signaling and Interaction	activation	activation of microglia	3.22E-03	5	CEBPB, IL10, IL1B, IL1RN, IL6
Cell-To-Cell Signaling and Interaction	stimulation	stimulation of cells	5.02E-05	11	FOS, GRP, IL10, IL11, IL12B, IL1B, IL1RN, IL6, INHBA, THBS1, TRH
Cell-To-Cell Signaling and Interaction	signaling	signaling of cells	6.05E-04	11	CCL17, CD14, CXCL10, GJA4, GJB2, IL10, IL1B, INHBA, PCDH8, SEMA5A, TRH
Cell-To-Cell Signaling and Interaction	excitatory postsynaptic potential	excitatory postsynaptic potential	1.23E-03	7	ARC, DOC2B, EGR3, GRIN2A, GRIN2B, IL1B, SEZ6
Cell-To-Cell Signaling and Interaction	action potential	action potential of nervous tissue	2.87E-03	5	EGR3, GRIN2B, IL1B, NFKB1, SEZ6
Cell-To-Cell Signaling and Interaction	NMDA-mediated synaptic current	NMDA-mediated synaptic current	3.79E-03	3	FOSB, GRIN2A, GRIN2B
Cell Signaling	synthesis	synthesis of nitric oxide	7.60E-04	10	CEBPB, GHSR, GRIN2B, IL10, IL12B, IL1B, IL1RN, IL6, PRKCD, TAC1
Cell Signaling	quantity	quantity of Ca2+	3.94E-03	12	CXCL10, FOS, GRIN2A, GRP, IL1B, IL6, NFKB1, TAC1, TRH, TRHR, TTR, WFS1
Protein Trafficking	secretion	secretion of protein	1.57E-03	7	ARL4D, CD14, CXCL10, IL10, IL1B, IL6, LRRC32
Neurological Disease	epileptic seizure	epileptic seizure	6.28E-27	28	ANGPTL4, ARC, ARRDC3, ATF3, BAG3, C11orf96, CDKN1A, CREM, CRYM, CYR61, DUSP1, DUSP5, EGR1, EGR2, EGR3, EGR4, FOS, FOSB, GADD45G, IER2, IL1B, INHBA, JUNB, NFIL3, NR4A1, NR4A3, TAC1, TIPARP
Neurological Disease	epilepsy	epilepsy	1.27E-24	32	ANGPTL4, ARC, ARRDC3, ATF3, BAG3, C11orf96, CDKN1A, CREM, CRYM, CYR61, DUSP1, DUSP5, EGR1, EGR2, EGR3, EGR4, FOS, FOSB, GADD45G, GRIN2A, GRIN2B, IER2, IL1B, INHBA, JUNB, KCNQ3, NFIL3, NR4A1, NR4A3, SLC2A1, TAC1, TIPARP
Neurological Disease	seizures	seizures	1.07E-22	35	ANGPTL4, ARC, ARRDC3, ATF3, BAG3, C11orf96, CDKN1A, CREM, CRYM, CYR61, DUSP1, DUSP5, EGR1, EGR2, EGR3, EGR4, FOS, FOSB, GADD45G, GRIN2A, GRIN2B, IER2, IL1B, IL1RN, IL6, INHBA, JUNB, KCNQ3, NFIL3, NR4A1, NR4A3, SEZ6, SLC2A1, TAC1, TIPARP
Neurological Disease	schizophrenia	Schizophrenia	1.13E-05	18	BTG2, CRYM, DUSP1, EGR3, EGR4, GRIN2A, GRIN2B, HCAR2, IL10, IL1B, IL1RN, PAX6, PCDH8, PRKCD, SEMA5A, TAC1, THBS1, TTR
Neurological Disease	movement disorder	Movement Disorders	2.03E-05	28	AFF1, CARTPT, CRYM, DUSP5, EGR1, EGR2, EGR3, EGR4, FOS, FOSB, GRIN2A, GRIN2B, IL10, IL1B, IL6, JUNB, MAFF, NFKB1, NPAS4, NR4A1, NR4A2, PAX6, RPH3A, SEMA5A, SEZ6, SLC2A1, TAC1, ZIC1
Neurological Disease	disorder of basal ganglia	disorder of basal ganglia	3.85E-05	22	CRYM, DUSP5, EGR1, EGR2, EGR4, FOS, FOSB, GRIN2A, GRIN2B, IL10, IL1B, IL6, JUNB, MAFF, NFKB1, NR4A1, NR4A2, RPH3A, SEMA5A, SEZ6, SLC2A1, TAC1
Neurological Disease	kindling	kindling	1.11E-04	3	CREM, FOS, GRIN2A
Neurological Disease	dyskinesia	dyskinesia	2.26E-04	18	CRYM, DUSP5, EGR1, EGR2, EGR4, FOS, FOSB, GRIN2A, GRIN2B, IL6, JUNB, MAFF, NFKB1, NR4A1, RPH3A, SEZ6, SLC2A1, TAC1
Neurological Disease	peroxisomal acyl CoA oxidase deficiency	peroxisomal acyl CoA oxidase deficiency	2.99E-04	3	CEBPB, IL1B, IL1RN

4 Conclusions and significance

4.1 Localization and miRNA-mediated regulation of GluA2 mRNA

At the start of the miR-124/GluA2 project, GluA2 mRNA seemed like a very favorable candidate for local translation: GluA2 protein is present at distal compartments, its levels at the synapse are tightly-regulated and recent studies showed that not only was GluA2 mRNA dendritically localized, GluA2 protein was locally translated in a stimulus-specific manner. Furthermore, the GluA2 transcript was known to undergo several interesting RNA processing steps: alternative splicing of the flip/flop isoforms, alternative 5' splice donors in the last coding exon that gave rise to different carboxy terminal tails and alternative 3'UTRs, and RNA editing. The 3'UTR of GluA2 is 3.8 kb long and probably rich with regulatory sequence and structure. It seemed plausible that GluA2 mRNA would be subject to further regulation at the post-transcriptional level by interactions with RNA binding proteins that localize it dendritically. However, the results presented in Chapter 2 provide clear evidence that GluA2 mRNA is not dendritically localized. While an occasional GluA2 mRNA puncta is observed in distal dendrites, the biological significance of translation from the rare dendritic GluA2 transcript is unclear.

The majority of GluA2 protein is probably translated in the cell body and transported out to synaptic sites, despite the great distances between synapses and cell bodies. In retrospect, there does not seem to be a significant energetic benefit to on-site versus somatic translation. In both cases, a macromolecule (protein or RNA) must be moved long distances. There does not seem to be a clear cell biological benefit to dendritic translation of GluA2 either. As a transmembrane receptor, GluA2 subunits are only functional when they are inserted in the

plasma membrane. This obviates the need for rapid translation, since a reserve pool of inactive GluA2 subunits can be (and is) maintained until the moment it is required. Other proteins that are not as easily regulated post-translationally have a greater need for rapid translation and turnover. In this regard, cytoplasmic proteins may be better candidates for local translation (e.g. Camk2α).

The miR-124/GluA2 mRNA interaction was identified by computational predictions before the availability of experimental data (e.g. Argonaute HITS-CLIP, which identifies miRNA targets in the mouse brain). While the HEK293T cell assays and overexpression studies in neurons show that miR-124 can down-regulate GluA2 mRNA, it is unclear whether this interaction normally occurs in neurons and how biologically important the interaction is. To fully address this question, the miR-124 target site would have to be deleted from the genomic GluA2 loci. The miR-124 target site in GluA2 was actually not identified as a hit in the Darnell lab Argonaute HITS-CLIP experiment [253], which suggests that the interaction is not strong endogenously. Hence, it is probably not worthwhile to try targeted deletion of the miR-124 site from genomic GluA2 loci. Genomic deletion of miRNA target sites has not been reported, to my knowledge, and would be an interesting experiment for the right miRNA/mRNA interaction. A good miRNA/mRNA candidate would probably not come from computational predictions, but should be identified by experimental screens. A good candidate interaction would also preferably involve a gene that is primarily regulated at the translational level so that post-translational modifications do not confound the interpretation of results.

4.2 Genome-wide gene regulation during long-lasting plasticity

In contrast to the miR-124/GluA2 project where the regulation of only one gene was studied, the chemLTP sequencing project studies the regulation of the entire transcriptome. Once

sample collection and sequencing of total, small, and polysomal RNA is complete, we will have a lot of data and our next challenge would be to glean useful information from it. A useful approach to analyzing the data would be to categorize it (e.g. by sequence, function, cell type, fold change, etc.) and make connections between groups. It will be important that we use appropriate analyses, although RNAseq is still a relatively young technique and the tools available for data analysis are a work in progress. It will also be important to validate our findings from bioinformatics with wet experiments. Hopefully, this project will enhance our understanding of how gene expression is regulated during synaptic plasticity.

APPENDIX

Protocol 1: Immunocytochemistry for surface receptors with cultured neurons

Perform all steps at room temperature unless otherwise noted.

1. Prepare fresh artificial cerebral spinal fluid (ACSF).
    a. Dissolve all chemicals except $CaCl_2$.
    b. Bubble ACSF with carboxygen until the pH is ~7.35.
    c. Add $CaCl_2$.
    d. Adjust osmolarity to ~293 mOsm with glucose or water.
    e. Filter with a 0.22 µm filter. Warm to 37 ^oC before use.

	Stock (M)	Final (mM)	Volume
NaCl	5	119	1.19 mL
$NaHCO_3$	0.5	26.2	2.62 mL
KCl	1	2.5	125 µL
NaH_2PO_4	0.5	1	100 µL
$MgCl_2$	1	1.3	65 µL
Glucose	1	10	500 µL
$CaCl_2$	1	2.5	125 µL
Milli-Q water	-	-	To 50 mL

2. Incubate in surface primary antibody.

Antibody should recognize an external epitope. Spin down antibody (13,000 rpm; 5 minutes; 4 ^{o}C) before taking an aliquot. Dilute antibody in pre-warmed ACSF. Replace media with antibody dilution. Incubate at 37^{o}C for 30 min.

3. Fix cells with freshly diluted 4% PFA, 10 min.
4. Wash cells 3 times with PBS.
5. Permeabilize with 0.1% Triton-X100, 5 min.
6. Wash cells 3 times with PBS.
7. Block in 10% goat serum, 30 min.
8. Incubate in cytoplasmic primary antibody.

   Spin down antibody before taking an aliquot. Dilute in 10% goat serum. Incubate overnight at 4^{o}C in humid chamber. Use 30 µL for each coverslip.
9. Wash 3 times with PBS, 10 min per wash.
10. Incubate in secondary antibody.

    Dilute antibody in 10% goat serum. Hoechst may be included at this step. Incubate 1 hour in humid chamber.
11. Wash 3 times with PBS, 10 min per wash.
12. Mount with Aqua Poly/Mount (Polysciences #18606). Let coverslips dry overnight before imaging. Let coverslips dry a couple days before storing them on their sides.

Protocol 2: Chemical treatment of acute slices to induce long-term potentiation [219,254]

Solution	Composition	Recipe
A	0.2% DMSO	25 mL ACSF + 50 µL DMSO
B	50 µM FSK	45 mL ACSF + 90 µL FSK
C	30 mM KCl, 10 mM $CaCl_2$, 0 mM $MgSO_4$, 50 µM forskolin	24.5 mL modACSF + 375 µL 2 M KCl + 125 µL 2 M Ca + 50 µL FSK
D	100 µM D-APV	15 mL ACSF + 30 µL APV
E	100 µM D-APV, solution B	15 uL solution B + 30 µL APV
F	100 µM D-APV, solution C	15 mL solution C + 30 µL APV

DMSO: dimethyl sulfoxide; ACSF: artificial cerebral spinal fluid; FSK: forskolin (25 mM stock in DMSO; LC Laboratories F-9929); modACSF: modified ACSF without potassium, calcium, phosphates, or magnesium; APV: 2-amino-5-phosphonopentanoic acid (50 mM stock in water)

Vehicle control

2 x 5 min DMSO (Solution A)

ChemLTP

5 min FSK (Solution B)

5 min high K/Ca + FSK (Solution C)

Forskolin only

2 x 5 min FSK (Solution B)

ChemLTP + APV

5 min APV (Solution D)

5 min FSK + APV (Solution E)

5 min high K/Ca + /FSK + APV (Solution F)

Procedure:

1. Acute slices of 500 μm are prepared and allowed to recover for 2 hours. Each mouse hippocampus yields 5 to 6 slices, which are distributed between different treatment chambers. Each treatment uses 5 to 6 slices.
2. Prepare all solutions. Warm up to 30 ^{o}C and bubble with carboxygen.
    a. Modified ACSF should be warmed and bubbled before the addition of KCl and $CaCl_2$. Presence of phosphates will cause the high concentration of calcium added later to precipitate.
    b. Prepare 10 mL of solution per treatment.
3. Stop ACSF perfusion for chamber undergoing treatment.
4. Apply treatment solution with a syringe and remove of the solution already present at the same time. During this step, the chamber is essentially rinsed with ~10 mL of the treatment solution. Once all the treatment solution has been added, stop aspiration and allow slices to incubate submerged.
5. After treatment, resume ACSF perfusion of the chambers.
6. Let slices sit for 3 hours before snap freezing in tubes pre-chilled in dry ice.

Protocol 3: Polysome fractionation and RNA extraction [205]

Prepare stock solutions in diethylpyrocarbonate (DEPC)-treated water and filter sterilize.

	Stock	Final concentration	Lysis buffer (2 mL)	20% sucrose (15 mL)	50% sucrose (15 mL)
Tris pH 7.5	1 M	20 mM	40 µL	0.3 mL	0.3 mL
NaCl	5 M	100 mM	40 µL	0.3 mL	0.3 mL
$MgCl_2$	1 M	12 mM	24 µL	0.18 mL	0.18 mL
NP-40	10%	1 %	(200 µL)	-	-
RNasin	40 U/µL	30 U/mL	1.5 µL	-	-
Protease inhibitor	7 x	1 x	286 µL	-	-
DTT	2 M	1 mM	1 µL	-	-
Cycloheximide	10 mg/mL	0.1 mg/mL	20 µL	150 µL	150 µL
Sucrose	-	15 or 50%	-	3 g	7.5 g
DEPC-treated water	-	-	1387.5 µL	To 15 mL	To 15 mL

1. Homogenize tissue in lysis buffer without NP-40 added yet.

   Use about 1 mL of lysis buffer for ~ 300 mg of brain tissue. If using adult forebrain, remove the white matter tracks to avoid a myelin peak among the polysomes (Figure A-1).

2. Add NP-40 to 1 % and incubate on ice for 10-20 minutes.
3. Clear the lysate. Spin at 4 ^{o}C for 10 min at 20,000 g.

4. Layer supernatant onto pre-chilled gradient.
5. Spin at 4 ^{o}C for 2 h at 39,000 rpm in a SW41 rotor (235,000 g). Set break and acceleration to 7 (slow).
6. Run gradient with continuous UV monitoring at 254 nm and collect fractions.

   If the gradients are cold, there is a risk of condensation forming on the UV monitor and causing any ribosome peaks to be occluded (Figure A-1). To avoid this, dry the UV gun in a drying incubator for a few hours before using. Or, warm the tubes before running.
7. Spike synthetic control RNA in each fraction (e.g. Invitrogen ERCC ExFold for sequencing or Thermo Solaris for RT-qPCR).
8. Proteinase K-treat fractions and phenol-chloroform extract RNA. Precipitate with glycogen carrier (e.g. Thermo #R0561).

Figure A-16. Troubleshooting polysome profiles.

(A) Example of a profile obtained while there was condensation inside the UV monitoring unit. Absorbance measured with a sensitivity setting of 0.5 absorbance units full scale (AUFS), shown on the y-axis in arbitrary units (a.u.). (B) Example of a profile from forebrain lysate with material from white matter tracts. This lysate was prepared without detergent and spun for 90 minutes at 39 krpm on a 5-50% gradient. Absorbance measured at 0.2 AUFS.

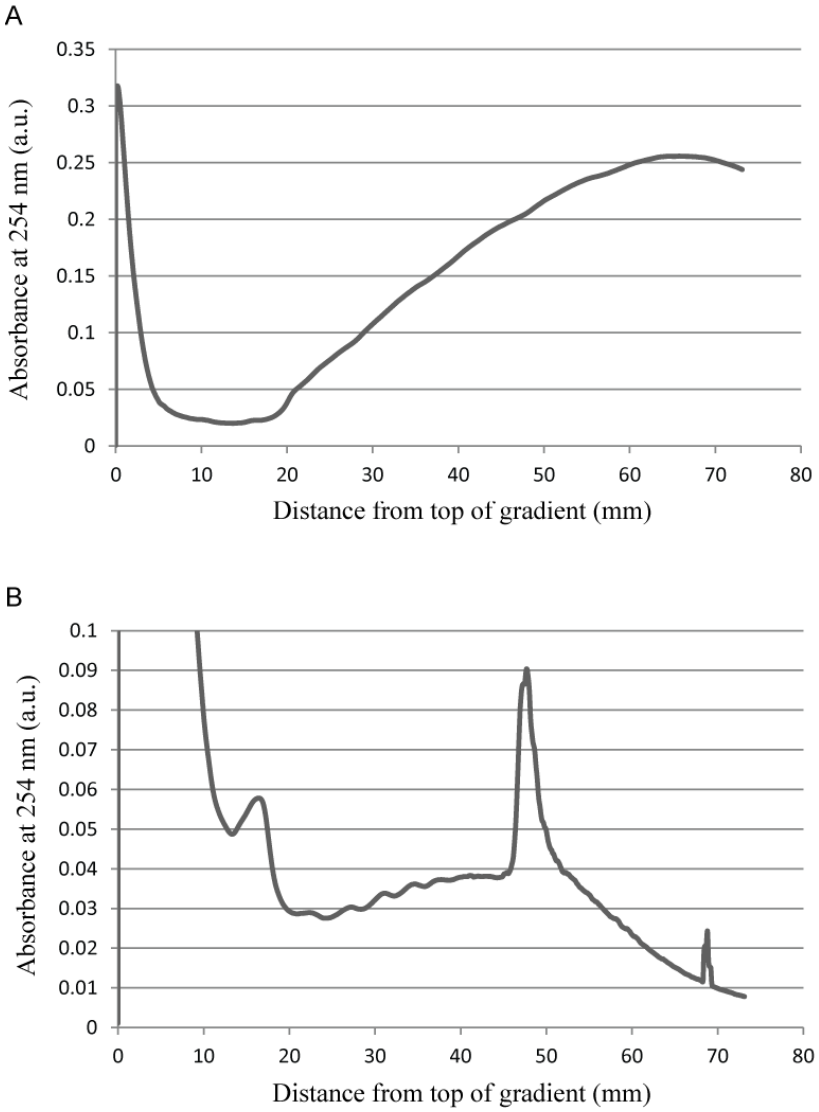

BIBLIOGRAPHY

[1] Cajal SRy. The Croonian Lecture: La Fine Structure des Centres Nerveux. Proc R Soc Lond 1894:444-68.

[2] Hebb DO. Organization of Behavior: A Neuropsychological Theory: New York, John Wiley and Sons; 1949.

[3] Cajal SRy. Histologie du système nerveux de l'homme & des vertébrés: Paris :Maloine; 1911.

[4] Bourne J, Harris KM. Do thin spines learn to be mushroom spines that remember? Current opinion in neurobiology 2007;17:381-6.

[5] Kandel ER. The molecular biology of memory storage: a dialogue between genes and synapses. Science (New York, NY) 2001;294:1030-8.

[6] Andersen P, Morris R, Amaral D, Bliss T, O'Keefe J, eds. The Hippocampus Book. New York: Oxford University Press; 2006.

[7] Bliss TV, Lomo T. Long-lasting potentiation of synaptic transmission in the dentate area of the anaesthetized rabbit following stimulation of the perforant path. J Physiol 1973;232:331-56.

[8] Dan Y, Poo MM. Spike timing-dependent plasticity: from synapse to perception. Physiological reviews 2006;86:1033-48.

[9] Cesca F, Baldelli P, Valtorta F, Benfenati F. The synapsins: key actors of synapse function and plasticity. Progress in neurobiology 2010;91:313-48.

[10] Rosahl TW, Spillane D, Missler M, et al. Essential functions of synapsins I and II in synaptic vesicle regulation. Nature 1995;375:488-93.

[11] Kaeser PS, Deng L, Wang Y, et al. RIM proteins tether Ca2+ channels to presynaptic active zones via a direct PDZ-domain interaction. Cell 2011;144:282-95.

[12] Han Y, Kaeser PS, Sudhof TC, Schneggenburger R. RIM determines Ca(2)+ channel density and vesicle docking at the presynaptic active zone. Neuron 2011;69:304-16.

[13] Deng L, Kaeser PS, Xu W, Sudhof TC. RIM proteins activate vesicle priming by reversing autoinhibitory homodimerization of Munc13. Neuron 2011;69:317-31.

[14] Castillo PE, Schoch S, Schmitz F, Sudhof TC, Malenka RC. RIM1alpha is required for presynaptic long-term potentiation. Nature 2002;415:327-30.

[15] Powell CM, Schoch S, Monteggia L, et al. The presynaptic active zone protein RIM1alpha is critical for normal learning and memory. Neuron 2004;42:143-53.

[16] Kirov SA, Harris KM. Dendrites are more spiny on mature hippocampal neurons when synapses are inactivated. Nature neuroscience 1999;2:878-83.

[17] Holtmaat A, Svoboda K. Experience-dependent structural synaptic plasticity in the mammalian brain. Nature reviews Neuroscience 2009;10:647-58.

[18] Engert F, Bonhoeffer T. Dendritic spine changes associated with hippocampal long-term synaptic plasticity. Nature 1999;399:66-70.

[19] Lynch G, Larson J, Kelso S, Barrionuevo G, Schottler F. Intracellular injections of EGTA block induction of hippocampal long-term potentiation. Nature 1983;305:719-21.

[20] Malenka RC, Kauer JA, Zucker RS, Nicoll RA. Postsynaptic calcium is sufficient for potentiation of hippocampal synaptic transmission. Science (New York, NY) 1988;242:81-4.

[21] Malenka RC, Kauer JA, Perkel DJ, et al. An essential role for postsynaptic calmodulin and protein kinase activity in long-term potentiation. Nature 1989;340:554-7.

[22] Malinow R, Schulman H, Tsien RW. Inhibition of postsynaptic PKC or CaMKII blocks induction but not expression of LTP. Science (New York, NY) 1989;245:862-6.

[23] Silva AJ, Paylor R, Wehner JM, Tonegawa S. Impaired spatial learning in alpha-calcium-calmodulin kinase II mutant mice. Science (New York, NY) 1992;257:206-11.

[24] Silva AJ, Stevens CF, Tonegawa S, Wang Y. Deficient hippocampal long-term potentiation in alpha-calcium-calmodulin kinase II mutant mice. Science (New York, NY) 1992;257:201-6.

[25] Colbran RJ, Brown AM. Calcium/calmodulin-dependent protein kinase II and synaptic plasticity. Current opinion in neurobiology 2004;14:318-27.

[26] Lisman J, Schulman H, Cline H. The molecular basis of CaMKII function in synaptic and behavioural memory. Nature reviews Neuroscience 2002;3:175-90.

[27] Buard I, Coultrap SJ, Freund RK, et al. CaMKII "autonomy" is required for initiating but not for maintaining neuronal long-term information storage. J Neurosci 2010;30:8214-20.

[28] Sacktor TC. How does PKMzeta maintain long-term memory? Nature reviews Neuroscience 2011;12:9-15.

[29] Hrabetova S, Sacktor TC. Bidirectional regulation of protein kinase M zeta in the maintenance of long-term potentiation and long-term depression. J Neurosci 1996;16:5324-33.

[30] Ling DS, Benardo LS, Serrano PA, et al. Protein kinase Mzeta is necessary and sufficient for LTP maintenance. Nature neuroscience 2002;5:295-6.

[31] Shema R, Sacktor TC, Dudai Y. Rapid erasure of long-term memory associations in the cortex by an inhibitor of PKM zeta. Science (New York, NY) 2007;317:951-3.

[32] Yao Y, Kelly MT, Sajikumar S, et al. PKM zeta maintains late long-term potentiation by N-ethylmaleimide-sensitive factor/GluR2-dependent trafficking of postsynaptic AMPA receptors. J Neurosci 2008;28:7820-7.

[33] Kauer JA, Malenka RC, Nicoll RA. A persistent postsynaptic modification mediates long-term potentiation in the hippocampus. Neuron 1988;1:911-7.

[34] Muller D, Joly M, Lynch G. Contributions of quisqualate and NMDA receptors to the induction and expression of LTP. Science (New York, NY) 1988;242:1694-7.

[35] Andrasfalvy BK, Magee JC. Changes in AMPA receptor currents following LTP induction on rat CA1 pyramidal neurones. J Physiol 2004;559:543-54.

[36] Lissin DV, Carroll RC, Nicoll RA, Malenka RC, von Zastrow M. Rapid, activation-induced redistribution of ionotropic glutamate receptors in cultured hippocampal neurons. J Neurosci 1999;19:1263-72.

[37] Lissin DV, Gomperts SN, Carroll RC, et al. Activity differentially regulates the surface expression of synaptic AMPA and NMDA glutamate receptors. Proceedings of the National Academy of Sciences of the United States of America 1998;95:7097-102.

[38] Shi SH, Hayashi Y, Petralia RS, et al. Rapid spine delivery and redistribution of AMPA receptors after synaptic NMDA receptor activation. Science (New York, NY) 1999;284:1811-6.

[39] Carroll RC, Lissin DV, von Zastrow M, Nicoll RA, Malenka RC. Rapid redistribution of glutamate receptors contributes to long-term depression in hippocampal cultures. Nature neuroscience 1999;2:454-60.

[40] Beattie EC, Carroll RC, Yu X, et al. Regulation of AMPA receptor endocytosis by a signaling mechanism shared with LTD. Nature neuroscience 2000;3:1291-300.

[41] Park M, Penick EC, Edwards JG, Kauer JA, Ehlers MD. Recycling endosomes supply AMPA receptors for LTP. Science (New York, NY) 2004;305:1972-5.

[42] Schnell E, Sizemore M, Karimzadegan S, Chen L, Bredt DS, Nicoll RA. Direct interactions between PSD-95 and stargazin control synaptic AMPA receptor number. Proceedings of the National Academy of Sciences of the United States of America 2002;99:13902-7.

[43] Tomita S, Stein V, Stocker TJ, Nicoll RA, Bredt DS. Bidirectional synaptic plasticity regulated by phosphorylation of stargazin-like TARPs. Neuron 2005;45:269-77.

[44] Wenthold RJ, Petralia RS, Blahos J, II, Niedzielski AS. Evidence for multiple AMPA receptor complexes in hippocampal CA1/CA2 neurons. J Neurosci 1996;16:1982-9.

[45] Man HY, Sekine-Aizawa Y, Huganir RL. Regulation of {alpha}-amino-3-hydroxy-5-methyl-4-isoxazolepropionic acid receptor trafficking through PKA phosphorylation of the Glu receptor 1 subunit. Proceedings of the National Academy of Sciences of the United States of America 2007;104:3579-84.

[46] Ehlers MD. Reinsertion or degradation of AMPA receptors determined by activity-dependent endocytic sorting. Neuron 2000;28:511-25.

[47] Lee HK, Takamiya K, Han JS, et al. Phosphorylation of the AMPA receptor GluR1 subunit is required for synaptic plasticity and retention of spatial memory. Cell 2003;112:631-43.

[48] Makino Y, Johnson RC, Yu Y, Takamiya K, Huganir RL. Enhanced synaptic plasticity in mice with phosphomimetic mutation of the GluA1 AMPA receptor. Proceedings of the National Academy of Sciences of the United States of America 2011;108:8450-5.

[49] Boehm J, Kang MG, Johnson RC, Esteban J, Huganir RL, Malinow R. Synaptic incorporation of AMPA receptors during LTP is controlled by a PKC phosphorylation site on GluR1. Neuron 2006;51:213-25.

[50] Delgado JY, Coba M, Anderson CN, et al. NMDA receptor activation dephosphorylates AMPA receptor glutamate receptor 1 subunits at threonine 840. J Neurosci 2007;27:13210-21.

[51] Dalva MB, McClelland AC, Kayser MS. Cell adhesion molecules: signalling functions at the synapse. Nature reviews Neuroscience 2007;8:206-20.

[52] Venero C, Herrero AI, Touyarot K, et al. Hippocampal up-regulation of NCAM expression and polysialylation plays a key role on spatial memory. The European journal of neuroscience 2006;23:1585-95.

[53] Bonfanti L. PSA-NCAM in mammalian structural plasticity and neurogenesis. Progress in neurobiology 2006;80:129-64.

[54] Kraev I, Henneberger C, Rossetti C, et al. A Peptide Mimetic Targeting Trans-Homophilic NCAM Binding Sites Promotes Spatial Learning and Neural Plasticity in the Hippocampus. PLoS One 2011;6:e23433.

[55] Lai KO, Ip NY. Synapse development and plasticity: roles of ephrin/Eph receptor signaling. Current opinion in neurobiology 2009;19:275-83.

[56] Contractor A, Rogers C, Maron C, Henkemeyer M, Swanson GT, Heinemann SF. Trans-synaptic Eph receptor-ephrin signaling in hippocampal mossy fiber LTP. Science (New York, NY) 2002;296:1864-9.

[57] Heifets BD, Castillo PE. Endocannabinoid signaling and long-term synaptic plasticity. Annu Rev Physiol 2009;71:283-306.

[58] Marsicano G, Wotjak CT, Azad SC, et al. The endogenous cannabinoid system controls extinction of aversive memories. Nature 2002;418:530-4.

[59] Varvel SA, Lichtman AH. Evaluation of CB1 receptor knockout mice in the Morris water maze. J Pharmacol Exp Ther 2002;301:915-24.

[60] Varvel SA, Anum EA, Lichtman AH. Disruption of CB(1) receptor signaling impairs extinction of spatial memory in mice. Psychopharmacology (Berl) 2005;179:863-72.

[61] Kamprath K, Marsicano G, Tang J, et al. Cannabinoid CB1 receptor mediates fear extinction via habituation-like processes. J Neurosci 2006;26:6677-86.

[62] Eroglu C, Barres BA. Regulation of synaptic connectivity by glia. Nature 2010;468:223-31.

[63] Henneberger C, Papouin T, Oliet SH, Rusakov DA. Long-term potentiation depends on release of D-serine from astrocytes. Nature 2010;463:232-6.

[64] Agulhon C, Fiacco TA, McCarthy KD. Hippocampal short- and long-term plasticity are not modulated by astrocyte Ca2+ signaling. Science (New York, NY) 2010;327:1250-4.

[65] Filosa A, Paixao S, Honsek SD, et al. Neuron-glia communication via EphA4/ephrin-A3 modulates LTP through glial glutamate transport. Nature neuroscience 2009;12:1285-92.

[66] Suzuki A, Stern SA, Bozdagi O, et al. Astrocyte-neuron lactate transport is required for long-term memory formation. Cell 2011;144:810-23.

[67] Ghosh A, Carnahan J, Greenberg ME. Requirement for BDNF in activity-dependent survival of cortical neurons. Science (New York, NY) 1994;263:1618-23.

[68] Ch'ng TH, Martin KC. Synapse-to-nucleus signaling. Current opinion in neurobiology 2011;21:345-52.

[69] Lai KO, Zhao Y, Ch'ng TH, Martin KC. Importin-mediated retrograde transport of CREB2 from distal processes to the nucleus in neurons. Proceedings of the National Academy of Sciences of the United States of America 2008;105:17175-80.

[70] Sweatt JD. Mitogen-activated protein kinases in synaptic plasticity and memory. Current opinion in neurobiology 2004;14:311-7.

[71] Lin Y, Bloodgood BL, Hauser JL, et al. Activity-dependent regulation of inhibitory synapse development by Npas4. Nature 2008;455:1198-204.

[72] Impey S, McCorkle SR, Cha-Molstad H, et al. Defining the CREB regulon: a genome-wide analysis of transcription factor regulatory regions. Cell 2004;119:1041-54.

[73] Flavell SW, Cowan CW, Kim TK, et al. Activity-dependent regulation of MEF2 transcription factors suppresses excitatory synapse number. Science (New York, NY) 2006;311:1008-12.

[74] Martin KC, Ephrussi A. mRNA localization: gene expression in the spatial dimension. Cell 2009;136:719-30.

[75] Steward O, Levy WB. Preferential localization of polyribosomes under the base of dendritic spines in granule cells of the dentate gyrus. J Neurosci 1982;2:284-91.

[76] Kang H, Schuman EM. A requirement for local protein synthesis in neurotrophin-induced hippocampal synaptic plasticity. Science (New York, NY) 1996;273:1402-6.

[77] Huber KM, Kayser MS, Bear MF. Role for rapid dendritic protein synthesis in hippocampal mGluR-dependent long-term depression. Science (New York, NY) 2000;288:1254-7.

[78] Raab-Graham KF, Haddick PC, Jan YN, Jan LY. Activity- and mTOR-dependent suppression of Kv1.1 channel mRNA translation in dendrites. Science (New York, NY) 2006;314:144-8.

[79] Wang DO, Kim SM, Zhao Y, et al. Synapse- and stimulus-specific local translation during long-term neuronal plasticity. Science (New York, NY) 2009;324:1536-40.

[80] Kiebler MA, Bassell GJ. Neuronal RNA granules: movers and makers. Neuron 2006;51:685-90.

[81] Doyle M, Kiebler MA. Mechanisms of dendritic mRNA transport and its role in synaptic tagging. EMBO J 2011;30:3540-52.

[82] Costa-Mattioli M, Gobert D, Harding H, et al. Translational control of hippocampal synaptic plasticity and memory by the eIF2alpha kinase GCN2. Nature 2005;436:1166-73.

[83] Costa-Mattioli M, Gobert D, Stern E, et al. eIF2alpha phosphorylation bidirectionally regulates the switch from short- to long-term synaptic plasticity and memory. Cell 2007;129:195-206.

[84] Richter JD. CPEB: a life in translation. Trends Biochem Sci 2007;32:279-85.

[85] Wu L, Wells D, Tay J, et al. CPEB-mediated cytoplasmic polyadenylation and the regulation of experience-dependent translation of alpha-CaMKII mRNA at synapses. Neuron 1998;21:1129-39.

[86] Wells DG, Dong X, Quinlan EM, et al. A role for the cytoplasmic polyadenylation element in NMDA receptor-regulated mRNA translation in neurons. J Neurosci 2001;21:9541-8.

[87] Pause A, Belsham GJ, Gingras AC, et al. Insulin-dependent stimulation of protein synthesis by phosphorylation of a regulator of 5'-cap function. Nature 1994;371:762-7.

[88] Lin TA, Kong X, Haystead TA, et al. PHAS-I as a link between mitogen-activated protein kinase and translation initiation. Science (New York, NY) 1994;266:653-6.

[89] Kelleher RJ, 3rd, Govindarajan A, Jung HY, Kang H, Tonegawa S. Translational control by MAPK signaling in long-term synaptic plasticity and memory. Cell 2004;116:467-79.

[90] Banko JL, Poulin F, Hou L, DeMaria CT, Sonenberg N, Klann E. The translation repressor 4E-BP2 is critical for eIF4F complex formation, synaptic plasticity, and memory in the hippocampus. J Neurosci 2005;25:9581-90.

[91] Jung MY, Lorenz L, Richter JD. Translational control by neuroguidin, a eukaryotic initiation factor 4E and CPEB binding protein. Molecular and cellular biology 2006;26:4277-87.

[92] Napoli I, Mercaldo V, Boyl PP, et al. The fragile X syndrome protein represses activity-dependent translation through CYFIP1, a new 4E-BP. Cell 2008;134:1042-54.

[93] Sempere LF, Freemantle S, Pitha-Rowe I, Moss E, Dmitrovsky E, Ambros V. Expression profiling of mammalian microRNAs uncovers a subset of brain-expressed microRNAs with possible roles in murine and human neuronal differentiation. Genome Biol 2004;5:R13.

[94] Banerjee S, Neveu P, Kosik KS. A coordinated local translational control point at the synapse involving relief from silencing and MOV10 degradation. Neuron 2009;64:871-84.

[95] Hegde AN, Goldberg AL, Schwartz JH. Regulatory subunits of cAMP-dependent protein kinases are degraded after conjugation to ubiquitin: a molecular mechanism underlying long-term synaptic plasticity. Proceedings of the National Academy of Sciences of the United States of America 1993;90:7436-40.

[96] Yashiro K, Riday TT, Condon KH, et al. Ube3a is required for experience-dependent maturation of the neocortex. Nature neuroscience 2009;12:777-83.

[97] Fonseca R, Vabulas RM, Hartl FU, Bonhoeffer T, Nagerl UV. A balance of protein synthesis and proteasome-dependent degradation determines the maintenance of LTP. Neuron 2006;52:239-45.

[98] Dong C, Upadhya SC, Ding L, Smith TK, Hegde AN. Proteasome inhibition enhances the induction and impairs the maintenance of late-phase long-term potentiation. Learn Mem 2008;15:335-47.

[99] Patrick GN, Bingol B, Weld HA, Schuman EM. Ubiquitin-mediated proteasome activity is required for agonist-induced endocytosis of GluRs. Current biology : CB 2003;13:2073-81.

[100] Ehlers MD. Activity level controls postsynaptic composition and signaling via the ubiquitin-proteasome system. Nature neuroscience 2003;6:231-42.

[101] Bingol B, Schuman EM. Activity-dependent dynamics and sequestration of proteasomes in dendritic spines. Nature 2006;441:1144-8.

[102] Ho VM, Lee JA, Martin KC. The cell biology of synaptic plasticity. Science (New York, NY) 2011;334:623-8.

[103] Shepherd JD, Huganir RL. The cell biology of synaptic plasticity: AMPA receptor trafficking. Annual review of cell and developmental biology 2007;23:613-43.

[104] Malinow R, Malenka RC. AMPA receptor trafficking and synaptic plasticity. Annual review of neuroscience 2002;25:103-26.

[105] Derkach VA, Oh MC, Guire ES, Soderling TR. Regulatory mechanisms of AMPA receptors in synaptic plasticity. Nature reviews Neuroscience 2007;8:101-13.

[106] Jackson AC, Nicoll RA. The expanding social network of ionotropic glutamate receptors: TARPs and other transmembrane auxiliary subunits. Neuron 2011;70:178-99.

[107] Lu W, Roche KW. Posttranslational regulation of AMPA receptor trafficking and function. Current opinion in neurobiology 2012;22:470-9.

[108] Nicoll RA, Tomita S, Bredt DS. Auxiliary subunits assist AMPA-type glutamate receptors. Science (New York, NY) 2006;311:1253-6.

[109] Santos SD, Carvalho AL, Caldeira MV, Duarte CB. Regulation of AMPA receptors and synaptic plasticity. Neuroscience 2009;158:105-25.

[110] Hirokawa N, Takemura R. Molecular motors and mechanisms of directional transport in neurons. Nature reviews Neuroscience 2005;6:201-14.

[111] Setou M, Seog DH, Tanaka Y, et al. Glutamate-receptor-interacting protein GRIP1 directly steers kinesin to dendrites. Nature 2002;417:83-7.

[112] Shin H, Wyszynski M, Huh KH, et al. Association of the kinesin motor KIF1A with the multimodular protein liprin-alpha. The Journal of biological chemistry 2003;278:11393-401.

[113] Wyszynski M, Kim E, Dunah AW, et al. Interaction between GRIP and liprin-alpha/SYD2 is required for AMPA receptor targeting. Neuron 2002;34:39-52.

[114] Adesnik H, Nicoll RA, England PM. Photoinactivation of native AMPA receptors reveals their real-time trafficking. Neuron 2005;48:977-85.

[115] Horton AC, Ehlers MD. Secretory trafficking in neuronal dendrites. Nature cell biology 2004;6:585-91.

[116] Cajigas IJ, Tushev G, Will TJ, tom Dieck S, Fuerst N, Schuman EM. The local transcriptome in the synaptic neuropil revealed by deep sequencing and high-resolution imaging. Neuron 2012;74:453-66.

[117] Grooms SY, Noh KM, Regis R, et al. Activity bidirectionally regulates AMPA receptor mRNA abundance in dendrites of hippocampal neurons. J Neurosci 2006;26:8339-51.

[118] Ju W, Morishita W, Tsui J, et al. Activity-dependent regulation of dendritic synthesis and trafficking of AMPA receptors. Nature neuroscience 2004;7:244-53.

[119] Kacharmina JE, Job C, Crino P, Eberwine J. Stimulation of glutamate receptor protein synthesis and membrane insertion within isolated neuronal dendrites. Proceedings of the National Academy of Sciences of the United States of America 2000;97:11545-50.

[120] Carthew RW, Sontheimer EJ. Origins and Mechanisms of miRNAs and siRNAs. Cell 2009;136:642-55.

[121] Yates LA, Norbury CJ, Gilbert RJ. The Long and Short of MicroRNA. Cell 2013;153:516-9.

[122] Djuranovic S, Nahvi A, Green R. A parsimonious model for gene regulation by miRNAs. Science (New York, NY) 2011;331:550-3.

[123] Fabian MR, Sonenberg N, Filipowicz W. Regulation of mRNA translation and stability by microRNAs. Annual review of biochemistry 2010;79:351-79.

[124] Huntzinger E, Izaurralde E. Gene silencing by microRNAs: contributions of translational repression and mRNA decay. Nature reviews Genetics 2011;12:99-110.

[125] Burnashev N, Monyer H, Seeburg PH, Sakmann B. Divalent ion permeability of AMPA receptor channels is dominated by the edited form of a single subunit. Neuron 1992;8:189-98.

[126] Geiger JR, Melcher T, Koh DS, et al. Relative abundance of subunit mRNAs determines gating and Ca2+ permeability of AMPA receptors in principal neurons and interneurons in rat CNS. Neuron 1995;15:193-204.

[127] Lewis BP, Shih IH, Jones-Rhoades MW, Bartel DP, Burge CB. Prediction of mammalian microRNA targets. Cell 2003;115:787-98.

[128] Benson DL, Gall CM, Isackson PJ. Dendritic localization of type II calcium calmodulin-dependent protein kinase mRNA in normal and reinnervated rat hippocampus. Neuroscience 1992;46:851-7.

[129] Blichenberg A, Rehbein M, Muller R, Garner CC, Richter D, Kindler S. Identification of a cis-acting dendritic targeting element in the mRNA encoding the alpha subunit of Ca2+/calmodulin-dependent protein kinase II. The European journal of neuroscience 2001;13:1881-8.

[130] Burgin KE, Waxham MN, Rickling S, Westgate SA, Mobley WC, Kelly PT. In situ hybridization histochemistry of Ca2+/calmodulin-dependent protein kinase in developing rat brain. J Neurosci 1990;10:1788-98.

[131] Miller S, Yasuda M, Coats JK, Jones Y, Martone ME, Mayford M. Disruption of dendritic translation of CaMKIIalpha impairs stabilization of synaptic plasticity and memory consolidation. Neuron 2002;36:507-19.

[132] Mori Y, Imaizumi K, Katayama T, Yoneda T, Tohyama M. Two cis-acting elements in the 3' untranslated region of alpha-CaMKII regulate its dendritic targeting. Nature neuroscience 2000;3:1079-84.

[133] Schratt GM, Tuebing F, Nigh EA, et al. A brain-specific microRNA regulates dendritic spine development. Nature 2006;439:283-9.

[134] Herrera DG, Robertson HA. Activation of c-fos in the brain. Progress in neurobiology 1996;50:83-107.

[135] Tomari Y, Zamore PD. Perspective: machines for RNAi. Genes & development 2005;19:517-29.

[136] Ebert MS, Neilson JR, Sharp PA. MicroRNA sponges: competitive inhibitors of small RNAs in mammalian cells. Nature methods 2007;4:721-6.

[137] Lagos-Quintana M, Rauhut R, Yalcin A, Meyer J, Lendeckel W, Tuschl T. Identification of tissue-specific microRNAs from mouse. Current biology : CB 2002;12:735-9.

[138] Micheva KD, Busse B, Weiler NC, O'Rourke N, Smith SJ. Single-synapse analysis of a diverse synapse population: proteomic imaging methods and markers. Neuron 2010;68:639-53.

[139] Kye MJ, Liu T, Levy SF, et al. Somatodendritic microRNAs identified by laser capture and multiplex RT-PCR. RNA (New York, NY) 2007;13:1224-34.

[140] Anggono V, Huganir RL. Regulation of AMPA receptor trafficking and synaptic plasticity. Current opinion in neurobiology 2012;22:461-9.

[141] Hanley JG. Endosomal sorting of AMPA receptors in hippocampal neurons. Biochemical Society transactions 2010;38:460-5.

[142] Hirling H. Endosomal trafficking of AMPA-type glutamate receptors. Neuroscience 2009;158:36-44.

[143] Malenka RC. Synaptic plasticity and AMPA receptor trafficking. Annals of the New York Academy of Sciences 2003;1003:1-11.

[144] Irier HA, Shaw R, Lau A, Feng Y, Dingledine R. Translational regulation of GluR2 mRNAs in rat hippocampus by alternative 3' untranslated regions. Journal of neurochemistry 2009;109:584-94.

[145] Muddashetty RS, Kelic S, Gross C, Xu M, Bassell GJ. Dysregulated metabotropic glutamate receptor-dependent translation of AMPA receptor and postsynaptic density-95 mRNAs at synapses in a mouse model of fragile X syndrome. J Neurosci 2007;27:5338-48.

[146] Edbauer D, Neilson JR, Foster KA, et al. Regulation of synaptic structure and function by FMRP-associated microRNAs miR-125b and miR-132. Neuron 2010;65:373-84.

[147] Saba R, Storchel PH, Aksoy-Aksel A, et al. Dopamine-regulated microRNA MiR-181a controls GluA2 surface expression in hippocampal neurons. Molecular and cellular biology 2012;32:619-32.

[148] Ho VM, Dallalzadeh LO, Karathanasis N, et al. GluA2 mRNA distribution and regulation by miR-124 in hippocampal neurons. In preparation 2013.

[149] Du L, Richter JD. Activity-dependent polyadenylation in neurons. RNA (New York, NY) 2005;11:1340-7.

[150] Iijima T, Wu K, Witte H, et al. SAM68 regulates neuronal activity-dependent alternative splicing of neurexin-1. Cell 2011;147:1601-14.

[151] Li Q, Lee JA, Black DL. Neuronal regulation of alternative pre-mRNA splicing. Nature reviews Neuroscience 2007;8:819-31.

[152] Mu Y, Otsuka T, Horton AC, Scott DB, Ehlers MD. Activity-dependent mRNA splicing controls ER export and synaptic delivery of NMDA receptors. Neuron 2003;40:581-94.

[153] Costa-Mattioli M, Sossin WS, Klann E, Sonenberg N. Translational control of long-lasting synaptic plasticity and memory. Neuron 2009;61:10-26.

[154] Nguyen PV, Abel T, Kandel ER. Requirement of a critical period of transcription for induction of a late phase of LTP. Science (New York, NY) 1994;265:1104-7.

[155] Ch'ng TH, Uzgil B, Lin P, Avliyakulov NK, O'Dell TJ, Martin KC. Activity-dependent transport of the transcriptional coactivator CRTC1 from synapse to nucleus. Cell 2012;150:207-21.

[156] Jeffrey RA, Ch'ng TH, O'Dell TJ, Martin KC. Activity-dependent anchoring of importin alpha at the synapse involves regulated binding to the cytoplasmic tail of the NR1-1a subunit of the NMDA receptor. J Neurosci 2009;29:15613-20.

[157] Thompson KR, Otis KO, Chen DY, Zhao Y, O'Dell TJ, Martin KC. Synapse to nucleus signaling during long-term synaptic plasticity; a role for the classical active nuclear import pathway. Neuron 2004;44:997-1009.

[158] Flavell SW, Greenberg ME. Signaling mechanisms linking neuronal activity to gene expression and plasticity of the nervous system. Annual review of neuroscience 2008;31:563-90.

[159] Greer PL, Greenberg ME. From synapse to nucleus: calcium-dependent gene transcription in the control of synapse development and function. Neuron 2008;59:846-60.

[160] Flavell SW, Kim TK, Gray JM, et al. Genome-wide analysis of MEF2 transcriptional program reveals synaptic target genes and neuronal activity-dependent polyadenylation site selection. Neuron 2008;60:1022-38.

[161] Park CS, Gong R, Stuart J, Tang SJ. Molecular network and chromosomal clustering of genes involved in synaptic plasticity in the hippocampus. The Journal of biological chemistry 2006;281:30195-211.

[162] Newton SS, Collier EF, Hunsberger J, et al. Gene profile of electroconvulsive seizures: induction of neurotrophic and angiogenic factors. J Neurosci 2003;23:10841-51.

[163] Altar CA, Laeng P, Jurata LW, et al. Electroconvulsive seizures regulate gene expression of distinct neurotrophic signaling pathways. J Neurosci 2004;24:2667-77.

[164] Greenberg ME, Ziff EB, Greene LA. Stimulation of neuronal acetylcholine receptors induces rapid gene transcription. Science (New York, NY) 1986;234:80-3.

[165] Bartel DP, Sheng M, Lau LF, Greenberg ME. Growth factors and membrane depolarization activate distinct programs of early response gene expression: dissociation of fos and jun induction. Genes & development 1989;3:304-13.

[166] Sheng M, McFadden G, Greenberg ME. Membrane depolarization and calcium induce c-fos transcription via phosphorylation of transcription factor CREB. Neuron 1990;4:571-82.

[167] Misra RP, Bonni A, Miranti CK, Rivera VM, Sheng M, Greenberg ME. L-type voltage-sensitive calcium channel activation stimulates gene expression by a serum response factor-dependent pathway. The Journal of biological chemistry 1994;269:25483-93.

[168] Belfield JL, Whittaker C, Cader MZ, Chawla S. Differential effects of Ca2+ and cAMP on transcription mediated by MEF2D and cAMP-response element-binding protein in hippocampal neurons. The Journal of biological chemistry 2006;281:27724-32.

[169] Timmusk T, Palm K, Metsis M, et al. Multiple promoters direct tissue-specific expression of the rat BDNF gene. Neuron 1993;10:475-89.

[170] Aid T, Kazantseva A, Piirsoo M, Palm K, Timmusk T. Mouse and rat BDNF gene structure and expression revisited. Journal of neuroscience research 2007;85:525-35.

[171] McMahon AC, Barnett MW, O'Leary TS, et al. SynGAP isoforms exert opposing effects on synaptic strength. Nature communications 2012;3:900.

[172] Barbosa-Morais NL, Irimia M, Pan Q, et al. The evolutionary landscape of alternative splicing in vertebrate species. Science (New York, NY) 2012;338:1587-93.

[173] Xie J, Black DL. A CaMK IV responsive RNA element mediates depolarization-induced alternative splicing of ion channels. Nature 2001;410:936-9.

[174] Proudfoot NJ. Ending the message: poly(A) signals then and now. Genes & development 2011;25:1770-82.

[175] Hoque M, Ji Z, Zheng D, et al. Analysis of alternative cleavage and polyadenylation by 3' region extraction and deep sequencing. Nature methods 2013;10:133-9.

[176] Tian B, Hu J, Zhang H, Lutz CS. A large-scale analysis of mRNA polyadenylation of human and mouse genes. Nucleic acids research 2005;33:201-12.

[177] Di Giammartino DC, Nishida K, Manley JL. Mechanisms and consequences of alternative polyadenylation. Molecular cell 2011;43:853-66.

[178] Edwalds-Gilbert G, Veraldi KL, Milcarek C. Alternative poly(A) site selection in complex transcription units: means to an end? Nucleic acids research 1997;25:2547-61.

[179] Licatalosi DD, Mele A, Fak JJ, et al. HITS-CLIP yields genome-wide insights into brain alternative RNA processing. Nature 2008;456:464-9.

[180] Sala C, Futai K, Yamamoto K, Worley PF, Hayashi Y, Sheng M. Inhibition of dendritic spine morphogenesis and synaptic transmission by activity-inducible protein Homer1a. J Neurosci 2003;23:6327-37.

[181] Sato M, Suzuki K, Nakanishi S. NMDA receptor stimulation and brain-derived neurotrophic factor upregulate homer 1a mRNA via the mitogen-activated protein kinase cascade in cultured cerebellar granule cells. J Neurosci 2001;21:3797-805.

[182] Vazdarjanova A, McNaughton BL, Barnes CA, Worley PF, Guzowski JF. Experience-dependent coincident expression of the effector immediate-early genes arc and Homer 1a in hippocampal and neocortical neuronal networks. J Neurosci 2002;22:10067-71.

[183] Berg MG, Singh LN, Younis I, et al. U1 snRNP determines mRNA length and regulates isoform expression. Cell 2012;150:53-64.

[184] Miura P, Shenker S, Andreu-Agullo C, Westholm JO, Lai EC. Widespread and extensive lengthening of 3' UTRs in the mammalian brain. Genome research 2013;23:812-25.

[185] McKee AE, Minet E, Stern C, Riahi S, Stiles CD, Silver PA. A genome-wide in situ hybridization map of RNA-binding proteins reveals anatomically restricted expression in the developing mouse brain. BMC developmental biology 2005;5:14.

[186] Ule J, Darnell RB. RNA binding proteins and the regulation of neuronal synaptic plasticity. Current opinion in neurobiology 2006;16:102-10.

[187] Lugli G, Torvik VI, Larson J, Smalheiser NR. Expression of microRNAs and their precursors in synaptic fractions of adult mouse forebrain. Journal of neurochemistry 2008;106:650-61.

[188] Pietrzykowski AZ, Friesen RM, Martin GE, et al. Posttranscriptional regulation of BK channel splice variant stability by miR-9 underlies neuroadaptation to alcohol. Neuron 2008;59:274-87.

[189] Filipowicz W, Bhattacharyya SN, Sonenberg N. Mechanisms of post-transcriptional regulation by microRNAs: are the answers in sight? Nature reviews Genetics 2008;9:102-14.

[190] Baek D, Villen J, Shin C, Camargo FD, Gygi SP, Bartel DP. The impact of microRNAs on protein output. Nature 2008;455:64-71.

[191] Selbach M, Schwanhausser B, Thierfelder N, Fang Z, Khanin R, Rajewsky N. Widespread changes in protein synthesis induced by microRNAs. Nature 2008;455:58-63.

[192] Bantscheff M, Schirle M, Sweetman G, Rick J, Kuster B. Quantitative mass spectrometry in proteomics: a critical review. Analytical and bioanalytical chemistry 2007;389:1017-31.

[193] Hendrickson DG, Hogan DJ, McCullough HL, et al. Concordant regulation of translation and mRNA abundance for hundreds of targets of a human microRNA. PLoS biology 2009;7:e1000238.

[194] Guo H, Ingolia NT, Weissman JS, Bartel DP. Mammalian microRNAs predominantly act to decrease target mRNA levels. Nature 2010;466:835-40.

[195] Misquitta CM, Chen T, Grover AK. Control of protein expression through mRNA stability in calcium signalling. Cell calcium 2006;40:329-46.

[196] Perry RB, Doron-Mandel E, Iavnilovitch E, et al. Subcellular knockout of importin beta1 perturbs axonal retrograde signaling. Neuron 2012;75:294-305.

[197] An JJ, Gharami K, Liao GY, et al. Distinct role of long 3' UTR BDNF mRNA in spine morphology and synaptic plasticity in hippocampal neurons. Cell 2008;134:175-87.

[198] Gkogkas C, Sonenberg N, Costa-Mattioli M. Translational control mechanisms in long-lasting synaptic plasticity and memory. The Journal of biological chemistry 2010;285:31913-7.

[199] Tang SJ, Reis G, Kang H, Gingras AC, Sonenberg N, Schuman EM. A rapamycin-sensitive signaling pathway contributes to long-term synaptic plasticity in the hippocampus. Proceedings of the National Academy of Sciences of the United States of America 2002;99:467-72.

[200] Bhakar AL, Dolen G, Bear MF. The pathophysiology of fragile X (and what it teaches us about synapses). Annual review of neuroscience 2012;35:417-43.

[201] Kelleher RJ, 3rd, Bear MF. The autistic neuron: troubled translation? Cell 2008;135:401-6.

[202] Ebert DH, Greenberg ME. Activity-dependent neuronal signalling and autism spectrum disorder. Nature 2013;493:327-37.

[203] Darnell JC, Jensen KB, Jin P, Brown V, Warren ST, Darnell RB. Fragile X mental retardation protein targets G quartet mRNAs important for neuronal function. Cell 2001;107:489-99.

[204] Darnell JC, Fraser CE, Mostovetsky O, et al. Kissing complex RNAs mediate interaction between the Fragile-X mental retardation protein KH2 domain and brain polyribosomes. Genes & development 2005;19:903-18.

[205] Darnell JC, Van Driesche SJ, Zhang C, et al. FMRP stalls ribosomal translocation on mRNAs linked to synaptic function and autism. Cell 2011;146:247-61.

[206] Zalfa F, Giorgi M, Primerano B, et al. The fragile X syndrome protein FMRP associates with BC1 RNA and regulates the translation of specific mRNAs at synapses. Cell 2003;112:317-27.

[207] Dictenberg JB, Swanger SA, Antar LN, Singer RH, Bassell GJ. A direct role for FMRP in activity-dependent dendritic mRNA transport links filopodial-spine morphogenesis to fragile X syndrome. Developmental cell 2008;14:926-39.

[208] Zalfa F, Eleuteri B, Dickson KS, et al. A new function for the fragile X mental retardation protein in regulation of PSD-95 mRNA stability. Nature neuroscience 2007;10:578-87.

[209] Gobert D, Topolnik L, Azzi M, et al. Forskolin induction of late-LTP and up-regulation of 5' TOP mRNAs translation via mTOR, ERK, and PI3K in hippocampal pyramidal cells. Journal of neurochemistry 2008;106:1160-74.

[210] Moccia R, Chen D, Lyles V, et al. An unbiased cDNA library prepared from isolated Aplysia sensory neuron processes is enriched for cytoskeletal and translational mRNAs. J Neurosci 2003;23:9409-17.

[211] Poon MM, Choi SH, Jamieson CA, Geschwind DH, Martin KC. Identification of process-localized mRNAs from cultured rodent hippocampal neurons. J Neurosci 2006;26:13390-9.

[212] Lau AG, Irier HA, Gu J, et al. Distinct 3'UTRs differentially regulate activity-dependent translation of brain-derived neurotrophic factor (BDNF). Proceedings of the National Academy of Sciences of the United States of America 2010;107:15945-50.

[213] Udagawa T, Swanger SA, Takeuchi K, et al. Bidirectional control of mRNA translation and synaptic plasticity by the cytoplasmic polyadenylation complex. Molecular cell 2012;47:253-66.

[214] Mendez R, Richter JD. Translational control by CPEB: a means to the end. Nature reviews Molecular cell biology 2001;2:521-9.

[215] Halbeisen RE, Galgano A, Scherrer T, Gerber AP. Post-transcriptional gene regulation: from genome-wide studies to principles. Cellular and molecular life sciences : CMLS 2008;65:798-813.

[216] Wang Y, Liu CL, Storey JD, Tibshirani RJ, Herschlag D, Brown PO. Precision and functional specificity in mRNA decay. Proceedings of the National Academy of Sciences of the United States of America 2002;99:5860-5.

[217] Huang YS, Jung MY, Sarkissian M, Richter JD. N-methyl-D-aspartate receptor signaling results in Aurora kinase-catalyzed CPEB phosphorylation and alpha CaMKII mRNA polyadenylation at synapses. EMBO J 2002;21:2139-48.

[218] Atkins CM, Nozaki N, Shigeri Y, Soderling TR. Cytoplasmic polyadenylation element binding protein-dependent protein synthesis is regulated by calcium/calmodulin-dependent protein kinase II. J Neurosci 2004;24:5193-201.

[219] Makhinson M, Chotiner JK, Watson JB, O'Dell TJ. Adenylyl cyclase activation modulates activity-dependent changes in synaptic strength and Ca2+/calmodulin-dependent kinase II autophosphorylation. J Neurosci 1999;19:2500-10.

[220] Abel T, Nguyen PV. Regulation of hippocampus-dependent memory by cyclic AMP-dependent protein kinase. Progress in brain research 2008;169:97-115.

[221] Elgersma Y, Sweatt JD, Giese KP. Mouse genetic approaches to investigating calcium/calmodulin-dependent protein kinase II function in plasticity and cognition. J Neurosci 2004;24:8410-5.

[222] Wayman GA, Lee YS, Tokumitsu H, Silva AJ, Soderling TR. Calmodulin-kinases: modulators of neuronal development and plasticity. Neuron 2008;59:914-31.

[223] Harris EW, Cotman CW. Long-term potentiation of guinea pig mossy fiber responses is not blocked by N-methyl D-aspartate antagonists. Neuroscience letters 1986;70:132-7.

[224] Amaral DG, Witter MP. The three-dimensional organization of the hippocampal formation: a review of anatomical data. Neuroscience 1989;31:571-91.

[225] Debanne D, Gahwiler BH, Thompson SM. Long-term synaptic plasticity between pairs of individual CA3 pyramidal cells in rat hippocampal slice cultures. J Physiol 1998;507 (Pt 1):237-47.

[226] Pavlidis P, Madison DV. Synaptic transmission in pair recordings from CA3 pyramidal cells in organotypic culture. Journal of neurophysiology 1999;81:2787-97.

[227] Selig DK, Nicoll RA, Malenka RC. Hippocampal long-term potentiation preserves the fidelity of postsynaptic responses to presynaptic bursts. J Neurosci 1999;19:1236-46.

[228] Zalutsky RA, Nicoll RA. Comparison of two forms of long-term potentiation in single hippocampal neurons. Science (New York, NY) 1990;248:1619-24.

[229] Parkhomchuk D, Borodina T, Amstislavskiy V, et al. Transcriptome analysis by strand-specific sequencing of complementary DNA. Nucleic acids research 2009;37:e123.

[230] CASAVA. 2013. at http://support.illumina.com/sequencing/sequencing_software/casava.ilmn.)

[231] FastQC. at http://www.bioinformatics.babraham.ac.uk/projects/fastqc.)

[232] Dobin A, Davis CA, Schlesinger F, et al. STAR: ultrafast universal RNA-seq aligner. Bioinformatics (Oxford, England) 2013;29:15-21.

[233] Flicek P, Amode MR, Barrell D, et al. Ensembl 2012. Nucleic acids research 2012;40:D84-90.

[234] Kent WJ, Sugnet CW, Furey TS, et al. The human genome browser at UCSC. Genome research 2002;12:996-1006.

[235] Li H, Handsaker B, Wysoker A, et al. The Sequence Alignment/Map format and SAMtools. Bioinformatics (Oxford, England) 2009;25:2078-9.

[236] Trapnell C, Hendrickson DG, Sauvageau M, Goff L, Rinn JL, Pachter L. Differential analysis of gene regulation at transcript resolution with RNA-seq. Nature biotechnology 2013;31:46-53.

[237] Taubenfeld SM, Stevens KA, Pollonini G, Ruggiero J, Alberini CM. Profound molecular changes following hippocampal slice preparation: loss of AMPA receptor subunits and uncoupled mRNA/protein expression. Journal of neurochemistry 2002;81:1348-60.

[238] Ho OH, Delgado JY, O'Dell TJ. Phosphorylation of proteins involved in activity-dependent forms of synaptic plasticity is altered in hippocampal slices maintained in vitro. Journal of neurochemistry 2004;91:1344-57.

[239] Dubner R, Ruda MA. Activity-dependent neuronal plasticity following tissue injury and inflammation. Trends in neurosciences 1992;15:96-103.

[240] Coba MP, Valor LM, Kopanitsa MV, Afinowi NO, Grant SG. Kinase networks integrate profiles of N-methyl-D-aspartate receptor-mediated gene expression in hippocampus. The Journal of biological chemistry 2008;283:34101-7.

[241] Saha RN, Wissink EM, Bailey ER, et al. Rapid activity-induced transcription of Arc and other IEGs relies on poised RNA polymerase II. Nature neuroscience 2011;14:848-56.

[242] Nguyen PV, Kandel ER. Brief theta-burst stimulation induces a transcription-dependent late phase of LTP requiring cAMP in area CA1 of the mouse hippocampus. Learn Mem 1997;4:230-43.

[243] Luscher C, Malenka RC. NMDA receptor-dependent long-term potentiation and long-term depression (LTP/LTD). Cold Spring Harbor perspectives in biology 2012;4.

[244] Zafra F, Hengerer B, Leibrock J, Thoenen H, Lindholm D. Activity dependent regulation of BDNF and NGF mRNAs in the rat hippocampus is mediated by non-NMDA glutamate receptors. EMBO J 1990;9:3545-50.

[245] Tao X, West AE, Chen WG, Corfas G, Greenberg ME. A calcium-responsive transcription factor, CaRF, that regulates neuronal activity-dependent expression of BDNF. Neuron 2002;33:383-95.

[246] Mignone F, Gissi C, Liuni S, Pesole G. Untranslated regions of mRNAs. Genome Biol 2002;3:REVIEWS0004.

[247] Christopherson KS, Ullian EM, Stokes CC, et al. Thrombospondins are astrocyte-secreted proteins that promote CNS synaptogenesis. Cell 2005;120:421-33.

[248] Allen NJ, Bennett ML, Foo LC, et al. Astrocyte glypicans 4 and 6 promote formation of excitatory synapses via GluA1 AMPA receptors. Nature 2012;486:410-4.

[249] Chung WS, Barres BA. The role of glial cells in synapse elimination. Current opinion in neurobiology 2012;22:438-45.

[250] Chowdhury S, Shepherd JD, Okuno H, et al. Arc/Arg3.1 interacts with the endocytic machinery to regulate AMPA receptor trafficking. Neuron 2006;52:445-59.

[251] Schwanhausser B, Busse D, Li N, et al. Global quantification of mammalian gene expression control. Nature 2011;473:337-42.

[252] Wilkening S, Pelechano V, Jarvelin AI, et al. An efficient method for genome-wide polyadenylation site mapping and RNA quantification. Nucleic acids research 2013;41:e65.

[253] Chi SW, Zang JB, Mele A, Darnell RB. Argonaute HITS-CLIP decodes microRNA-mRNA interaction maps. Nature 2009;460:479-86.

[254] Chotiner JK, Khorasani H, Nairn AC, O'Dell TJ, Watson JB. Adenylyl cyclase-dependent form of chemical long-term potentiation triggers translational regulation at the elongation step. Neuroscience 2003;116:743-52.